Kinematics and Hydrodynamics of Undulatory Locomotion in Hagfishes (Myxinidae) and Hagfish-like Robotic Models

Kinematics and hydrodynamics of undulatory locomotion in hagfishes (Myxinidae) and hagfish-like robotic models

A dissertation presented

by

Jeanette Li Li Lim

to

The Department of Organismic and Evolutionary Biology

in partial fulfillment of the requirements
for the degree of
Doctor of Philosophy
in the subject of
Organismic and Evolutionary Biology

Harvard University
Cambridge, Massachusetts

May 2013

Dissertation Advisor: Professor George V. Lauder Jeanette Li Li Lim

Kinematics and hydrodynamics of undulatory locomotion in hagfishes (Myxinidae) and hagfish-like robotic models

Abstract

Hagfishes have both intrigued and confused biologists since Linnaeus first mistakenly classified one as an "intestinal worm." Modern hagfishes (Myxinidae) are elongate, marine fishes often described by what they lack: jaws, scales, paired fins, or a vertebral column. Accompanying this reduced morphology was a long-held view that hagfish are lazy animals that mostly lay about on the ocean floor, but more recent research has revealed them to be active hunters and scavengers in the benthic community. Routine swimming is a requisite part of these activities, yet knowledge of how these exceptionally flexible fishes swim is limited. Here, I use an integrative experimental approach to provide a more comprehensive, quantitative understanding of locomotory mechanisms in hagfishes.

In Chapters 1 and 2, I use high-speed videography to quantify whole-body kinematics of steady and unsteady swimming in *Eptatretus stoutii* and *Myxine glutinosa*, representing the two main lineages within Myxinidae. Both species generally swim with high amplitude head movements and use tail beat frequency to control swim speed, but inter- and intra-specific variation in other undulatory wave variables suggests multiple mechanisms to modulate speed. Changes in the shape of the body wave characterize the observed unsteady swimming behaviors. During positive linear accelerations, hagfish transiently adopt a larger, longer body wave. During lateral maneuvers, hagfish approximate "sidewinding" behavior as anterior body regions interact

with the substrate while posterior body regions propagate waves of lateral bending toward the tail tip.

Chapter 3 integrates kinematics with hydrodynamics, using particle image velocimetry to visualize the flow field around swimming *E. stoutii*. The steady swimming wake consists of caudolateral fluid jets, which turn caudally during linear accelerations. Wake jets orient asymmetrically during lateral swimming, contributing both forward and lateral thrust over a complete tail beat. The hydrodynamic patterns observed reinforce kinematics-based hypotheses on how hagfishes enact their various swimming behaviors.

In Chapter 4, I use simple robotically-controlled physical models to examine functional relationships between body flexural stiffness, shape, kinematics, hydrodynamics, and swimming performance. I relate model swim performance to characteristics of hagfish swimming, and describe lessons that passively undulating models impart for understanding locomotion by live elongate undulatory swimmers.

Table of Contents

Introduction…….1

Chapter 1: Diverse steady swimming kinematics in two species of hagfish, *Eptatretus stoutii* and *Myxine glutinosa*……..…6

Chapter 2: Maneuvering by flexible finless fishes: kinematics of linear accelerations and lateral maneuvers in hagfishes (Myxinidae)…….43

Chapter 3: Hydrodynamics of steady and unsteady swimming in the Pacific hagfish, *Eptatretus stoutii*……...…….…….88

Chapter 4: Flexible fish-like robotic models reveal functional relationships between body stiffness, kinematics, and hydrodynamics in undulatory swimming…….…..121

Acknowledgements

I am honored and humbled that I get to express sincere gratitude to a number of wonderful people who helped make graduate school and life outside of it a better experience than I could have imagined. Thank you, Dr. George Lauder, my advisor, for your support, wisdom, and unstoppable energy. There is no better advisor that a grad student could ask for. Thank you, Timothy Winegard and Dr. Douglas Fudge, for being my hagfish providers and gurus. Your help made this entire thesis possible. Special thanks to Tim for ferrying the hagfish from Ontario to Massachusetts, and staying to film the hagfish with me, a sometimes tedious process for a fish that tires out pretty quickly. Thank you, Doug, for the mentorship and friendship, and for introducing me to the hagfish ten years ago at UBC. Thank you, Drs. Stacey Combes, Andrew Biewener, Karel Liem, and Farish Jenkins, Jr., my thesis committee. Your encouragement and caring has been and will be an inspiration. Thank you, present and past members of the Lauder Lab for years of camaraderie and talks about science and not science. Special thanks to Drs. Nicole Danos and Erin Blevins, who were there from the pre-doctor start. Your friendship has been one of the best perks of being here. Thank you to the new friends I made here for the laughs, trips, and dance parties. And thank you to the old friends from home for the laughs, care packages, and continued love.

A deep thank you to my parents and sister – Evelyn, Philip, and Vania. You have been endlessly supportive, loving, and patient since the very beginning. Thank you for taking me to Stanley Park, and letting me decorate the living room with dioramas of underwater scenes. Thank you Andy Klein, my partner and best friend. Your encouragement and love have made all the difference. And lastly, thank you to the hagfish, for putting up with my prodding and poking, and being the stars of my work.

Introduction

Fishes are the most diverse group of vertebrates on the planet (Bone et al., 1995). Within this diversity of species exists a remarkable array of distinct body forms and behaviors as each species presents its own solutions to the challenges of living in an underwater environment. Locomotion through water is a task that nearly all fishes face daily, and one where different fishes must obey the same physical laws. Water is dense yet deformable, giving way when pushed against but still exerting the reaction forces that enable swimming through a fluid medium (Vogel, 1994). Decades of study and technological advancement in experimental biology have allowed researchers to understand increasingly more about the different ways in which fishes swim through water, and the relationships between form and function that characterize different patterns of swimming (Lauder, 2006; Lauder, 2011). Over the course of these studies on various fishes, champions of swimming have emerged. Bullet-shaped tunas, for example, are undoubtedly champions of high-speed, open ocean cruising (Katz et al., 2001; Walters and Fierstine, 1964). Meanwhile, slender but muscular-bodied pike are champions of accelerating strikes (Harper and Blake, 1990; Harper and Blake, 1991). And bluegill sunfish, while not the most visually spectacular fish, are champions of precise maneuvering, using paired and median fins in concert to swim forward, turn, and hold station (Drucker and Lauder, 2001; Flammang and Lauder, 2009; Standen and Lauder, 2005).

Hagfishes have never been described as champions of swimming. Rather, members of this 300 million year-old clade (Myxinidae) (Bardack, 1991) of marine, temperate fishes have historically been noted for their exceptional inactivity. In early accounts of their behavior, hagfishes were described as lazy, sluggish, and degenerate animals that spent long stretches of time simply lying on the ocean floor or concealed in burrows beneath it (Braun and Northcutt,

1998; Jensen, 1966). Coincident with this apparent lack of activity, living representatives of the Myxinidae are relatively simple in external appearance as they lack many of the anatomical features one typically associates with a fish: scales, paired fins, or a spine consisting of vertebrae (Bardack, 1991; Jensen, 1966). The hagfish body is a slightly modified tube, elongate and cylindrical with moderate lateral compression toward the caudal end where a narrow fin margin extends from the body (Hart, 1973; Nelson, 2006). The whole body is also quite flexible as a cartilaginous notochord serves as its main axial support (Long et al., 2002).

By passing waves of lateral bending down their flexible bodies, hagfishes push on the surrounding water and swim forward using a mode of locomotion broadly termed "anguilliform" swimming (Long et al., 2002). Breder originally classified several different modes of swimming among fishes, naming each after a representative champion or exemplar of the mode, such as the tuna, pike, and eel (Breder, 1926). Experimental studies on these exemplars of swimming have allowed researchers to examine specialized cases of how specific form associates with specific function, but also incorporating studies of non-champions can broaden our understanding of the collective diversity in locomotory behavior among aquatic animals (Gillis, 1996).

Hagfishes present a valuable opportunity to further explore mechanisms of locomotion among fishes. The combination of their relatively uniform external morphology, plesiomorphic condition of retaining a notochord into adulthood, and position as an early lineage in the evolution of fishes (Nelson, 2006) makes hagfishes ideal candidates for studying fundamental patterns of locomotion in vertebrates. In addition, more recent research on their ecology has shown that hagfish are much more active than their early reputation suggests (Martini, 1998). Individuals may travel long distances along the ocean floor to scavenge on fallen carcasses, using their tooth plates and undulating bodies to tear pieces of flesh off the decaying body

(Jensen, 1966; Martini, 1998). During predatory bouts, some hagfish will actively scour and swim into muddy substrates in search of live buried prey (Zintzen et al., 2011). Swimming is likely a requisite activity in a hagfish's daily life, but limited quantitative information on their swimming behavior is available (Long et al., 2002; Long et al., 2010).

Here, I use an integrative experimental approach to characterize hagfish swimming behavior and work toward a more comprehensive, quantitative understanding of their mechanisms of locomotion. First, I quantify the whole-body kinematics of steady swimming in two species of hagfish (*Eptatretus stoutii* and *Myxine glutinosa*) from the two main lineages within Myxinidae (Fernholm, 1998), and use these data to formulate mechanistic hypotheses on how hagfishes control swimming speed during routine locomotion (Chapter 1). I then further explore the locomotory repertoire of hagfishes and examine how a body lacking discrete fins accomplishes maneuvering behaviors by quantifying the kinematics of linear accelerations and lateral maneuvers (Chapter 2). The patterns of hagfish body motion revealed from these two chapters are then integrated with the hydrodynamics of steady and unsteady swimming to better understand how hagfish manipulate their fluid environment while performing different swimming behaviors (Chapter 3). Finally, I take advantage of the experimental freedom that physical modeling affords and use robotically-controlled fish-like models to examine functional relationships between body stiffness, kinematics, and hydrodynamics in undulatory swimming by elongate anguilliform swimmers, particularly the flexible-bodied hagfish (Chapter 4).

References

Bardack, D. (1991). First fossil hagfish (Myxinoidea): a record from the Pennsylvanian of Illinois. *Science* **254**, 701-703.

Bone, Q., Marshall, N. B. and Blaxter, J. H. S. (1995). *Biology of Fishes*. London: Chapman & Hall.

Braun, C. B. and Northcutt, R. G. (1998). Cutaneous exteroreceptors and their innervation in hagfishes. In *The Biology of Hagfishes* (eds. J. M. Jørgensen, J. P. Lomholt, R. E. Weber and H. Malte), pp. 512-532. London: Chapman & Hall.

Breder, C. M. (1926). The locomotion of fishes. *Zoologica* **4**, 159-297.

Drucker, E. G. and Lauder, G. V. (2001). Wake dynamics and fluid forces of turning maneuvers in sunfish. *J. Exp. Biol.* **204**, 431-442.

Fernholm, B. (1998). Hagfish systematics. In *The Biology of Hagfishes* (eds. J. M. Jørgensen, J. P. Lomholt, R. E. Weber and H. Malte), pp. 33-44. London: Chapman & Hall.

Flammang, B. E. and Lauder, G. V. (2009). Caudal fin shape modulation and control during acceleration, braking and backing maneuvers in bluegill sunfish, *Lepomis macrochirus*. *J. Exp. Biol.* **212**, 277-286.

Gillis, G. B. (1996). Undulatory locomotion in elongate aquatic vertebrates: Anguilliform swimming since Sir James Gray. *Amer. Zool.* **36**, 656-665.

Harper, D. G. and Blake, R. W. (1990). Fast-start performance of rainbow trout *Salmo gairdneri* and northern pike *Esox lucius*. *J. Exp. Biol.* **150**, 321-342.

Harper, D. G. and Blake, R. W. (1991). Prey capture and the fast-start performance of northern pike *Esox lucius*. *J. Exp. Biol.* **155**, 175-192.

Hart, J. L. (1973). Pacific fishes of Canada. *Fish. Res. Board Can. Bull.* **180**, 1-740.

Jensen, D. (1966). The hagfish. *Sci. Am.* **214**, 82-90.

Katz, S. L., Syme, D. A. and Shadwick, R. E. (2001). High-speed swimming: Enhanced power in yellowfin tuna. *Nature* **410**, 770-771.

Lauder, G. V. (2006). Locomotion. In *The Physiology of Fishes* (eds. D. H. Evans and J. B. Claiborne), pp. 3-46. Boca Raton: CRC Press.

Lauder, G. V. (2011). Swimming hydrodynamics: ten questions and the technical approaches needed to resolve them. *Exp. Fluids* **51**, 23-35.

Long, J. H., Jr., Koob-Emunds, M., Sinwell, B. and Koob, T. J. (2002). The notochord of hagfish *Myxine glutinosa*: visco-elastic properties and mechanical functions during steady swimming. *J. Exp. Biol.* **205**, 3819-3831.

Long, J. H., Porter, M. E., Root, R. G. and Liew, C. W. (2010). Go reconfigure: how fish change shape as they swim and evolve. *Integr. Comp. Biol.* **50**, 1120-1139.

Martini, F. H. (1998). The ecology of hagfishes. In *The Biology of Hagfishes* (eds. J. M. Jørgensen, J. P. Lomholt, R. E. Weber and H. Malte), pp. 57-77. London: Chapman & Hall.

Nelson, J. S. (2006). *Fishes of the World*. Hoboken: John Wiley & Sons, Inc.

Standen, E. M. and Lauder, G. V. (2005). Dorsal and anal fin function in bluegill sunfish Lepomis macrochirus: Three-dimensional kinematics during propulsion and maneuvering. *J. Exp. Biol.* **208**, 2753-2763.

Vogel, S. (1994). *Life in Moving Fluids: The Physical Biology of Flow*. Princeton: Princeton University Press.

Walters, V. and Fierstine, H. L. (1964). Measurements of swimming speeds of yellowfin tuna and wahoo. *Nature* **202**, 208-209.

Zintzen, V., Roberts, C. D., Anderson, M. J., Stewart, A. L., Struthers, C. D. and Harvey, E. S. (2011). Hagfish predatory behaviour and slime defence mechanism. *Sci. Rep.* **1**:131 doi: 10.1038/srep00131.

Chapter 1

Diverse steady swimming kinematics in two species of hagfish, *Eptatretus stoutii* and *Myxine glutinosa*

Abstract

Animals that swim in the anguilliform mode pass waves of lateral bending down their elongate bodies to propel forward. Hagfishes (Myxinidae) are generally classified as anguilliform swimmers, but the family's unique habits and reduced morphology—including a flexible body lacking a vertebral column and capable of tying itself into a knot—may also translate into unique swimming behavior within this broad classification. Their ecological roles as active scavengers and hunters can require considerable bouts of swimming, yet quantitative data on hagfish swimming abilities are limited. Here, I quantify whole-body kinematics of steady undulatory swimming in Pacific hagfish (*Eptatretus stoutii*) and Atlantic hagfish (*Myxine glutinosa*), species representing the two main lineages of Myxinidae. I analyzed body midlines obtained from high-speed video of hagfishes swimming between 0.33 and 0.86 body lengths/second, and found that both species swim using large lateral head movements that initiate high amplitude undulatory waves. Swim speed is generally frequency-modulated, but patterns in wave speed, wavelength, and amplitude along the body and across swim speeds are variable, implying versatile mechanisms for the control of swim speed in these highly flexible fishes. I compare my results to kinematics published for other elongate swimmers and propose mechanistic hypotheses on how hagfishes might modulate swim speed through interacting body wave properties. I demonstrate that hagfishes possess a rich locomotory repertoire and add diversity to an already broad assemblage of anguilliform swimmers.

Introduction

With their seemingly primitive appearance and unique habits among fishes, hagfishes have both intrigued and confused biologists since Linnaeus first mistakenly classified one as an "intestinal worm" (Jensen, 1966). Modern hagfishes (Myxinidae) are elongate, marine fishes whose anatomy is often described by what it lacks: jaws, scales, paired fins, or a fully developed set of eyes or vertebral column (Bardack, 1991; Jensen, 1966). Accompanying these reduced anatomical features was a long-held view that hagfish are lazy, sensory-limited animals that lay about on the ocean floor or in burrows, moving infrequently only to feed on dead or dying prey (Jensen, 1966); however, more recent research has revealed hagfishes to be active hunters (Zintzen et al., 2011) and scavengers in the benthic and epibenthic community (Koob and Long, 2000; Martini, 1998), covering potentially large distances to find often scarce prey (Braun and Northcutt, 1998). Routine swimming represents a non-trivial part of these activities, yet only a few studies have explored swimming movements in hagfishes (Adam, 1960; Campbell, 1940; Long et al., 2002; Long et al., 2010).

Early qualitative descriptions of swimming motions in Pacific hagfish (*Eptatretus stoutii,* (Campbell, 1940)) and Atlantic hagfish (*Myxine glutinosa*, (Adam, 1960)) called their swimming "snake-like." Hagfishes pass a wave of bending down their body to propel themselves forward, but they will also reverse this undulatory wave and swim backward if stimulated near the head (Adam, 1960; Campbell, 1940). Their bodies are cylindrical with moderate lateral compression toward the posterior, where a narrow caudal fin margin is supported by cartilaginous fin rays (Hart, 1973; Koob and Long, 2000). While hagfish were once thought to completely lack vertebrae, workers recently found vestigial vertebral elements along the notochord in the inshore hagfish, *E. burgeri* (Ota et al., 2011). This anatomical discovery combined with the latest genetic

evidence place hagfishes and similarly jawless lampreys in a monophyletic group within the vertebrates (Heimberg et al., 2010).

The cartilaginous notochord remains the adult hagfish's main propulsive axis, and research on its locomotory function in *M. glutinosa* has led to our current quantitative knowledge on hagfish swimming (Long et al., 2002). One study by Long and his colleagues reported basic motion patterns of isolated points on the body over a moderate range of steady swim speeds (Long et al., 2002), while another study provided detailed motion patterns along the body but for a short range of swim speeds (Long et al., 2010). Accordingly, we can improve our mechanistic understanding of the hagfish undulatory waveform from a quantitative analysis that spans the animal's body length and speed capabilities. Hagfish have been characterized as anguilliform-mode swimmers, but we have yet to determine how their kinematics relate to those of other elongate swimmers. Furthermore, while hagfishes as a group have rather distinct morphologies and physiologies when compared to other fishes, several differences between myxinid and eptatretid hagfishes suggest that the two major lineages might differ in their swimming abilities. In general, myxinids appear to be the more specialized burrowers (Lesser et al., 1996; Martini, 1998), while eptatretids appear to have a greater capacity for aerobic exercise (Forster, 1990). A more comprehensive and comparative analysis of hagfish swimming may help identify where hagfishes are unique and where convergence in elongate form is accompanied by convergence in behavior and function.

This paper aims to broaden our current understanding of locomotory behavior in hagfishes by (1) quantifying whole-body kinematics of steady undulatory swimming in *E. stoutii* and *M. glutinosa,* two representative species from the main lineages within Myxinidae (Fernholm, 1998); (2) comparing specific waveform characteristics in hagfish to published data

from other elongate, anguilliform swimmers; and (3) proposing several mechanistic hypotheses on how hagfishes modulate their swimming speed during routine locomotion.

Materials and Methods

Experimental animals

Pacific hagfish (*Eptatretus stoutii*, Lockington) were collected from Barkley Sound, British Columbia, with assistance from the Bamfield Marine Sciences Centre. Atlantic hagfish (*Myxine glutinosa*, Linnaeus) were collected from the Huntsman Science Centre in St. Andrews, New Brunswick, Canada. At both locations, hagfish were caught using baited traps. The animals were housed in a recirculating artificial seawater tank (8 – 9°C, 35 ‰) at a Harvard University aquarium facility, and were maintained on a 12:12 hour light:dark cycle and fed frozen squid monthly. Swimming behavior was recorded from four Atlantic hagfish ranging from 26.0 – 30.9 cm in body length (BL) (mean BL ± standard deviation., 28.5 ± 2.0 cm) and four Pacific hagfish ranging from 26.1 – 30.3 cm BL (mean BL ± standard deviation., 28.4 ± 2.1 cm). All procedures and experiments adhered to Harvard University animal care guidelines (protocol # 20-03).

Filming and kinematic analysis of hagfish swimming

Video recordings of steady undulatory swimming were obtained from individual hagfish swimming in a recirculating flow tank filled with artificial seawater (9°C, 35 ‰). The working section of the flow tank where hagfish could swim was 84 x 28 x 28 cm. As the speed of water flow in the tank was slowly increased from zero, hagfish were encouraged to swim by gently prodding the underside of the caudal end. Flow tank speed was adjusted until hagfish appeared to be swimming steadily; steady swimming was defined and later verified as less than a 10%

change in center of mass (COM) velocity over a complete tail beat (see below for COM measurement procedure). Because steady swimming sequences sufficiently far from tank walls were rare, I could not impose specific swim speeds on individual hagfish. The range of speeds at which *M. glutinosa* voluntarily swam was 9.5 to 21.3 cm/s (0.33 to 0.69 BL/s), while *E. stoutii* swam from 13.6 to 26.0 cm/s (0.52 to 0.86 BL/s); however, the difference in mean swim speed between the two species was not significant (Student's t-test, $t = -1.8$, $p = 0.10$). *M. glutinosa* tended to swim near the surface of the water, while *E. stoutii* tended to swim at the bottom of the tank. Previous studies using the same flow tank at flow speeds comparable to the lowest swim speed observed in this study found that the thickness of the boundary layer at the tank's solid surfaces was approximately 0.2 – 0.7 cm (Carlson and Lauder, 2011; Tytell and Lauder, 2004); because these values are an order of magnitude lower than the typical depth of a hagfish body, and because the boundary layer thins as flow speed increases (Schlichting, 1979), it was assumed that boundary layer flows had a negligible effect on swimming. Ventral views of swimming hagfish (Figure 1.1) were filmed at a rate of 500 frames/s using a Photron PCI1024 Fastcam high-speed video camera (1024 x 1024 pixels, San Francisco, CA) aimed at a 45 degree-angled mirror below the flow tank.

Swimming sequences that were further analyzed consisted of 2 to 5 complete tail beat cycles per individual hagfish. A custom Matlab (R2011a, The Mathworks Inc., Natick, MA) program was used to record two-dimensional (x, y) coordinates of hagfish body position from the video images. Because hagfish body movements tended to be slow, analysis was performed on a subset of video images down-sampled to 25 frames/s. For each video image, ten to 15 manually-digitized points along the midline of the hagfish body were fit with a cubic spline to

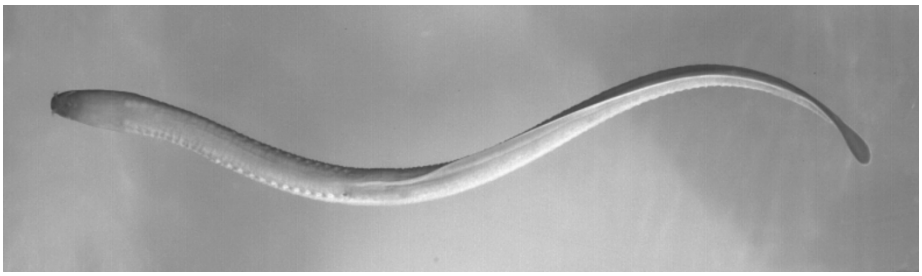

Figure 1.1. Ventral view image from a video recording of steady swimming in a Pacific hagfish, *Eptatretus stoutii*. This individual is 26 cm-long and is swimming at 0.68 BL/s toward the left of the image.

generate an interpolated and smoothed line consisting of 200 equally-spaced data points and representing the body midline for that instant in the tail beat cycle. At each hagfish swim speed (independent variable), kinematic variables were calculated from these smoothed midline coordinate data using custom Matlab routines.

Tail beat amplitude (TBA) was calculated as half the distance covered by the caudal tip between maximum lateral excursions within a tail beat cycle. Tail beat frequency (TBF) was calculated as the inverse of the period of one tail beat cycle. Tail tip speed was the total lateral distance travelled by the caudal tip over a whole tail beat divided by the tail beat period. Strouhal number (*St*), a dimensionless index that relates propulsor flapping behavior to the body's forward velocity, was calculated as the product between $2 \cdot$TBA and TBF, divided by forward swim speed (Triantafyllou et al., 1993; Vogel, 2003). As such, tail beat behavior that results in faster forward swim speeds is associated with lower *St* values and higher locomotor efficiency.

To examine the kinematics of the undulatory wave along the length of the hagfish body, the body was divided into 5 segments (20% BL increments) and the following variables were computed within and then averaged over each segment: undulatory amplitude along the body was calculated in a similar way as TBA, except that the points of interest were body midline points; undulatory wave frequency was calculated using the formula for TBF applied to body midline points; undulatory wave speed was determined by measuring the distance a wave crest travelled between consecutive video frames and dividing by the frame interval; and wavelength was computed as wave speed divided by wave frequency. Wave speed was subsequently averaged over the entire hagfish body and used to calculate slip, a measure of the efficiency of a propulsive wave given by the ratio between the body's forward swim speed and the rearward wave speed (Lighthill, 1970; Shadwick and Gemballa, 2006).

All measurements were averaged over multiple tail beats to provide a more reliable estimate of the kinematic quantity, and when appropriate, divided by body length to normalize the data. Additional variables that were calculated to characterize and compare hagfish swimming patterns included COM velocity and Reynolds (*Re*) number. The average position of the COM on a hagfish was approximately 0.4 BL, determined by placing a fully extended dead hagfish on a rigid beam, and balancing the beam on a fulcrum (Westneat et al., 1998). COM velocity was then calculated in the direction of travel to confirm steady swimming behavior. Reynolds number, a dimensionless index that characterizes the general fluid flow regime, was calculated as the product between fluid density, hagfish body length, and forward swim speed, divided by the dynamic viscosity of the fluid (Vogel, 2003).

Statistical analysis

Kinematic data were $\log_{10}$ transformed prior to statistical analysis. An analysis of covariance (ANCOVA) tested for the effects of species, swim speed, and the interaction between species and speed on kinematic variables with one measure per individual: TBA, TBF, tail tip speed, *St*, and slip. Because individual hagfish swam at voluntary speeds and not prescribed speeds, swimming speed was treated as a continuous covariate. ANCOVA assumes a linear relationship between the dependent variable and covariate (Sokal and Rohlf, 1981), and existing literature on steady undulatory fish swimming has provided evidence that kinematic values can vary linearly with swim speed, depending on the species (e.g. Gillis, 1998; Long et al., 2002). *Post-hoc* Spearman's non-parametric correlation tests were performed on single-measure kinematics with significant swim speed or interaction effects. A multivariate analysis of covariance (MANCOVA) was performed on kinematics that were calculated along the hagfish body

(undulatory amplitude, wave frequency, wave speed, and wavelength), treating longitudinal position (LP) along the body as a repeated measure. Between-individual effects were species, swim speed, and species x swim speed, while within-individual effects were longitudinal position, and interactions between LP, species, and swim speed. To help illustrate patterns between kinematic measurements and these within-individual effects, an Ordinary Least Squares trend line was fit to kinematic data from each 0.2 BL-long body segment and plotted with the data; fits with a magnitude of the correlation coefficient $r > 0.9$ are represented by solid thick lines on the plots. Adjusted test statistics were used where appropriate to satisfy the assumptions of the MANCOVA. Only descriptive statistics were applied to *Re*. All statistical analyses were performed with JMP Pro 9 (SAS Institute, Inc., Cary, NC).

Results

General patterns in hagfish swimming

Both Pacific and Atlantic hagfish swam with large lateral head movements, passing an undulatory wave down the entire body as they swam forward at a range of swimming speeds (Figures 1.1, 1.2). Plotting midline drawings of the body as it would have appeared swimming forward in the water shows that successive parts of the body would occasionally follow a similar path of forward travel, or exhibit partial "path-following" behavior (Pace and Gibb, 2011) (Figure 1.2D, F, H). The speed of the hagfish body's COM tended to oscillate around a mean value, indicating small accelerations and decelerations that averaged to "steady" behavior over an entire tail beat (Figure 1.3). For the swimming speeds observed in this study, the average *Re* for both species of hagfish was approximately 38,000.

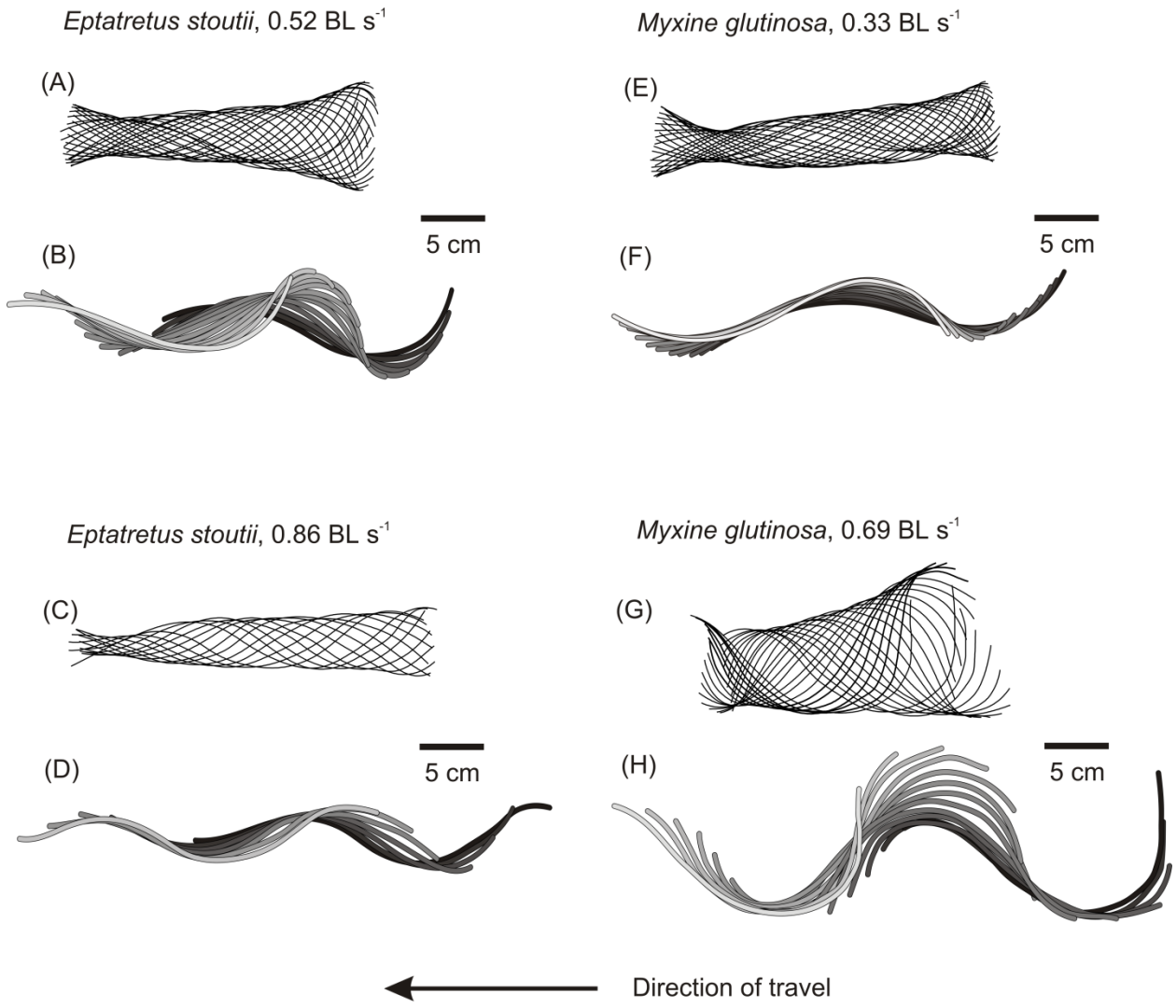

Figure 1.2. Ventral body midline tracings from (A-D) Pacific (*Eptatretus stoutii*) and (E-H) Atlantic (*Myxine glutinosa*) hagfish swimming at a range of speeds illustrate whole-body undulatory waves and large lateral head movements during steady swimming. A complete tail beat cycle is shown in each drawing, with each midline representing an instant in time. (A, C, E, G) Overlapping midlines are each separated by 0.04 seconds. (B, D, F, H) Midlines moving in the direction of travel illustrate that hagfish can exhibit partial path-following behavior. Progressing midlines are each separated by 0.08 seconds and line shading becomes lighter as time passes. All scale bars are 5 cm.

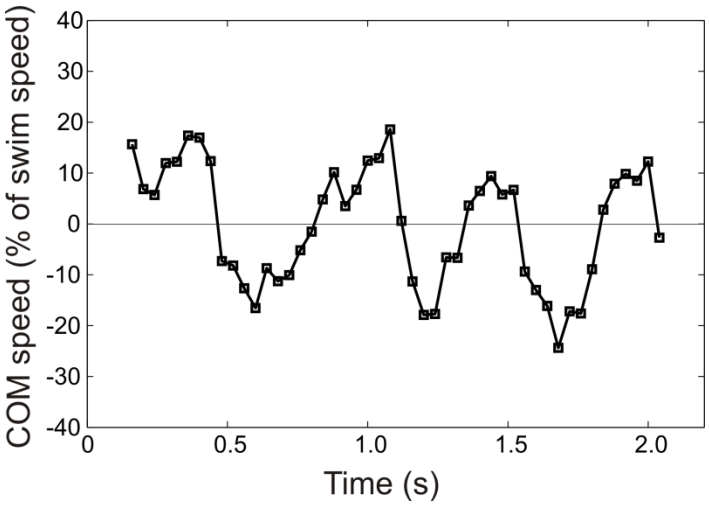

Figure 1.3. Representative plot for speed of a hagfish body's center of mass in the axial direction, showing small oscillations in COM speed around a mean "steady" value over the course of two consecutive tail beats. The hagfish is *E. stoutii*, swimming at 0.52 BL/s.

Kinematics of hagfish swimming

Tail beat amplitude (TBA) was typically less than 0.15 BL in both *E. stoutii* and *M. glutinosa* (Figure 1.4A, but see Figure 1.2G, H for an outlier). A significant species x swim speed interaction effect indicated that the two species differed in how TBA changed with swim speed. *Post-hoc* correlation tests showed that, within the range of swim speeds each species achieved, TBA in *M. glutinosa* exhibited a significant positive correlation with speed, while TBA in *E. stoutii* exhibited a significant negative correlation with speed (Figure 1.4A; Table 1.1). Undulatory amplitude along the body also showed a significant species x swim speed interaction effect, and a borderline significant species effect between individual hagfish (Table 1.1). Within individual hagfish, longitudinal position along the body had a significant effect on undulatory amplitude, which showed a characteristic pattern of large amplitude at the rostral tip (>50% of amplitude at the tail tip) decreasing to a minimum at 0.2 – 0.4 BL before steadily growing toward the tail (Figure 1.5A, B). However, the two species differed in how amplitude varied with swim speed along the body (Figure 1.5C, D), as a significant LP x species x swim speed interaction effect was also present. Echoing the observed relationships between TBA and swim speed reported above, in *E. stoutii* undulatory amplitude generally decreased with swim speed (most prominently for the last 40% of the body, Figure 1.5C), while in *M. glutinosa* amplitude generally increased with swim speed (Figure 1.5D).

Tail beat frequency (TBF) varied significantly with swim speed only, ranging from 0.87 to 2.08 Hz and showing a positive linear correlation with speed for combined data from both species (Figure 1.4B; Table 1.1). Similarly, undulatory wave frequency showed only a significant swim speed effect between individuals, with no effects due to species, longitudinal position along the body, or any interactions (Table 1.1). Tail tip speed, which is proportional to

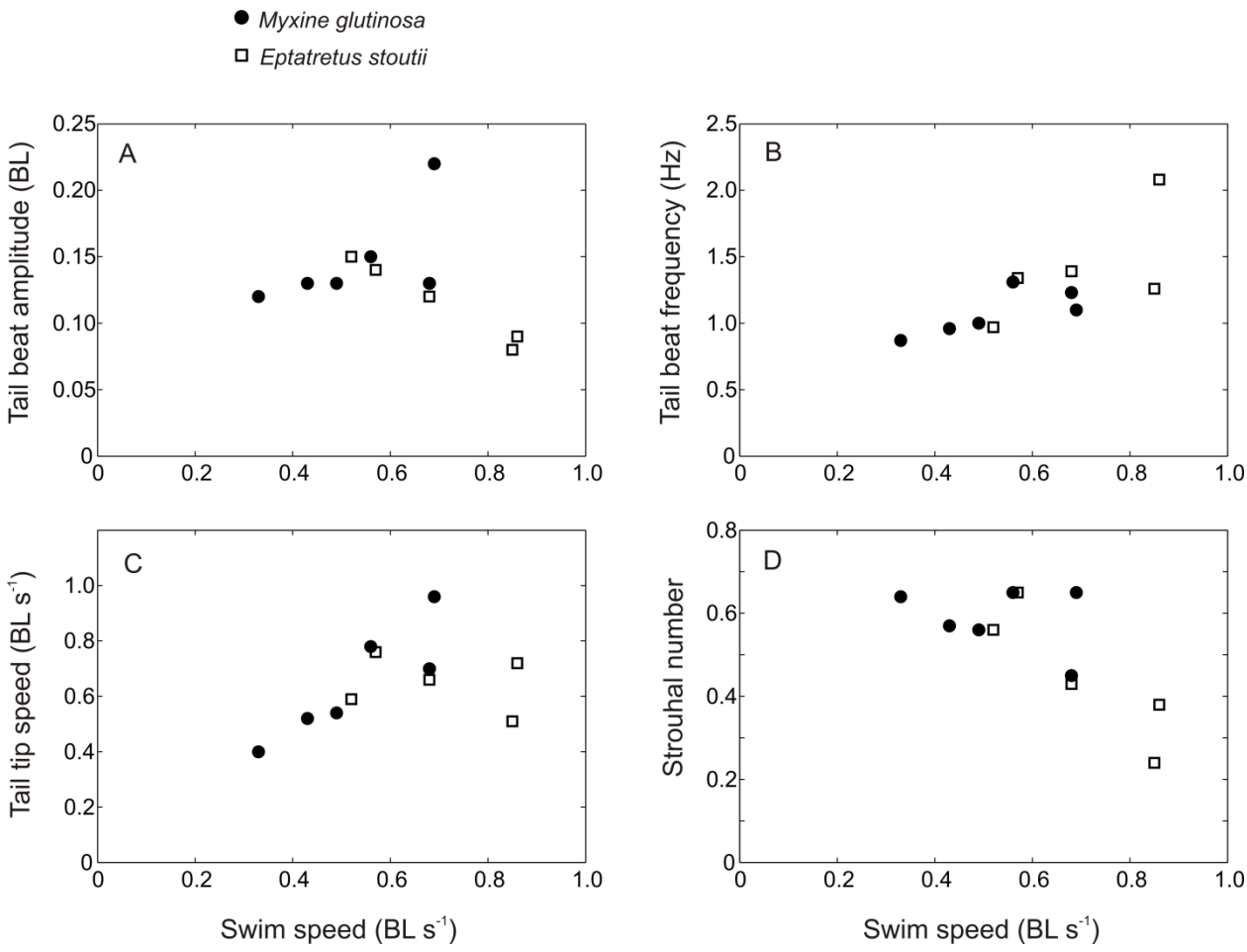

Figure 1.4. Relationship between tail tip kinematics and Strouhal number with swim speed in *E. stoutii* (open squares) and *M. glutinosa* (filled circles). (A) Tail beat amplitude increases with swim speed in *M. glutinosa* but decreases in *E. stoutii* (see Table 1.1 for statistical results). (B) Combined tail beat frequencies from both species of hagfish increase with swim speed. (C) Tail tip speed increases in *M. glutinosa*, but is independent of swim speed in *E. stoutii*. (D) Strouhal number tends to decrease with increasing swim speed for both species of hagfish, though the more conservative, non-parametric Spearman's correlation test did not find a statistically significant trend (see Table 1.1).

Table 1.1. ANCOVA and MANCOVA results for kinematic measurements on steady swimming *E. stoutii* and *M. glutinosa.*

Kinematic variable with single measure	ANCOVA: Effect tests						Post-hoc correlation tests					
	Species		Swim speed		Species x Swim speed		Overall correlation with swim speed		Species-specific correlation with swim speed			
									Myxine		*Eptatretus*	
	F ratio	*p*	*F* ratio	*p*	*F* ratio	*p*	Spearman's ρ	*p*	Spearman's ρ	*p*	Spearman's ρ	*p*
Tail beat amplitude (BL)	2.24	0.178	0.05	0.831	11.01	**0.013**	n/a		0.82	**0.046**	-0.90	**0.037**
Tail beat frequency (Hz)	0.35	0.574	6.68	**0.036**	0.39	0.554	0.76	**0.007**	n/a		n/a	
Tail tip speed (BL/s)	1.09	0.332	5.83	**0.046**	9.17	**0.019**	n/a		0.94	**0.005**	0	1
Strouhal number	0.47	0.514	8.39	**0.023**	4.15	0.081	-0.47	0.145	n/a		n/a	
Slip (propeller efficiency)	0.23	0.647	17.73	**0.004**	1.43	0.270	0.89	**<0.001**	n/a		n/a	

Kinematic variable with repeated measures along the body	MANCOVA: Between-individuals effect tests						MANCOVA: Within-individuals effect tests							
	Species		Swim speed		Species x Swim speed		Longitudinal position (LP)		LP x Species		LP x Swim speed		LP x Species x Swim speed	
	F ratio	*p*	*F* ratio	*p*	*F* ratio	*p*	*F* ratio	*p*	*F* ratio	*p*	*F* ratio	*p*	*F* ratio	*p*
Undulatory amplitude (BL)	5.62	**0.049**	0.07	0.800	10.67	**0.014**	10.77	**<0.001**	0.65	0.591	0.40	0.749	6.21	**0.004**
Undulatory wave frequency (Hz)	0.69	0.432	10.94	**0.013**	3.88	0.089	0.43	0.787	0.35	0.843	0.39	0.816	1.11	0.370
Undulatory wave speed (BL/s)	0.77	0.413	1.19	0.317	1.45	0.275	7.00	**<0.001**	2.98	**0.039**	5.63	**0.002**	1.28	0.305
Undulatory wavelength (BL)	0.10	0.764	9.05	**0.024**	0.57	0.479	7.04	**<0.001**	3.04	**0.037**	5.64	**0.002**	1.33	0.287

p- values in bold denote significance at the alpha = 0.05 level

Within-individual MANCOVA F tests use adjusted univariate H-F values

Random effects tests indicated that individual had no effect on any variables

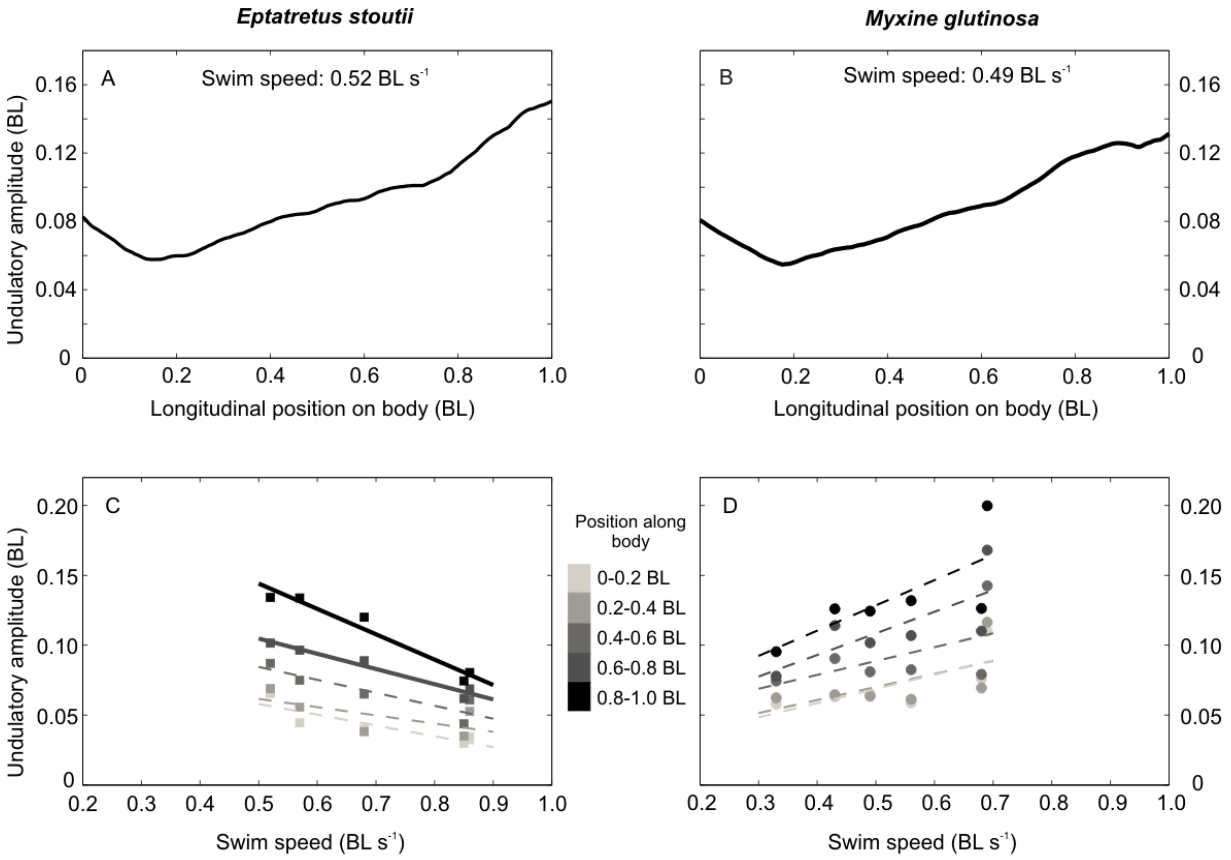

Figure 1.5. Undulatory amplitude along the body in representative swimming sequences from (A) *E. stoutii* and (B) *M. glutinosa.* The rostral tip is at 0 BL and the caudal tip is at 1.0 BL. The minimum in amplitude just posterior to the head is characteristic of both species of hagfish. (C, D) Undulatory amplitude as a function of swim speed, averaged within 0.20 BL-long segments of the body, shows that (C) *E. stoutii* and (D) *M. glutinosa* differed in how amplitude varied with swim speed along the body. Darker shades correspond to more caudal positions along the body. Trend lines are Ordinary Least Squares fits, where solid thick lines represent correlation coefficient magnitudes $r > 0.9$ and dashed lines represent coefficient magnitudes of $r < 0.9$.

the product of TBA and TBF, varied significantly with swim speed for only *M. glutinosa*; as swim speed increased, tail tip speed also increased (Figure 1.4C; Table 1.1). Strouhal number (*St)* ranged from 0.24 to 0.65, with the ANCOVA identifying swim speed as a significant effect (Table 1.1). While *St* did tend to decrease with increasing swim speed (Figure 1.4D), the more conservative non-parametric correlation test did not suggest a significant linear relationship between *St* and swim speed (Table 1.1).

The rearward speed of the undulatory wave was not constant along the length of a hagfish's body at a given swim speed (Figure 1.6), in one instance ranging between 0.5 and 1.4 BL/s within an individual hagfish (Figure 1.6A). The pattern of variation along the body was also generally quite variable across swim speeds. MANCOVA revealed that longitudinal position (LP), LP x species, and LP x swim speed all had significant effects on wave speed within individuals (Table 1.1), indicating that wave speed varied along the body differently for the two species of hagfish (Figure 1.6A, B), and also varied with swim speed differently for different segments of the body (Figure 1.6C, D). Wave speed tended to increase with swim speed for the caudal portion of the body in *E. stoutii* (Figure 1.6C) and for the mid-body in *M. glutinosa* (Figure 1.6D). None of the effects tests were significant for between-subjects comparisons of wave speed (Table 1.1). Slip, the ratio between average forward swimming speed and average rearward wave speed, showed a significant positive correlation with swim speed (Table 1.1). These average slip values increased from 0.41 to 0.97 with increasing swim speed (Figure 1.7), but local values of slip calculated along the body sometimes exceeded 1.0 (Figure 1.6C, D, data points below unity line), indicating that the undulatory wave was travelling slower than the forward-moving body at these regions.

Undulatory wavelength was also variable along the hagfish body and across swim speeds,

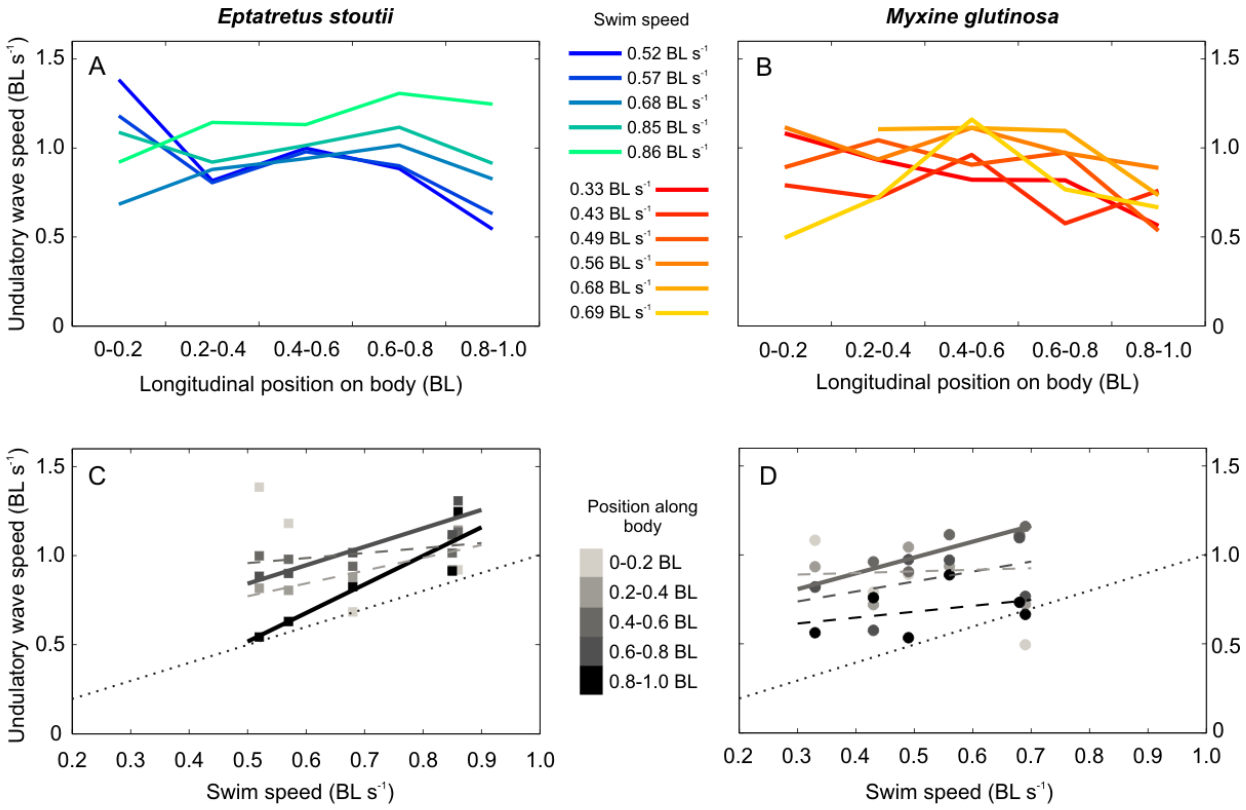

Figure 1.6. Undulatory wave speed as a function of position along the body and swim speed in (A, C) *E. stoutii* and (B, D) *M. glutinosa*. (A, B) Wave speed varies along the body differently for the two species of hagfish. Lighter colors correspond to faster swim speeds. (C, D) Wave speed also varies with swim speed differently for different segments of the body. Darker shades correspond to more caudal positions along the body. Trend lines are Ordinary Least Squares fits, where solid thick lines represent correlation coefficient magnitudes $r > 0.9$ and dashed lines represent coefficient magnitudes of $r < 0.9$. The single dotted line represents unity between wave speed and swim speed. For points below this line, the rearward undulatory wave is travelling slower than the forward moving body.

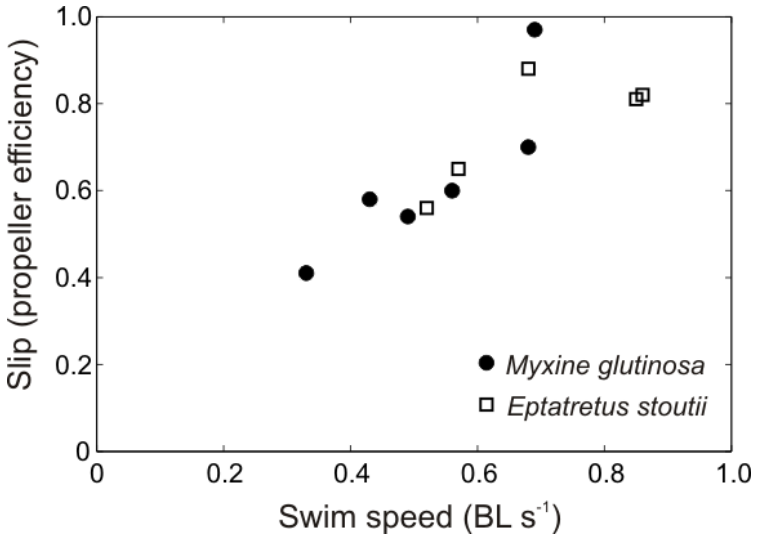

Figure 1.7. Slip (the ratio between forward swim speed and average rearward undulatory wave speed) increases with swim speed in both species of hagfish. The linear relationship reflects that wave speed averaged over the entire body takes a value near 1.0 BL/s and does not vary significantly with swim speed (see Table 1.1).

ranging from 0.4 (more than one complete wave on the body) to 1.4 BL (less than one complete wave on the body) (Figure 1.8). The factors that significantly affected wavelength were a combination of those that affected wave frequency and wave speed (Table 1.1), in part likely reflecting the dependency of wavelength calculations on both variables. Among individual hagfish, wavelength was significantly influenced by swim speed only, with its average over the entire body tending to decrease with increasing swim speed (Spearman's $\rho = -0.71$, $p = 0.015$, not shown on graph). Within individuals, wavelength was significantly influenced by LP, LP x species (Figure 1.8A *vs*. 1.8B), and LP x swim speed (Figure 1.8C, D).

Discussion

In this paper I quantified the kinematics of the body undulatory wave during steady swimming in two species of hagfish, *Eptatretus stoutii* and *Myxine glutinosa*, representing the two main lineages of hagfishes. I examined how kinematic variables change over a range of swim speeds and along the bodies of individual hagfish. Hagfish swam at a range of voluntary speeds, and while Pacific hagfish (*E. stoutii*) tended to swim faster on average than Atlantic hagfish (*M. glutinosa*), the difference in average swim speed was not statistically significant. Furthermore, *M. glutinosa* have been previously recorded swimming through a still-water tank at speeds beyond the range observed here (Long et al., 2002). Under the present study's experimental conditions, the higher swimming speeds achieved by *E. stoutii* may reflect eptatretids's more aerobic lifestyle when compared to the burrowing specialist myxinids (Forster, 1990); however, because few clear kinematic patterns emerged to distinguish between species, and because kinematics among individual hagfish were often highly variable, here I will refer to hagfishes altogether as a unique group within anguilliform swimmers. I focus on how trends in hagfish

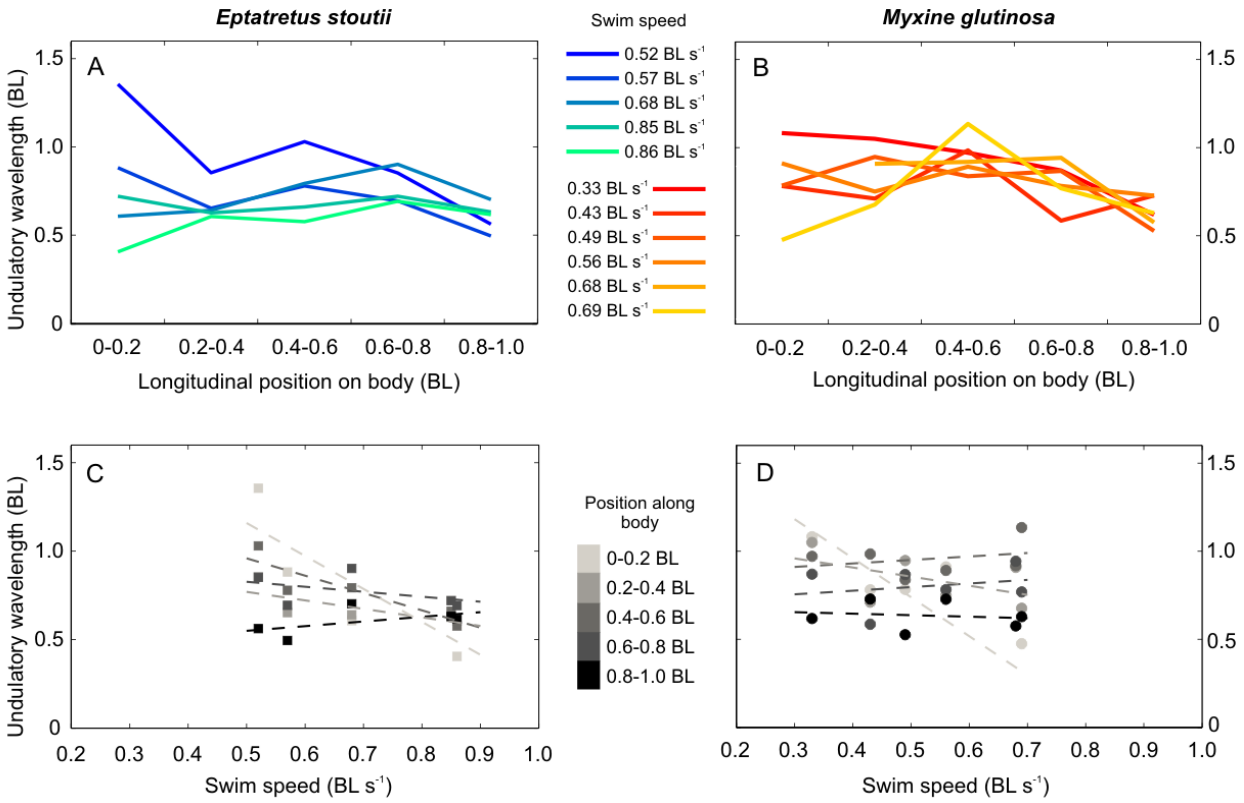

Figure 1.8. Undulatory wavelength as a function of position along the body and swim speed in (A, C) *E. stoutii* and (B, D) *M. glutinosa*. (A, B) Wavelength varies along the body differently for the two species of hagfish. Lighter colors correspond to faster swim speeds. (C, D) Wavelength also varies with swim speed differently for different segments of the body. Darker shades correspond to more caudal positions along the body. Trend lines are Ordinary Least Squares fits, where dashed lines represent a correlation coefficient magnitude of $r < 0.9$.

steady swimming kinematics compare to those in other animals that locomote with body undulations, and then propose several mechanistic scenarios that begin to address the diversity seen in hagfish locomotor patterns and abilities.

Hagfish swim with large body waves

When observing the overall appearance of steady swimming in hagfishes, the most striking feature one notices is the relatively large side-to-side swaying of the head, which initiates the large amplitude, whole-body undulatory wave that travels down the body as a hagfish swims forward (Figure 1.2). This pattern corresponds well with the original description of the anguilliform swimming mode made by Breder (Breder, 1926); interestingly, it contrasts with eels (*Anguilla rostrata*), the exemplars of anguilliform swimming, where at comparable swimming speeds the head yaws very little and undulatory waves start further along the body (Gillis, 1998; Lauder and Tytell, 2006; Tytell, 2004a). The general pattern of body midlines observed in this study is consistent with body waveform descriptions from previous work on swimming hagfish (Adam, 1960; Campbell, 1940; Long et al., 2002; Long et al., 2010), as well as other more flexible and elongate swimmers (lamprey (Root et al., 2007; Williams et al., 1995); leeches swimming with dorso-ventral undulations (Chen et al., 2011)). In hagfish, it is possible that these large head oscillations are a consequence of the body's mechanical properties or motor program constraints, though they may serve a function in surveying water in front of the animal during searches for prey, in concert with touch-sensitive barbels and a single nostril at the snout (Jensen, 1966).

Kinematics of the body wave in hagfishes and other undulating swimmers

Both *E. stoutii* and *M. glutinosa* increase the frequency of their body undulations as they swim faster. The linear relationship between tail beat frequency and swim speed (Figure 1.4B) has previously been reported for *M. glutinosa* (Long et al., 2002), and is well-documented in other anguilliform swimmers including American eels (Gillis, 1998; Tytell, 2004a), salamanders (Gillis, 1997), and swimming snakes (Jayne, 1985; Munk, 2008). But is altering undulation frequency the main way for a hagfish to change its swimming speed? If the correlation between tail beat frequency and swim speed is high, we might expect little change in other kinematic variables. However, the relationship between swimming speed and body waveform characteristics may be more complex for highly flexible undulatory swimmers like hagfishes and lamprey, which retain notochords and lack fully developed vertebrae even as adults; other variables may modulate speed in addition to — and sometimes rather than — wave frequency (Long, 1995). Indeed, the correlation between frequency and swim speed observed here was not particularly high, and as discussed below, other waveform quantities varied considerably with swim speed and along the hagfish body. Wave frequency was the only variable that was constant along the body in hagfish, but varying frequencies have been found in the notochord-bearing lamprey (Root et al., 2007).

At a given swim speed, undulatory amplitude changed with longitudinal position along the body in a similar fashion for both hagfish species: amplitude reached a minimum just posterior to the head and then steadily grew toward the tail (Figure 1.5A, B). This pattern of increasing amplitude occurs in a diversity of undulating swimmers (e.g. salamanders (Gillis, 1997), eels (Gillis, 1998), garter snakes (Munk, 2008), ropefish (Pace and Gibb, 2011)). Interestingly, as hagfish increased swim speed over their respective ranges, amplitude along the

body and at the tail tip were the only variables that obviously varied between the two species (Figures 1.4A, 1.5C, D). As hagfishes swam faster, amplitude in *M. glutinosa* increased, while amplitude in *E. stoutii* decreased. These relationships appeared to be strongest at the tail, especially for *E. stoutii* (Figure 1.5C). In contrast to the present findings, Long et al. (Long et al., 2002) reported decreasing tail beat amplitude in *M. glutinosa* swimming from 0.4 to 1.0 BL/s. The present study's dataset does include an individual *M. glutinosa* that swam with particularly large body undulations and likely skewed the average for *Myxine* upward; but even excluding this outlier, the *M. glutinosa* in this study show no apparent decrease in TBA as they swim faster. These contrasting findings reinforce the idea that in very flexible-bodied swimmers, kinematic parameters can influence swim speed in variable and interrelated ways (Long, 1995). Magnitudes of amplitude and how they change with swim speed appear to vary among anguilliform swimmers in general. Hagfishes, swimming snakes (Jayne, 1985), and elongate salamanders (Gillis, 1996) tend to beat their tails with amplitudes higher than those typical of other undulatory swimmers (approximately 0.09 BL) (Videler, 1993). American eels swimming in water have a TBA of 0.08 BL, but eels undulating on land during short terrestrial bouts alter their kinematics and also move with a larger TBA (Gillis, 1998). As salamanders and eels swim faster, they tend to keep TBA constant and instead increase undulatory amplitude along other parts of the body or recruit more anterior regions (Gillis, 1997; Gillis, 1998). Hagfish employ whole-body undulations even for slow speeds within their range, but as they swim faster they do appear to modulate amplitude all along the body and not only at the tail (Figure 1.5C, D). The increasing undulatory amplitudes and tail tip speed with swim speed in *M. glutinosa* (Figure 1.4C) can lead to higher energetic costs (D'Août and Aerts, 1999; Root et al., 1999; Tytell, 2004a), but one needs to know the muscle activity associated with these kinematics to determine whether costs of

swimming differ among species (Jayne, 1985).

The speed of the undulatory wave varied along the length of the hagfish body, though not in a consistent manner within or between species (Figure 1.6A, B). This highly variable pattern contrasts with previous findings that mechanical waves accelerate caudally (e.g. salamanders at high speeds (Gillis, 1997); swimming snakes (Jayne, 1985; Munk, 2008)) or are constant along the body (e.g. eels (Gillis, 1998); salamanders at low speeds (Gillis, 1997)). Variability in wave speed seems to appear also in lamprey, however, as both changing (Root et al., 2007) and constant wave speeds (Williams et al., 1989) along the body have been reported in previous work. Faster body wave speeds are commonly correlated with faster swim speeds in anguilliform swimmers (Gillis, 1997; Gillis, 1998; Tytell, 2004b), but how wave speed contributes to swim speed in hagfishes is not obvious. Average wave speed over the entire body does not change with swim speed, but a positive correlation between wave speed and swim speed does occur at particular regions of the hagfish body: at the caudal portions of *E. stoutii* (Figure 1.6C), and the mid-body in *M. glutinosa* (Figure 1.6D). Because of the inverse relationship between wavelength and wave frequency given a constant average wave speed, average wavelength over the whole body decreased as swim speed increased. The anterior regions of the hagfish body seemed to drive this trend, though, as more posterior regions tended to have relatively short and constant wavelengths over increasing swim speeds (Figure 1.8C, D). We again see an array of relationships between wavelength, body position, and swim speed among other elongate swimmers. Like hagfish, swimming lamprey can display shorter wavelengths closer to the tail (Root et al., 2007); but water snakes (Jayne, 1985), garter snakes (Munk, 2008), and ropefish (Pace and Gibb, 2011) swim with longer wavelengths near the tail. Yet the water snake *Nerodia f. pictiventris* studied by Jayne (Jayne, 1985) shares with hagfish the inverse correlation between

undulatory wavelength and swim speed. Burrowing specialist and non-specialist eels (*Heteroconger hassi* and *Pisodonophis boro*, respectively) swim with wavelengths that are independent of swim speed (Herrel et al., 2011), as do aquatic salamanders (Gillis, 1997).

The functional implications of changing wave speed and wavelength are discussed further below, but it is unknown whether these changes are passive or active. Frequency-dependent changes in internal dynamics (i.e. notochord behavior, (Long et al., 2002)) or external dynamics (i.e. hydrodynamic load) can passively influence emergent kinematics in swimming fish (Tytell et al., 2010). But varying patterns in the wave of muscle activation down the body can also produce different wave speeds (Gillis, 1996), and mechanical waves can be initiated nearly anywhere along the hagfish body (Campbell, 1940), suggesting that precise control is possible. Root et al. (Root et al., 2007) propose that steadiness in swimming is actually a result of actively reducing unsteady body movements that can be energetically expensive; fluctuations in wave kinematics along the body reflect localized unsteadiness where parts of the body are accelerating and decelerating over the course of a tail beat. This local unsteady behavior may be related to the small oscillations in speed measured at the hagfish body's center of mass (Figure 1.3), which have also been observed in garter snakes that swim with body undulations (*Thamnophis sirtalis* (Munk, 2008)). One important issue that the current data conclusively support is the need for multiple kinematic measurements along the length of a swimming body. Studies on animal undulatory swimming commonly assume that wave speed and wavelength are constant along the body, but the hagfish in the present study demonstrate that the body wave can be quite variable.

This is not to say that hagfishes are inherently inefficient swimmers, however. Strouhal number (*St*) and slip (the ratio between swim speed and undulatory wave speed) are regularly

applied to swimming animals as simplified indices of efficiency, and both suggest that hagfishes can swim with greater efficiency at higher speeds. Heaving aero- and hydrofoils peak in thrust efficiency between *St* values of 0.25 – 0.35 (Triantafyllou et al., 1993); many swimming or flying animals maintain Strouhal numbers within or near this so-called optimal range (Taylor et al., 2003), including American eels (Tytell, 2004a) and *E. stoutii* swimming at the fastest speeds achieved in this study (Figure 1.4D). Strouhal numbers are as high as 0.65, though, at slower swim speeds in both *M. glutinosa* and *E. stoutii*. Comparably high *St* values have also been measured for slow-swimming Pacific salmon (Lauder and Tytell, 2006). Slip values similarly suggested lower efficiency of the hagfish undulatory wave at slow speeds, but perhaps more interesting were slip values nearing unity at faster swim speeds (Figure 1.7). Rearward-travelling body waves push on the water to propel an animal forward; but water is deformable, so not all of the backward wave speed is translated into forward swim speed (Shadwick and Gemballa, 2006). Increasing concordance between wave speed and swim speed (slip approaching 1) increases mechanical wave efficiency, reduces thrust power requirements (Webb et al., 1984; Wu, 1977), and reflects an increase in path-following by trailing regions of the undulating body (e.g. Figure 1.2H) (Gillis, 1998; Maladen et al., 2009; Pace and Gibb, 2011). Increasing slip with swim speed also occurs in salamanders (Gillis, 1997), and eels are among other undulating swimmers that can similarly operate at relatively high slip values ((Gillis, 1998), and see Videler for a review (Videler and Hess, 1984)). Surprisingly, slip actually exceeded 1 for some regions of the body in the fastest swimming *M. glutinosa* (Figure 1.6D, data points below line of unity), again signifying that parts of the body were decelerating and not contributing to forward propulsion (Jayne, 1985; Müller et al., 2002).

Mechanistic hypotheses on hagfish steady swimming

Taking into account this diversity in how waveform kinematics relate to steady swimming speed, both within and between hagfish species, I propose three mechanistic scenarios (Figure 1.9) that could explain how hagfish increase swimming speed and achieve greater efficiencies at higher speeds. Here, I aim to sort through some of the kinematic variability and interpret the emerging patterns in form and motion with respect to locomotory function. I focus on the potential for mechanical tuning in swimming behavior, which predicts that a body's movements and mechanical properties can adjust and interact to enhance performance or reduce the cost of locomotion (Alexander, 1988; Blight, 1977; Daniel and Tu, 1999; Long and Nipper, 1996). The scenarios are based on the present experimental results, account for increasing levels of variability, and are not mutually exclusive given the variation in kinematics one sees within hagfishes.

First (Figure 1.9A), hagfishes could simply increase whole-body undulation frequency to swim faster (Figure 1.4B). The speed of the undulatory wave down the body does not change with swim speed, but the average wavelength shortens (Table 1.1). This tendency for wavelength to shorten with increasing frequency is the result of the constant body wave speed, which can arise, according to mechanical theory, if body stiffness remains constant during swimming (McHenry et al., 1995). Changes in undulatory amplitude could largely be consequences of changes in other linked kinematic variables, rather than actively modulated. Higher swimming efficiency at faster speeds follows from a greater proportion of power contributing to forward thrust rather than maintaining stability (Videler, 1993).

Second (Figure 1.9B), hagfishes could still increase undulation frequency to swim faster, but with caudal regions of the body contributing more to propulsion through altered kinematics

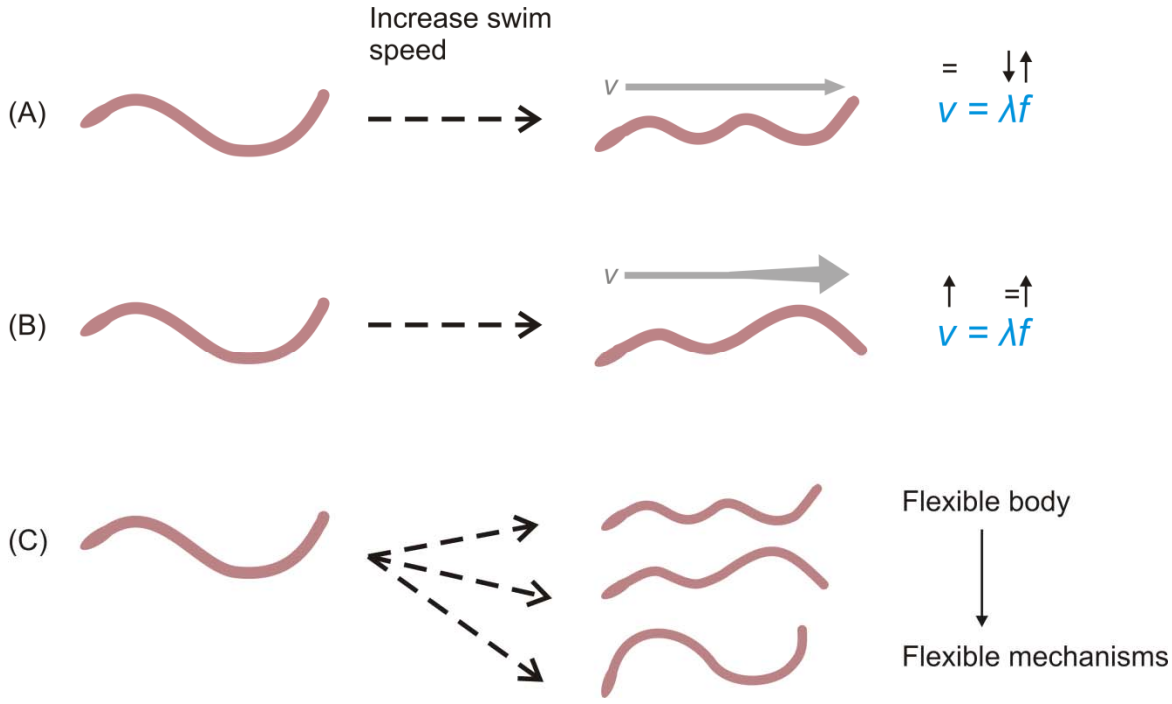

Figure 1.9. Schematic representation of mechanistic hypotheses on how hagfish alter their undulatory wave to increase steady swimming speed. v, undulatory wave speed; λ, undulatory wavelength; f, undulatory wave frequency. The black symbols above the blue formula indicate whether the variable in the formula remains constant (equal sign), increases (upward arrow), or decreases (downward arrow) with increasing swim speed.

and mechanics. The role of the tail in augmenting thrust production in undulating swimmers has been recognized before (Bainbridge, 1963; Jayne, 1985; Koob and Long, 2000; Lauder, 2000), and support for this hypothesis in hagfish comes from the present study's data on *E. stoutii*. The increase in undulatory wave speed at the caudal end adds to wake momentum and increases swim speed (Figure 1.6C). Wavelength is relatively independent of swim speed at the tail (Figure 1.8C), but tail beat amplitude decreases with faster swim speeds (Figure 1.4A). While a reduction in amplitude would tend to decrease thrust power (Wu, 1977), this effect may be mitigated by high swimming efficiencies at faster speeds (Figures 1.4D, 1.7) (Long et al., 2002).

The potential causes for these local differences in kinematics at the tail include altered muscle activation patterns (Gillis, 1996) and passive or active changes in the tail's mechanical properties that influence body wave propagation (Long and Nipper, 1996). Several workers have previously demonstrated the importance of propulsor stiffness in locomotion (Lauder et al., 2011; Long, 1998; Long and Nipper, 1996; McHenry et al., 1995), with some predicting that undulatory swimmers actively use muscle contractions to tune the mechanical properties of their bodies and achieve efficient swimming (Long, 1998; McHenry et al., 1995; Root et al., 1999). The patterns of kinematic variation seen at the tail in swimming *E. stoutii* are concordant with localized changes in body flexural stiffness. Wave speed, in particular, should increase with increasing stiffness, and this prediction based on wave theory is supported experimentally by work on longnose gar (Long et al., 1996) and physical fish models (McHenry et al., 1995). In hagfish, the presence of cartilaginous caudal fin rays may passively stiffen the tail relative to the rest of the body (Koob and Long, 2000), while over increasing swim speeds, the viscoelastic behavior of the notochord results in a stiffer body at higher bending frequencies (Long et al., 2002).

Third (Figure 1.9C), various kinematic and mechanical variables could interact non-linearly and/or in combination to modulate swimming speed in hagfishes. Within and between species, hagfish may be capable of achieving similar swim speeds through different mechanisms. For instance, the experimental data presented here for *M. glutinosa* do not obviously support the above "stiffened tail" hypothesis, as wave speed varies only slightly with swim speed in the caudal region (Figure 1.6D). Rather, it appears that *M. glutinosa* in this study tended to increase tail beat amplitude in concert with tail beat frequency to generate more propulsive thrust (Figure 1.4A) (Bainbridge, 1958; Bainbridge, 1963). It is unclear if and how body stiffness is influencing waveform kinematics here, especially considering that in one instance of high-speed swimming *M. glutinosa* appeared to be more flexible, with greater lateral bending and body wave amplitudes (Figure 1.2G, H); yet, in another individual at a similar speed and wave frequency, amplitudes along the body were noticeably smaller (Figures 1.4A, 1.5D). For the free-swimming *M. glutinosa* that Long and his colleagues (Long et al., 2002; Long et al., 2010) observed, the authors predicted that reductions in tail beat amplitude and body postural changes were consequences of increased body stiffness at faster swim speeds. Combining these distinct accounts of swimming behavior in *M. glutinosa* and *E. stoutii* offers support for the broadest scenario, which affords flexible-bodied swimmers a number of ways to gain speed (Long, 1995). This scenario is further supported by the hagfish's "contortionist" abilities that are not displayed during routine locomotion. The body is flexible enough to tie into a knot, but the knot can still be forcefully propagated in either direction to escape a predator's grasp or gain leverage while tearing chunks off large pieces of prey (Jensen, 1966).

Diversity of anguilliform locomotion

The results I present here complement previous work showing that a great deal of variability can exist within the anguilliform mode of swimming, and that what researchers refer to as "eel-like" actually encompasses a wide array of body shapes and motion patterns (Gillis, 1996; Gillis, 1997). Hagfishes converged on a generally anguilliform body shape and swimming pattern, but still have distinctive physiological, anatomical, and behavioral features that undoubtedly influence their routine locomotion.

Continued study of hagfish locomotion will contribute to our growing understanding of collective diversity in elongate animals and how they navigate their environments (Gillis, 1996; Herrel et al., 2011; Jayne, 1985). From the varying degrees of specificity in the mechanisms proposed above, it is clear that hagfishes can display a rich repertoire of body movements to attain steady swimming. But we have yet to fully understand the functional relationships that dictate how the hagfish's exceedingly flexible body modulates swim speed. Subsequent work that I anticipate will help explain the mechanics of hagfish swimming includes a study of passive kinematics in hagfish-like physical models actuated with a robotic device (Chapter 4); by comparing the emergent kinematics of a passive body with that of a live one, the influence of body stiffness on hagfish swimming may be revealed.

List of symbols and abbreviations

BL Body length

COM Center of mass

TBA Tail beat amplitude

TBF Tail beat frequency

St	Strouhal number
Re	Reynolds number
LP	Longitudinal position along the body
r	Linear coefficient of correlation
v	Undulatory wave speed
λ	Undulatory wavelength
f	Undulatory wave frequency

Acknowledgements

I am grateful to George Lauder, Erin Blevins, and other members of the Lauder Lab for helpful discussions about this work and manuscript, Douglas Fudge for collecting hagfish, and Chuck Witt for his Matlab expertise. Funding for this work was provided by NSF grant EFRI-0938043 to George Lauder, the Harvard University OEB Department, and an NSERC Canada Graduate Scholarship to Jeanette Lim.

References

Adam, H. (1960). Different types of body movement in the hagfish, *Myxine glutinosa* L. *Nature* **188**, 595-596.

Alexander, R. M. (1988). *Elastic Mechanisms in Animal Movement*. New York: Cambridge University Press.

Bainbridge, R. (1958). The speed of swimming of fish as related to size and to the frequency and amplitude of the tail beat. *J. Exp. Biol.* **35**, 109-133.

Bainbridge, R. (1963). Caudal fin and body movement in the propulsion of some fish. *J. Exp. Biol.* **40**, 23-56.

Bardack, D. (1991). First fossil hagfish (Myxinoidea): a record from the Pennsylvanian of Illinois. *Science* **254**, 701-703.

Blight, A. R. (1977). The muscular control of vertebrate swimming movements. *Biol. Rev.* **52**, 181-218.

Braun, C. B. and Northcutt, R. G. (1998). Cutaneous exteroreceptors and their innervation in hagfishes. In *The Biology of Hagfishes* (eds. J. M. Jørgensen, J. P. Lomholt, R. E. Weber and H. Malte), pp. 512-532. London: Chapman & Hall.

Breder, C. M. (1926). The locomotion of fishes. *Zoologica* **4**, 159-297.

Campbell, B. (1940). Integration of locomotor behavior patterns of the hagfish. *J. Neurophysiol.* **3**, 323-328.

Carlson, R. L. and Lauder, G. V. (2011). Escaping the flow: boundary layer use by the darter *Etheostoma tetrazonum* (Percidae) during benthic station holding. *J. Exp. Biol.* **214**, 1181-1193.

Chen, J., Friesen, W. O. and Iwasaki, T. (2011). Mechanisms underlying rhythmic locomotion: body-fluid interaction in undulatory swimming. *J. Exp. Biol.* **214**, 561-274.

D'Août, K. and Aerts, P. (1999). A kinematic comparison of forward and backward swimming in the eel *Anguilla anguilla*. *J. Exp. Biol.* **202**, 1511-1521.

Daniel, T. L. and Tu, M. S. (1999). Animal movement, mechanical tuning and coupled systems. *J. Exp. Biol.* **202**, 3415-3421.

Fernholm, B. (1998). Hagfish systematics. In *The Biology of Hagfishes* (eds. J. M. Jørgensen, J. P. Lomholt, R. E. Weber and H. Malte), pp. 33-44. London: Chapman & Hall.

Forster, M. E. (1990). Confirmation of the low metabolic rate of hagfish. *Comp. Biochem. Physiol. A* **96**, 113-116.

Gillis, G. B. (1996). Undulatory locomotion in elongate aquatic vertebrates: Anguilliform swimming since Sir James Gray. *Amer. Zool.* **36**, 656-665.

Gillis, G. B. (1997). Anguilliform locomotion in an elongate salamander (*Siren intermedia*): effects of speed on axial undulatory movements. *J. Exp. Biol.* **200**, 767-784.

Gillis, G. B. (1998). Environmental effects on undulatory locomotion in the American eel *Anguilla rostrata*: kinematics in water and on land. *J. Exp. Biol.* **201**, 949-961.

Hart, J. L. (1973). Pacific fishes of Canada. *Fish. Res. Board Can. Bull.* **180**, 1-740.

Heimberg, A. M., Cowper-Sal-lari, R., Sémon, M., Donoghue, P. C. J. and Peterson, K. J. (2010). microRNAs reveal the interrelationships of hagfish, lampreys, and gnathostomes and the nature of the ancestral vertebrate. *Proc. Nat. Acad. Sci. USA* **107**, 19379-19383.

Herrel, A., Choi, H.-F., De Schepper, N., Aerts, P. and Adriaens, D. (2011). Kinematics of swimming in two burrowing anguilliform fishes. *Zoology* **114**, 78-84.

Jayne, B. C. (1985). Swimming in constricting (*Elaphe g. guttata*) and nonconstricting (*Nerodia fasciata pictiventris*) colubrid snakes. *Copeia* **1985**, 195-208.

Jensen, D. (1966). The hagfish. *Sci. Am.* **214**, 82-90.

Koob, T. J. and Long, J. H., Jr. (2000). The vertebrate body axis: evolution and mechanical function. *Amer. Zool.* **40**, 1-18.

Lauder, G. V. (2000). Function of the caudal fin during locomotion in fishes: kinematics, flow visualization, and evolutionary patterns. *Amer. Zool.* **40**, 101-122.

Lauder, G. V., Lim, J. L., Shelton, R., Witt, C., Anderson, E. J. and Tangorra, J. L. (2011). Robotic models for studying undulatory locomotion in fishes. *Mar. Technol. Soc. J.* **45**, 45-55.

Lauder, G. V. and Tytell, E. D. (2006). Hydrodynamics of undulatory propulsion. In *Fish Biomechanics* (eds. R. E. Shadwick and G. V. Lauder), pp. 425-468. London: Elsevier Inc.

Lesser, M. P., Martini, F. H. and Heiser, J. B. (1996). Ecology of the hagfish, *Myxine glutinosa* L. in the Gulf of Maine I. Metabolic rates and energetics. *J. Exp. Mar. Biol. Ecol.* **208**, 215-225.

Lighthill, M. J. (1970). Aquatic animal propulsion of high hydromechanical efficiency. *J. Fluid Mech.* **44**, 265-301.

Long, J. H. (1995). Morphology, mechanics, and locomotion: the relation between the notochord and swimming motions in sturgeon. *Environ. Biol. Fish.* **44**, 199-211.

Long, J. H., Hale, M. E., McHenry, M. J. and Westneat, M. W. (1996). Functions of fish skin: flexural stiffness and steady swimming of longnose gar *Lepisosteus osseus*. *J. Exp. Biol.* **199**, 2139-2151.

Long, J. H., Jr. (1998). Muscles, elastic energy, and the dynamics of body stiffness in swimming eels. *Amer. Zool.* **38**, 771-792.

Long, J. H., Jr., Koob-Emunds, M., Sinwell, B. and Koob, T. J. (2002). The notochord of hagfish *Myxine glutinosa*: visco-elastic properties and mechanical functions during steady swimming. *J. Exp. Biol.* **205**, 3819-3831.

Long, J. H., Jr. and Nipper, K. S. (1996). The importance of body stiffness in undulatory propulsion. *Amer. Zool.* **36**, 678-694.

Long, J. H., Porter, M. E., Root, R. G. and Liew, C. W. (2010). Go reconfigure: how fish change shape as they swim and evolve. *Integr. Comp. Biol.* **50**, 1120-1139.

Maladen, R. D., Ding, Y., Li, C. and Goldman, D. I. (2009). Undulatory swimming in sand: subsurface locomotion of the sandfish lizard. *Science* **325**, 314-318.

Martini, F. H. (1998). The ecology of hagfishes. In *The Biology of Hagfishes* (eds. J. M. Jørgensen, J. P. Lomholt, R. E. Weber and H. Malte), pp. 57-77. London: Chapman & Hall.

McHenry, M. J., Pell, C. A. and Long, J. H., Jr. (1995). Mechanical control of swimming speed: stiffness and axial wave form in undulating fish models. *J. Exp. Biol.* **198**, 2293-2305.

Müller, U. K., Stamhuis, E. J. and Videler, J. J. (2002). Riding the waves: the role of the body wave in undulatory fish swimming. *Integr. Comp. Biol.* **42**, 981-987.

Munk, Y. (2008). Kinematics of swimming garter snakes (*Thamnophis sirtalis*). *Comp. Biochem. Physiol. A* **150**, 131-135.

Ota, K. G., Fujimoto, S., Oisi, Y. and Kuratani, S. (2011). Identification of vertebra-like elements and their possible differentiation from sclerotomes in the hagfish. *Nat. Commun.* **2**:373 doi: 10.1038/ncomms1355.

Pace, C. M. and Gibb, A. C. (2011). Locomotor behavior across an environmental transition in the ropefish, *Erpetoichthys calabaricus*. *J. Exp. Biol.* **214**, 530-537.

Root, R. G., Courtland, H. W., Pell, C. A., Hobson, B., Twohig, E. J., Suter, R. B., Shepherd, W. R. I., Boetticher, N. C. and Long, J. H., Jr. (1999). Swimming fish and fish-like models: the harmonic structure of undulatory waves suggest that fish actively tune their bodies. In *Proceedings of the 11th International Symposium on Unmanned Untethered Submersible Technology* vol. 11, pp. 378-388: Autonomous Undersea Systems Institute.

Root, R. G., Courtland, H. W., Shepherd, W. and Long, J. H. J. (2007). Flapping flexible fish: periodic and secular body reconfigurations in swimming lamprey, *Petromyzon marinus*. *Exp. Fluids* **43**, 779-797.

Schlichting, H. (1979). *Boundary-layer theory*. New York: McGraw-Hill.

Shadwick, R. E. and Gemballa, S. (2006). Structure, kinematics, and muscle dynamics in undulatory swimming. In *Fish Biomechanics* (eds. R. E. Shadwick and G. V. Lauder), pp. 241-280. London: Elsevier Inc.

Taylor, G. K., Nudds, R. L. and Thomas, A. L. R. (2003). Flying and swimming animals cruise at a Strouhal number tuned for high power efficiency. *Nature* **425**, 707-711.

Triantafyllou, G. S., Triantafyllou, M. S. and Grosenbaugh, M. A. (1993). Optimal thrust development in oscillating foils with application to fish propulsion. *J. Fluids Struct.* **7**, 205-224.

Tytell, E. D. (2004a). The hydrodynamics of eel swimming II. Effect of swimming speed. *J. Exp. Biol.* **207**, 3265-3279.

Tytell, E. D. (2004b). Kinematics and hydrodynamics of linear acceleration in eels, *Anguilla rostrata*. *Proc. R. Soc. Lond. B* **271**, 2535-2540.

Tytell, E. D., Hsu, C.-Y., Williams, T. L., Cohen, A. H. and Fauci, L. J. (2010). Interactions between internal forces, body stiffness, and fluid environment in a neuromechanical model of lamprey swimming. *Proc. Nat. Acad. Sci. USA* **107**, 19832-19837.

Tytell, E. D. and Lauder, G. V. (2004). The hydrodynamics of eel swimming I. Wake structure. *J. Exp. Biol.* **207**, 1825-1841.

Videler, J. J. (1993). *Fish Swimming*. London: Chapman & Hall.

Videler, J. J. and Hess, F. (1984). Fast continuous swimming of two pelagic predators, saithe (*Pollachius virens*) and mackerel (*Scomber scombrus*): a kinematic analysis. *J. Exp. Biol.* **109**, 209-228.

Vogel, S. (2003). *Comparative Biomechanics: Life's Physical World*. Princeton: Princeton University Press.

Webb, P. W., Kostecki, P. T. and Stevens, E. D. (1984). The effect of size and swimming speed on locomotor kinematics of rainbow trout. *J. Exp. Biol.* **109**.

Westneat, M. W., Hale, M. E., McHenry, M. J. and Long, J. H. (1998). Mechanics of the fast-start: muscle function and the role of intramuscular pressure in the escape behavior of *Amia calva* and *Polypterus palmas*. *J. Exp. Biol.* **201**, 3041-3055.

Williams, T. L., Bowtell, G., Carling, J. C., Sigvardt, K. A. and Curtin, N. A. (1995). Interactions between muscle activation, body curvature and the water in the swimming lamprey. In *Symposia of the Society for Experimental Biology XLIX: Biological Fluid Dynamics* vol. 49 (eds. C. P. Ellington and T. J. Pedley), pp. 49-59. Cambridge: The Company of Biologists.

Williams, T. L., Grillner, S., Smoljaninov, V. V., Wallén, P., Kashin, S. and Rossignol, S. (1989). Locomotion in lamprey and trout: the relative timing of activation and movement. *J. Exp. Biol.* **143**, 559-566.

Wu, T. Y. (1977). Introduction to the scaling of aquatic animal locomotion. In *Scale effects in animal locomotion* (ed. T. J. Pedley), pp. 203-232. New York: Academic Press.

Zintzen, V., Roberts, C. D., Anderson, M. J., Stewart, A. L., Struthers, C. D. and Harvey, E. S. (2011). Hagfish predatory behaviour and slime defence mechanism. *Sci. Rep.* **1**:131 doi: 10.1038/srep00131.

Chapter 2

Maneuvering by flexible finless fishes: kinematics of linear accelerations and lateral maneuvers in hagfishes (Myxinidae)

Abstract

Likely making up a large portion of routine locomotion for most fishes, unsteady swimming behaviors – such as fast-starts, obstacle navigation, and vertical maneuvers – have received growing attention from researchers. Most of these studies, however, are on fishes that have discrete, movable fins to help enact their maneuvers. The hagfish is an elongate undulatory swimmer that lacks all paired and median fins except for a narrow caudal fin margin. In their marine benthic environments, hagfishes must maneuver while negotiating fallen prey items and burrowing into sediments, but little is known about unsteady swimming behaviors in these flexible yet finless fishes. In this study, I examine how hagfish accomplish swimming maneuvers by quantifying whole-body kinematics of two unsteady swimming behaviors: linear accelerations in Pacific (*Eptatretus stoutii*) and Atlantic hagfish (*Myxine glutinosa*), and lateral maneuvers in Pacific hagfish. Body midline coordinates were obtained from high-speed video of hagfishes accelerating at -0.86 – 0.11 BL/s^2 during linear accelerations, or swimming against flow speeds from 0.45 – 0.90 BL/s during lateral maneuvers. Positive linear accelerations are generally characterized by increased amplitude, wavelength, and flexion along the hagfish body, with greater engagement of the head and anterior regions. Lateral maneuvers are characterized by a repeating pattern of unsteady, unilateral motion of the anterior body as it interacts with the ground, while the posterior body propagates waves of lateral bending toward the tail tip. I show that without discrete, movable fins, hagfish can employ whole-body dexterity and differential patterns of motion along the body to control their maneuvers.

Introduction

The vast diversity that fishes display in their morphologies is accompanied by equally impressive diversity in how they move about their environment. Our understanding of relationships between form and locomotory function in fishes has grown tremendously from work on steady swimming, but given that the majority of routine swimming is unsteady (Webb, 1997), attempting to comprehend the full repertoire of fish locomotory behaviors involves studying unsteady swimming as well. Many workers have recognized the importance of transient behaviors as a part of routine swimming in fishes, and as such, have quantified the kinematics and hydrodynamics of several types of unsteady swimming behaviors. These include fast-starts, which are particularly high-acceleration maneuvers often performed as an escape response or a predator strike (for a review, see Domenici and Blake, 1997); turns associated with foraging or navigating obstacles (Danos and Lauder, 2007; Schrank and Webb, 1998); routine burst-and-coast swimming (Müller et al., 2000); and vertical maneuvers (Liao and Lauder, 2000; Wilga and Lauder, 2002).

The majority of these studies, however, are on fishes that have discrete, movable fins that can act as control surfaces for steering or can directly power maneuvers throughout the water column (Webb, 2004). Paired pectoral fins move individually to assist slow turns in bluegill sunfish (Drucker and Lauder, 2001), while asymmetrical caudal fin lobes direct fluid forces during vertical maneuvers in sharks (Wilga and Lauder, 2002) and sturgeon (Liao and Lauder, 2000). These distinct control surfaces are absent in hagfishes. The hagfish (Myxinidae) body is elongate and cylindrical with moderate lateral compression at the caudal end. They lack all paired and median fins except for a caudal fin consisting of a narrow fin margin supported by cartilaginous fin rays (Hart, 1973). Like many other elongate aquatic animals, hagfishes move

about their environment by activating axial muscles and propagating undulatory waves along the length of their bodies (Adam, 1960; Campbell, 1940; Long et al., 2002; Long et al., 1997).

Most of our quantitative knowledge on locomotion by elongate undulatory swimmers comes from studies of steady, forward swimming (Chapter 1; Gillis, 1997; Long et al., 2002; Tytell, 2004a; Tytell and Lauder, 2004). The relatively smaller body of work focusing on maneuvers or unsteady swimming includes theoretical models of maneuvering in fin-less, elongate swimmers (Singh and Pedley, 2008; Singh and Pedley, 2012), and experimental studies on backward swimming (D'Août and Aerts, 1999; Long et al., 1997) and linear accelerations (Tytell, 2004b) in freshwater eels. An analysis of unsteady swimming behaviors in hagfishes would expand our understanding of locomotor diversity among aquatic animals. Despite sharing a similar external morphology, hagfishes and eels appear to employ different undulatory motion patterns during steady swimming (see Chapter 1). In addition, unlike most vertebrates, hagfish lack fully-formed vertebrae, leaving their bodies with a high degree of flexibility that has functional consequences on their swimming behavior (Long et al., 2002). While having more fins available as control surfaces is generally associated with greater maneuverability, having a flexible body can enhance maneuverability as well (Webb, 1997).

In their role as scavengers and occasional hunters in marine benthic environments (Koob and Long, 2000; Martini, 1998; Zintzen et al., 2011), hagfishes likely spend most of their active time moving unsteadily. Navigating around and within decaying prey items, burrowing into sediments, and escaping their own slime all require some degree of maneuvering. Yet, despite making up a large portion of their locomotory activity, little is known about unsteady swimming behaviors in hagfishes.

In this chapter, I aim to broaden our comprehension of the hagfish locomotory repertoire by (1) quantifying whole-body kinematics of two different unsteady swimming behaviors in Pacific hagfish (*Eptatretus stoutii*) and Atlantic hagfish (*Myxine glutinosa*); (2) describing the mechanisms by which these unsteady behaviors are modulated in comparison to steady swimming in hagfishes; and (3) qualitatively comparing unsteady swimming behaviors in hagfish and other elongate vertebrates.

Materials and Methods

Experimental animals

Pacific hagfish (*Eptatretus stoutii*, Lockington) were caught in baited traps in Barkley Sound, British Columbia, with assistance from the Bamfield Marine Sciences Centre. Atlantic hagfish (*Myxine glutinosa*, Linnaeus) were collected from the Huntsman Science Centre in St. Andrews, New Brunswick, Canada. The animals were transported to a Harvard University aquarium facility and housed in a tank of recirculating artificial seawater (8 – 9°C, 35‰), where they were maintained on a 12:12 hour light:dark cycle and fed frozen squid monthly. Swimming behaviors were recorded from four Atlantic hagfish ranging from 26.0 – 30.9 cm in body length (BL) (mean BL ± standard deviation, 28.5 ± 2.0 cm) and three Pacific hagfish ranging from 26.1 – 30.2 cm BL (mean BL ± standard deviation, 28.8 ± 2.3 cm). All procedures and experiments adhered to Harvard University IACUC guidelines (protocol # 20-03).

Filming and kinematic analysis

Individual hagfish were placed in a variable-speed flow tank that contained artificial seawater (9°C, 35‰) and had a working section of 84 x 28 x 28 cm. A Photron PCI1024 Fastcam high-

speed video camera (500 frames/s, 1024 x 1024 pixels, Photron USA Inc., San Diego, CA) aimed at a 45 degree-angled mirror below the flow tank filmed ventral views of hagfish performing various unsteady swimming behaviors. While initiation of swimming was encouraged by slowly increasing the speed of water flow in the tank or by gently prodding the underside of the caudal end, hagfish voluntarily executed specific swimming behaviors. Two distinct unsteady behaviors were observed and recorded: linear accelerations and lateral maneuvers (detailed quantitative definitions below). Linear accelerations tended to occur in middle or top portion of the flow tank, while lateral maneuvers occurred on the bottom of the tank. Previous studies using the same flow tank at speeds comparable to the lowest speeds observed in this study found that the thickness of the boundary layer at the tank's solid surfaces was approximately 0.2 – 0.7 cm (Carlson and Lauder, 2011; Tytell and Lauder, 2004). Because these values are an order of magnitude lower than the typical depth of a hagfish body, and because the boundary layer thins as flow speed increases (Schlichting, 1979), it was assumed that boundary layer flows had a negligible effect on swimming.

Video sequences that were further analyzed consisted of 2 to 6 consecutive tail beats of a given unsteady swimming behavior. A custom Matlab (R2011a, The Mathworks Inc., Natick, MA) program was used to record two-dimensional (*x, y*) coordinates of hagfish body position from the video images. Because hagfish body movements were typically low frequency, videos were first down-sampled to 25 frames/s. For each video image, ten to 15 manually-digitized points along the midline of the hagfish body were fit with a cubic spline to generate an interpolated and smoothed line consisting of 200 equally-spaced data points and representing the body midline for that instant in the tail beat cycle. All subsequent analyses of hagfish body movements used these smoothed midline coordinate data. Swim speeds were measured at the

hagfish body's center of mass (COM), located at approximately 0.4 BL. Average COM position was determined by placing a fully extended dead hagfish on a rigid beam, and balancing the beam on a fulcrum (Westneat et al., 1998).

Linear accelerations were defined as a greater than 10% change in the hagfish COM axial velocity over a whole tail beat, while the average body midline and direction of travel is kept parallel to the oncoming water flow. Because the axial velocity of the COM actually oscillates throughout a tail beat during even steady swimming (Chapter 1), acceleration was measured as the slope of an ordinary least squares regression line fit to the COM velocity data. The range of accelerations measured for voluntarily swimming *M. glutinosa* was -0.86 to 0.09 BL/s^2, while accelerations for *E. stoutii* were -0.17 to 0.11 BL/s^2. Lateral maneuvers involved lateral body undulations that moved the whole hagfish across the flow tank, perpendicular to the oncoming flow and the long axis of the hagfish body. Changes in COM axial velocity were less than 10%, reflecting that hagfish largely maintained position in the upstream-downstream direction. *E. stoutii* swam at flow speeds from 0.45 to 0.90 BL/s, while only one individual of *M. glutinosa* performed a lateral maneuver and was excluded from analysis.

Custom Matlab routines were used to calculate kinematic variables for each type of swimming behavior. Tail beat amplitude (TBA) was calculated as half the distance covered by the caudal tip between maximum lateral excursions within a tail beat cycle. Tail beat frequency (TBF) was calculated as the inverse of the period of one tail beat cycle. Tail tip speed was the total lateral distance travelled by the caudal tip over a whole tail beat divided by the tail beat period. Strouhal number (*St*), a dimensionless index that relates the rate of oscillatory motion of a propulsor to its forward motion, was calculated as the product between 2·TBA and TBF, divided by forward swim speed (Triantafyllou et al., 1993; Vogel, 2003). The oscillation

amplitude of the rostral tip was also measured and used to calculate the nose:tail tip amplitude ratio.

To examine the kinematics of the undulatory wave along the length of the hagfish body, the body was divided into 5 segments (20% BL increments) and the following variables were computed within and then averaged over each segment: undulatory amplitude along the body was calculated using the formula for TBA applied to midline points along the body; undulatory wave frequency was calculated using the formula for TBF applied to body midline points; undulatory wave speed was determined by measuring the distance a wave crest travelled between consecutive video frames and dividing by the frame interval; and wavelength was computed as wave speed divided by wave frequency. Wave speed was subsequently averaged over the entire hagfish body and used to calculate slip, a measure of the efficiency of a propulsive wave given by the ratio between the body's forward swim speed and the rearward wave speed (Lighthill, 1970; Shadwick and Gemballa, 2006). Lastly, the maximum angle reached by each body segment relative to the oncoming flow was measured as a proxy for body flexion; here, the body segment was approximated as the straight line connecting the end points of each segment.

For linear accelerations, the change in these kinematic quantities over consecutive tail beats or over half tail beats was calculated to demonstrate the effect of a change in speed during swimming. For lateral maneuvers, kinematic values were measured for each tail beat in a sequence and then averaged. Additional variables were calculated for lateral maneuvers to illustrate the whole-body behavior of the hagfish as it traversed the tank. To estimate the overall orientation of the hagfish body during a maneuver, a generalized linear regression model was fit to the body midline in each frame and then regression coefficients were averaged over a tail beat cycle. The angle between the average regression line and the oncoming flow was defined as the

body orientation angle. Component velocities of body points along the hagfish midline were also measured with respect to the oncoming flow. Resultant velocities were calculated from the axial and lateral velocities using the Pythagorean Theorem. When appropriate, kinematic measurements were divided by body length to normalize the data.

Statistical analysis

Kinematic data were $\log_{10}$ transformed prior to statistical analysis. For linear accelerations, an analysis of covariance (ANCOVA) tested for the effects of species, acceleration, and the interaction between species and acceleration on the change in single-measure kinematic variables: TBA, TBF, tail tip speed, nose:tail tip amplitude ratio, *St*, and slip. ANCOVA assumes a linear relationship between the dependent variable and continuous covariate (Sokal and Rohlf, 1981), and I predicted that larger changes in swim speed (acceleration) would be accompanied by larger changes in kinematic variables. Furthermore, previous work on swimming in eels has provided evidence for linear relationships between kinematic values and changes in swim speed (Tytell, 2004a; Tytell, 2004b). A multivariate analysis of covariance (MANCOVA) analyzed the change in kinematics that were calculated along the hagfish body: undulatory amplitude, body segment angle, wave speed, and wavelength. Longitudinal position (LP) along the body was treated as a repeated measure. Between-individual effects were species, acceleration, and species x acceleration, while within-individual effects were longitudinal position, and interactions between LP, species, and acceleration. Adjusted test statistics were used where appropriate to satisfy the assumptions of the MANCOVA. For lateral maneuvers, the relationship between flow speed (= axial swim speed) and single-measure kinematics was determined with Spearman's non-parametric correlation test. A repeated measures general linear model tested for the effects

of flow speed, LP, and LP x flow speed on kinematic variables measured along the body. To help illustrate patterns between kinematic measurements and these within-individual effects for both types of swimming behaviors, an Ordinary Least Squares trend line was fit to kinematic data from each 0.2 BL-long body segment and plotted with the data versus acceleration or speed; fits with a magnitude of the correlation coefficient $r > 0.9$ are represented by solid thick lines on the plots. All statistical analyses were performed with JMP Pro 10 (SAS Institute, Inc., Cary, NC).

Results

Linear accelerations

Both negative and positive linear accelerations were characterized by large amplitude undulations along the whole body in swimming hagfish (Figure 2.1). Amplitude tended to be smaller for positive accelerations than for negative accelerations, likely reflecting that decelerations occurred while hagfish were already swimming at a high swim speed with large amplitude undulations. Midline drawings of representative linear accelerations in each species suggest that *M. glutinosa* generally swam with larger amplitude waves than *E. stoutii* (Figure 2.1C, D *vs.* A, B).

It was common for kinematic variables to both grow and decline throughout accelerating tail beats (Figure 2.2). As a result, an analysis of covariance did not detect significant effects of species, acceleration, or species x acceleration on any of the single-measure kinematic variables (tail beat amplitude, tail beat frequency, tail tip speed, Strouhal number, and nose:tail amplitude ratio) (Table 2.1). The magnitude of the change in tail beat amplitude (ΔTBA) as hagfish decelerated or accelerated was usually less than 0.04 BL (Figure 2.2A), approximately 25% of absolute TBA. TBA did tend to decline while hagfish decelerated, but showed no distinct pattern

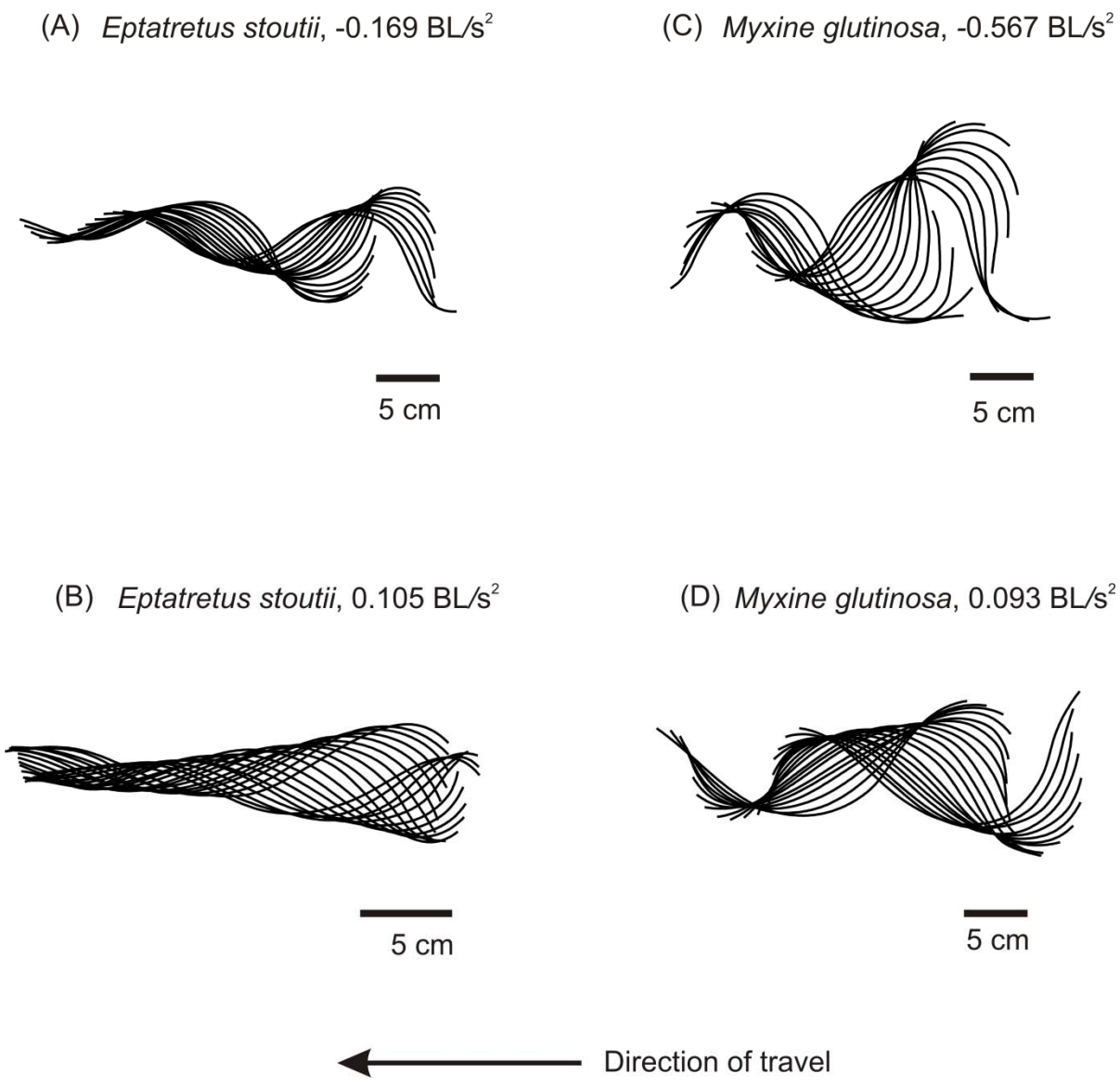

Figure 2.1. Ventral body midline drawings from (A, B) Pacific (*Eptatretus stoutii*) and (C, D) Atlantic (*Myxine glutinosa*) hagfish decelerating (negative acceleration) or accelerating illustrate whole-body, large amplitude undulatory waves during linear unsteady swimming. A complete tail beat cycle is shown in each drawing, with each midline representing an instant in time separated by 0.040 seconds (A, C, D) or 0.036 seconds (B). The head is at the left and the tail is at the right.

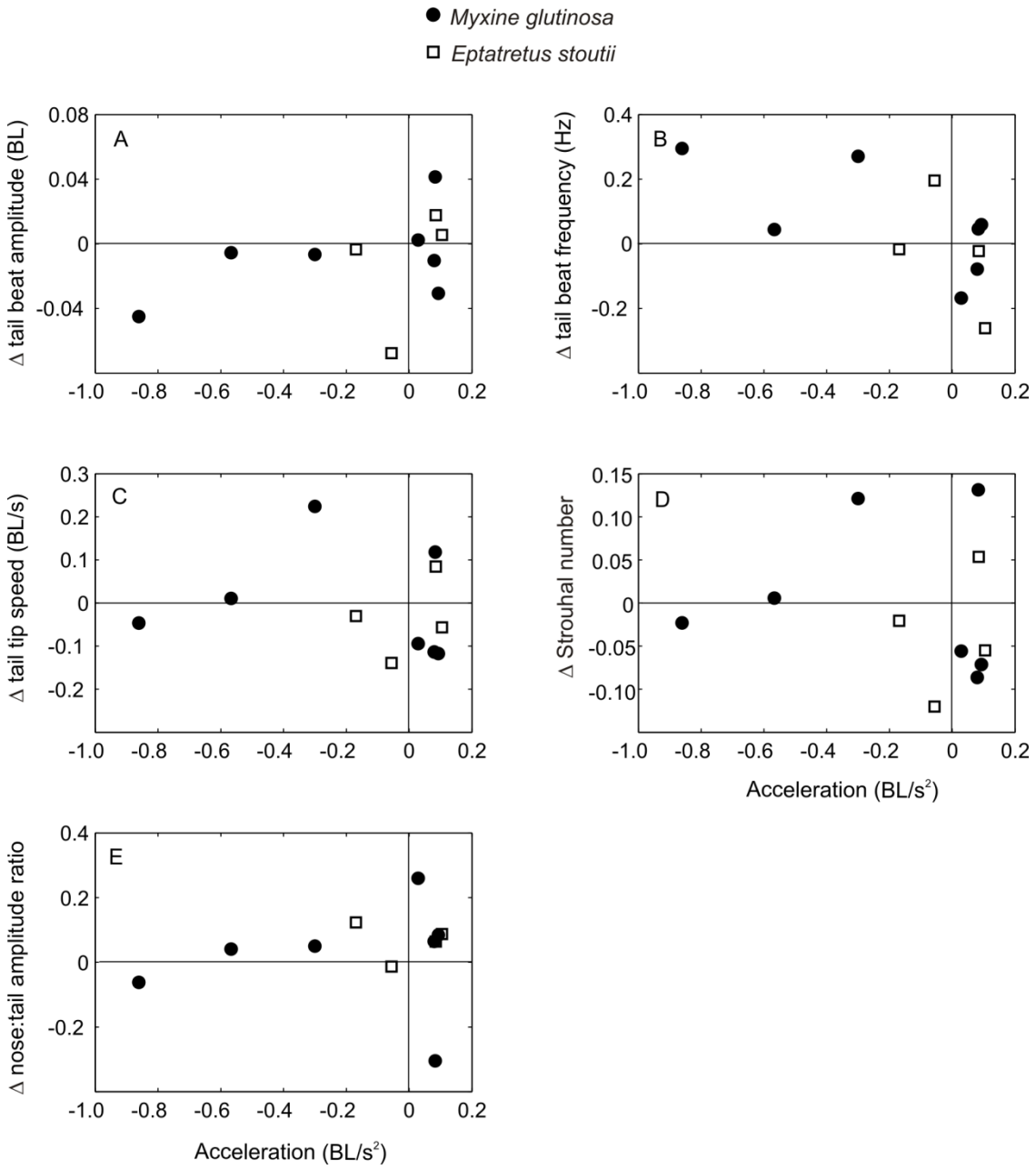

Figure 2.2. Relationships between changes in tail tip kinematics and acceleration in *M. glutinosa* (filled circles) and *E. stoutii* (open squares). A positive change means that the variable grew, while a negative change means that the variable decreased while the hagfish changed swimming speed. Because measured kinematic variables both grew and declined throughout accelerating tail beats, no significant effects of species, acceleration, or species x acceleration on the tail tip kinematics were found by an ANCOVA (see Table 2.1).

Table 2.1. ANCOVA and MANCOVA results for kinematic measurements on *E. stoutii* and *M. glutinosa* performing linear accelerations.

	ANCOVA: Effect tests					
	Species		Acceleration		Species x Acceleration	
Kinematic variable with single measure	*F* ratio	*p*	*F* ratio	*p*	*F* ratio	*p*
Δ tail beat amplitude (BL)	0.85	0.432	3.74	0.107	2.04	0.209
Δ tail beat frequency (Hz)	0.06	0.814	2.53	0.156	0.65	0.445
Δ tail tip speed (BL/s)	0.20	0.691	1.42	0.287	0.33	0.589
Δ nose:tail tip amplitude ratio	0.17	0.700	0.95	0.382	0.31	0.608
Δ Strouhal number	0.42	0.562	1.58	0.261	0.54	0.493
Δ slip (propeller efficiency)	0.57	0.498	0.21	0.665	0.17	0.690

	MANCOVA: Between-individuals effect tests						MANCOVA: Within-individuals effect tests							
	Species		Acceleration		Species x Acceleration		Longitudinal position (LP)		LP x Species		LP x Acceleration		LP x Species x Acceleration	
Kinematic variable with repeated measures along the body	*F* ratio	*p*	*F* ratio	*p*	*F* ratio	*p*	*F* ratio	*p*	*F* ratio	*p*	*F* ratio	*p*	*F* ratio	*p*
Δ undulatory amplitude (BL)	1.91	0.209	9.70	**0.017**	6.56	**0.038**	0.65	0.626	2.14	0.106	1.36	0.274	1.19	0.335
Δ max body segment angle (deg)	0.59	0.469	3.32	0.111	8.75	**0.021**	2.45	0.069	1.24	0.315	1.70	0.179	2.58	0.059
Δ undulatory wave speed (BL/s)	2.55	0.155	2.38	0.167	1.07	0.335	0.46	0.768	5.64	**0.002**	5.39	**0.002**	5.97	**0.001**
Δ undulatory wavelength (BL)	3.58	0.100	6.09	**0.043**	2.96	0.129	0.94	0.455	5.07	**0.003**	3.74	**0.015**	4.11	**0.010**

p-values in bold denote significance at the alpha = 0.05 level

Within-individual MANCOVA F tests use adjusted univariate H-F values

Random effects tests indicated that individual had no effect on any variables

of increase or decrease during positive accelerations. In contrast, tail beat frequency tended to decrease as hagfish accelerated through a tail beat, and grow as hagfish decelerated (Figure 2.2B).

Acceleration did significantly covary with changes in undulatory amplitude measured along the whole body (Table 2.1). A significant species x acceleration effect was also detected, indicating that *E. stoutii* and *M. glutinosa* differed in how undulatory amplitude varied with acceleration. Longitudinal position (LP) along the body did not have any significant effects on change in undulatory amplitude within individual hagfish. However, *E. stoutii* did show a general trend of reducing amplitudes along the body while decelerating and increasing amplitudes while accelerating, particularly at the head and tail (Figure 2.3A).

Changes in the maximum angle reached by segments along the body varied with acceleration differently for each species of hagfish, given by the significant species x acceleration interaction (Table 2.1). Position along the body had no significant effects on change in maximum body segment angle, though trends along the body were visible in *E. stoutii*: while accelerating, the head and tail tended to bend at greater angles, while the mid-body tended to bend at smaller angles (Figure 2.4B).

Changes in undulatory wave speed and wavelength differed along the body for the two species of hagfish and across accelerations (Figures 2.5, 2.6), as the MANCOVA identified LP x species, LP x acceleration, and LP x species x acceleration as significant effects for both variables (Table 2.1). In *E. stoutii*, the pattern of wave speed change was variable across body segments, with the head region showing the strongest linear trend of wave speed decline during deceleration and wave speed growth during acceleration (Figure 2.5B). Undulatory wavelength also tends to shorten during deceleration and increase during acceleration (Figure 2.6A, C).

Figure 2.3. Change in undulatory amplitude as a function of position along the body and acceleration in (A, B) *E. stoutii* and (C, D) *M. glutinosa*. (A, C) Positive accelerations are represented by solid bars, decelerations (negative accelerations) are represented by hatched bars, and darker colors denote greater magnitude acceleration/deceleration. *E. stoutii* showed a general trend of reducing amplitudes while decelerating and increasing amplitudes while accelerating (A), but the effect of longitudinal position along the body was not statistically significant. (B, D) The two species of hagfish did differ in how undulatory amplitude varied with acceleration at different segments of the body. Darker shades correspond to more caudal positions along the body. Trend lines are Ordinary Least Squares fits, where a dashed line represents a coefficient magnitude of $r < 0.9$.

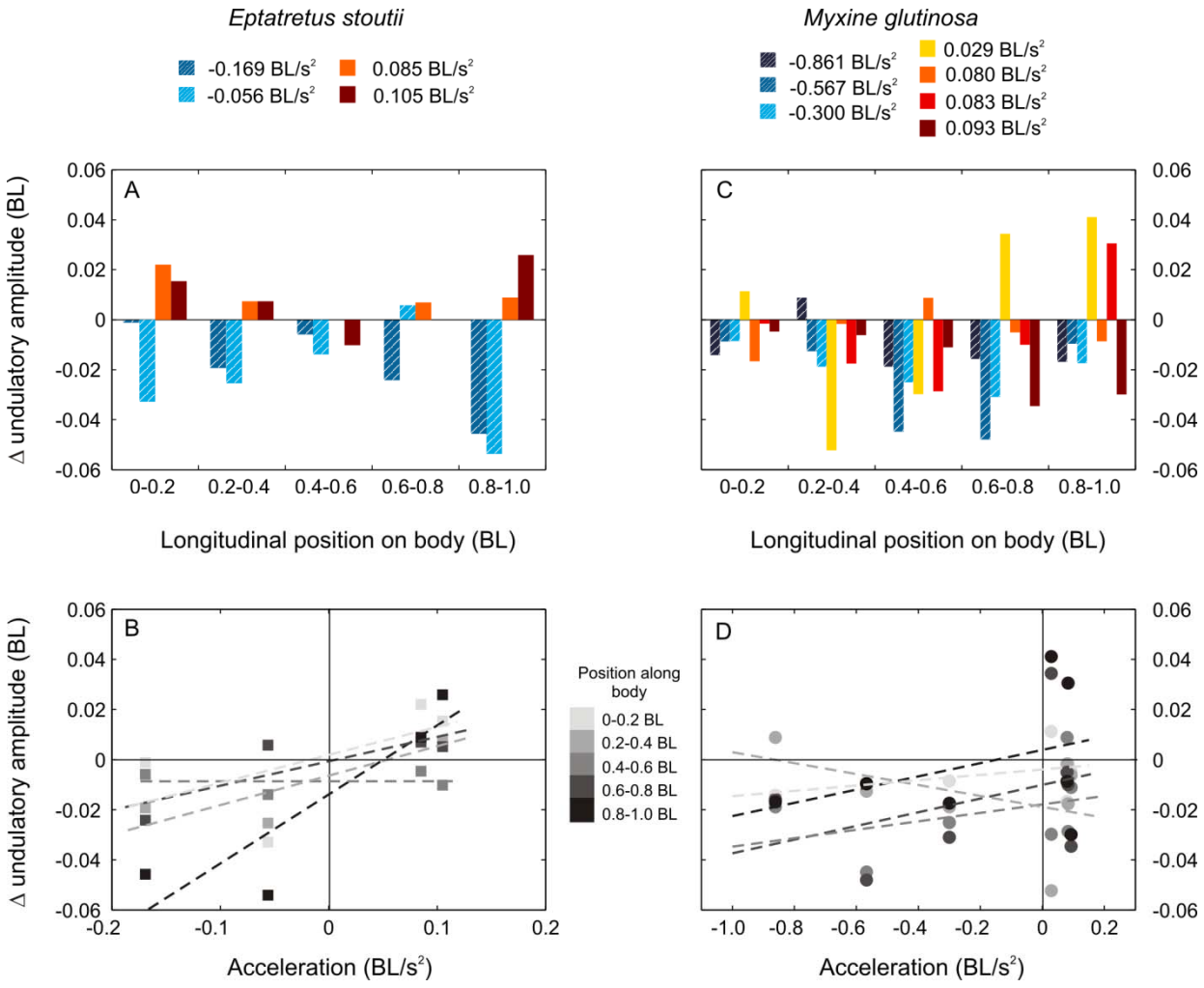

Figure 2.3 (Continued)

Figure 2.4. Change in maximum body segment angle as a function of position along the body and acceleration in (A, B) *E. stoutii* and (C, D) *M. glutinosa*. (A, C) Positive accelerations are represented by solid bars, decelerations (negative accelerations) are represented by hatched bars, and darker colors denote greater magnitude acceleration/deceleration. Position along the body had no statistically significant effect of the change in maximum body angle in either species. (B, D) *E. stoutii* and *M. glutinosa* differed in how changes in body segment angle co-varied with acceleration at different segments along the body. For *E. stoutii*, a trend along the body is visible where the head and tail tend to bend at larger angles while the mid-body bends at smaller angles while accelerating. Darker shades correspond to more caudal positions along the body. Trend lines are Ordinary Least Squares fits, where solid thick lines represent correlation coefficient magnitudes $r > 0.9$, and dashed lines represent coefficient magnitudes of $r < 0.9$.

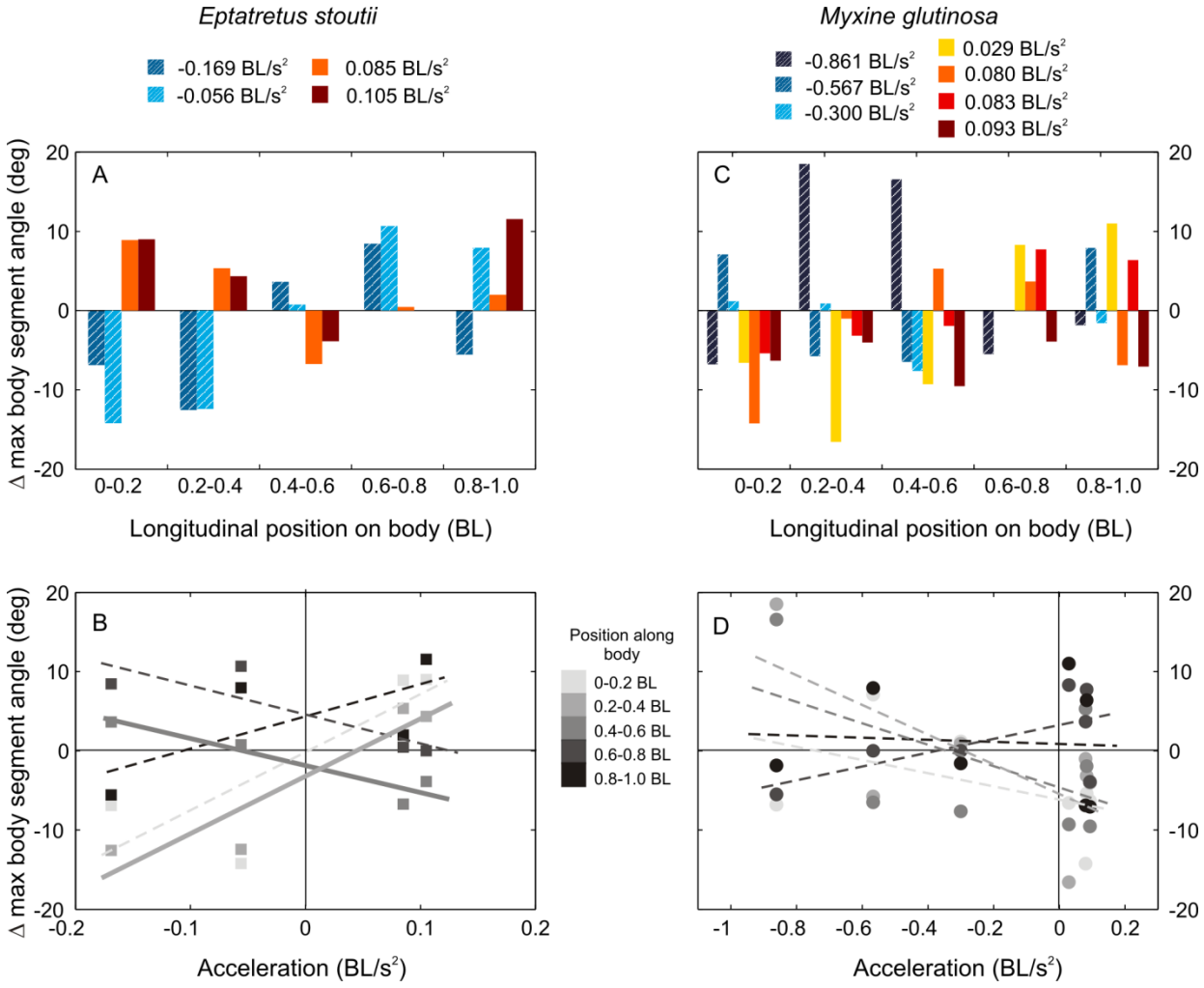

Figure 2.4 (Continued)

Figure 2.5. Change in undulatory wave speed as a function of position along the body and acceleration in (A, B) *E. stoutii* and (C, D) *M. glutinosa*. (A, C) Positive accelerations are represented by solid bars, decelerations (negative accelerations) are represented by hatched bars, and darker colors denote greater magnitude acceleration/deceleration. Change in wave speed varied along the body differently for the two species of hagfish. (B, D) Change in wave speed also significantly co-varied with acceleration differently for both species. For *E. stoutii*, the pattern of wave speed change was variable across body segments, with the head region showing a strong trend of wave speed decline during deceleration and wave speed growth during acceleration (B). Darker shades correspond to more caudal positions along the body. Trend lines are Ordinary Least Squares fits, where solid thick lines represent correlation coefficient magnitudes $r > 0.9$, and dashed lines represent coefficient magnitudes of $r < 0.9$.

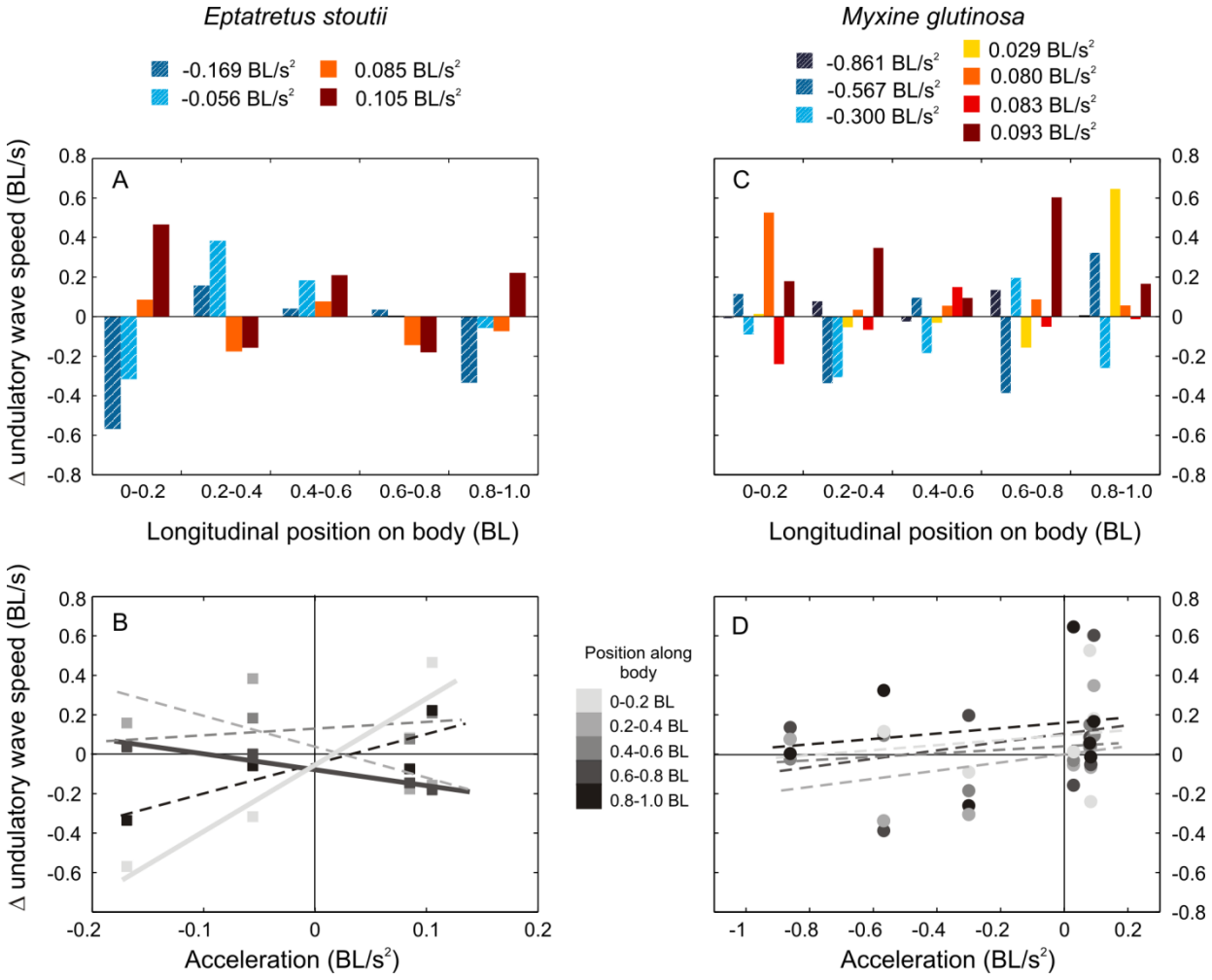

Figure 2.5 (Continued)

Figure 2.6. Change in undulatory wavelength as a function of position along the body and acceleration in (A, B) *E. stoutii* and (C, D) *M. glutinosa*. (A, C) Positive accelerations are represented by solid bars, decelerations (negative accelerations) are represented by hatched bars, and darker colors denote greater magnitude acceleration/deceleration. Change in wavelength varied along the body differently for the two species of hagfish. (B, D) Change in wavelength also significantly co-varied with acceleration differently between species. Wavelength at the tail tended to increase during acceleration for *E. stoutii* (B), but showed no obvious variation with acceleration in *M. glutinosa* (D). Darker shades correspond to more caudal positions along the body. Trend lines are Ordinary Least Squares fits, where solid thick lines represent correlation coefficient magnitudes $r > 0.9$, and dashed lines represent coefficient magnitudes of $r < 0.9$.

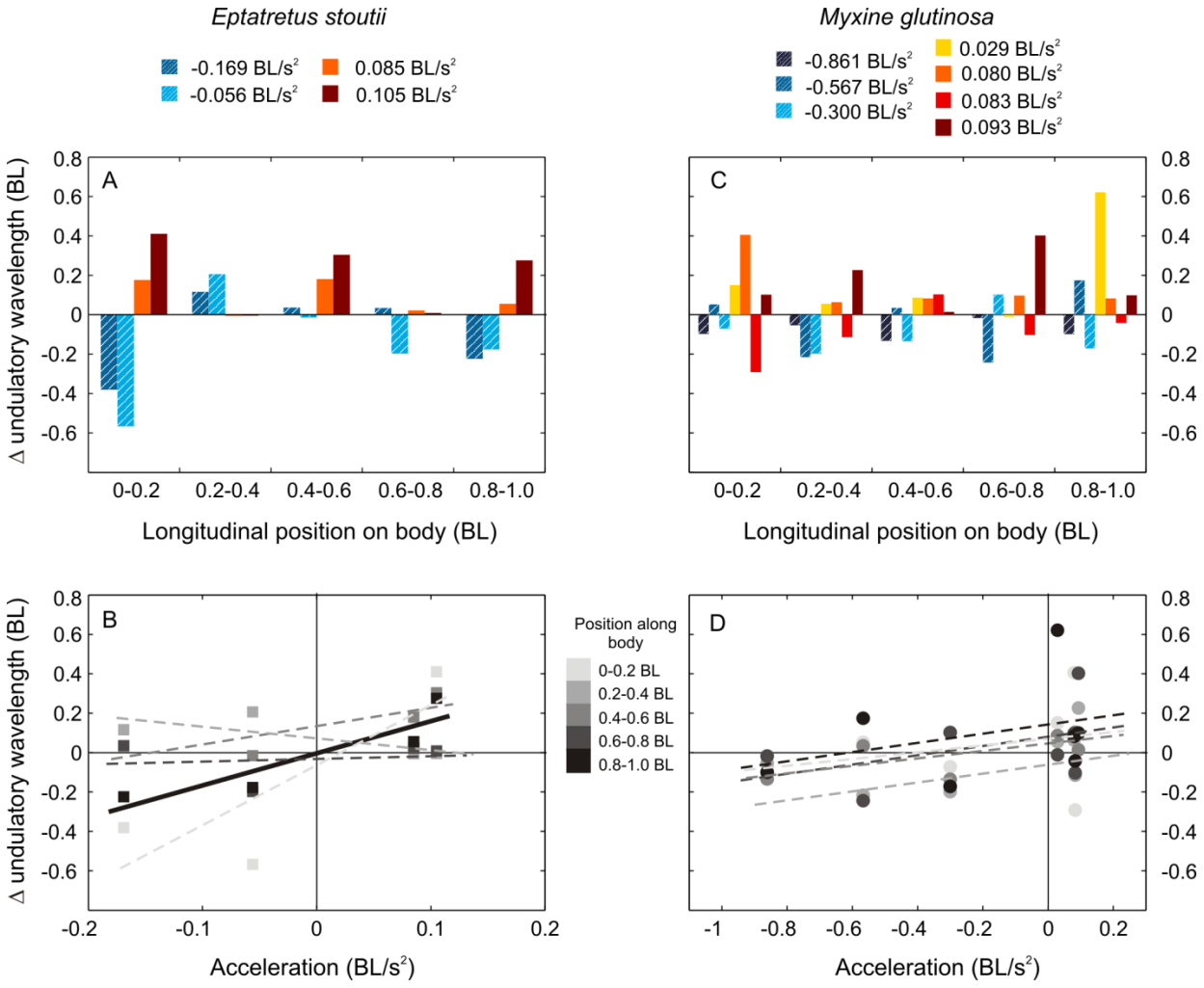

Figure 2.6 (Continued)

In contrast, no obvious patterns between acceleration and wave speed or wavelength change emerged in *M. glutinosa* (Figures 2.5C, D, 2.6C, D). For both species combined, however, wavelength did vary significantly with acceleration when averaged across the whole body (Table 2.1). Slip, the ratio between average forward swim speed and average rearward wave speed, did not show a consistent pattern of variation with acceleration for either species of hagfish (Figure 2.7). Rather, instances of growth and decline in slip were observed for both accelerating and decelerating hagfish.

Lateral maneuvers

During lateral maneuvers, Pacific hagfish (*E. stoutii*) modified their normal pattern of body undulation to traverse the flow tank floor while facing upstream into oncoming water flow. The head would first sweep laterally, then pause and come into contact with the ground while the undulatory wave travelled posteriorly (Figure 2.8A, B). As such, the anterior portion of the hagfish body is characterized by mostly unidirectional lateral travel with little midline overlap during a tail beat cycle, while caudal regions execute larger amplitude undulations (Figure 2.8A). Plotted trajectories of 25 equally-spaced points along the hagfish body clearly illustrate this cranio-caudal difference in lateral displacement, as well as the instances where points near the head pause in place (visible as small "knots" in the trajectory lines) while posterior body points continue to move laterally with increasing path overlap (bolded trajectories, Figure 2.8B).

Representative plots of body point velocity over time confirm the presence of static contact points at the head (Figure 2.8C). The lateral component velocity of a body point at 0.09 BL reaches zero or near-zero values between bouts of movement in the positive direction (Figure 2.8C, middle panel). Due to little motion in the axial direction, the resultant velocity shows a

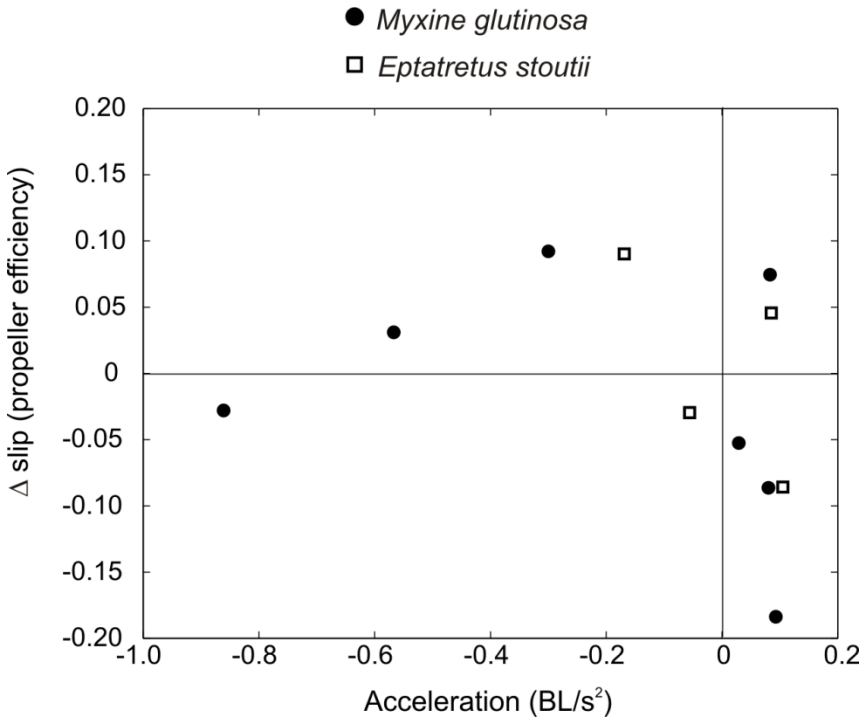

Figure 2.7. Change in slip (the ratio between forward swim speed and average rearward undulatory wave speed) did not show a consistent pattern of variation with acceleration for either *E. stoutii* (open squares) or *M. glutinosa* (filled circles).

Figure 2.8. A representative sequence of lateral maneuver swimming behavior by *E. stoutii* (BL 30.2 cm, flow speed 0.82 BL/s). (A) Ventral body midline drawings show that the overall direction of travel is perpendicular to the oncoming water flow. (B) Trajectories of 25 individual points along the body plotted through time illustrate that the anterior hagfish body moves largely unidirectionally, while the posterior body executes larger amplitude side-to-side movements. The trajectories of body points at 0.09 BL and 0.93 BL are represented by thick lines. Approximately 5 tail beat cycles are shown in (A) and (B). Axial, lateral, and resultant velocities of body points at (C) 0.09 BL and (D) 0.93 BL plotted over the course of approximately 3.5 tail beats demonstrate the presence of static contact points near the head (C) and lack thereof near the tail (D). Note the different scales of the y-axis in (C) and (D).

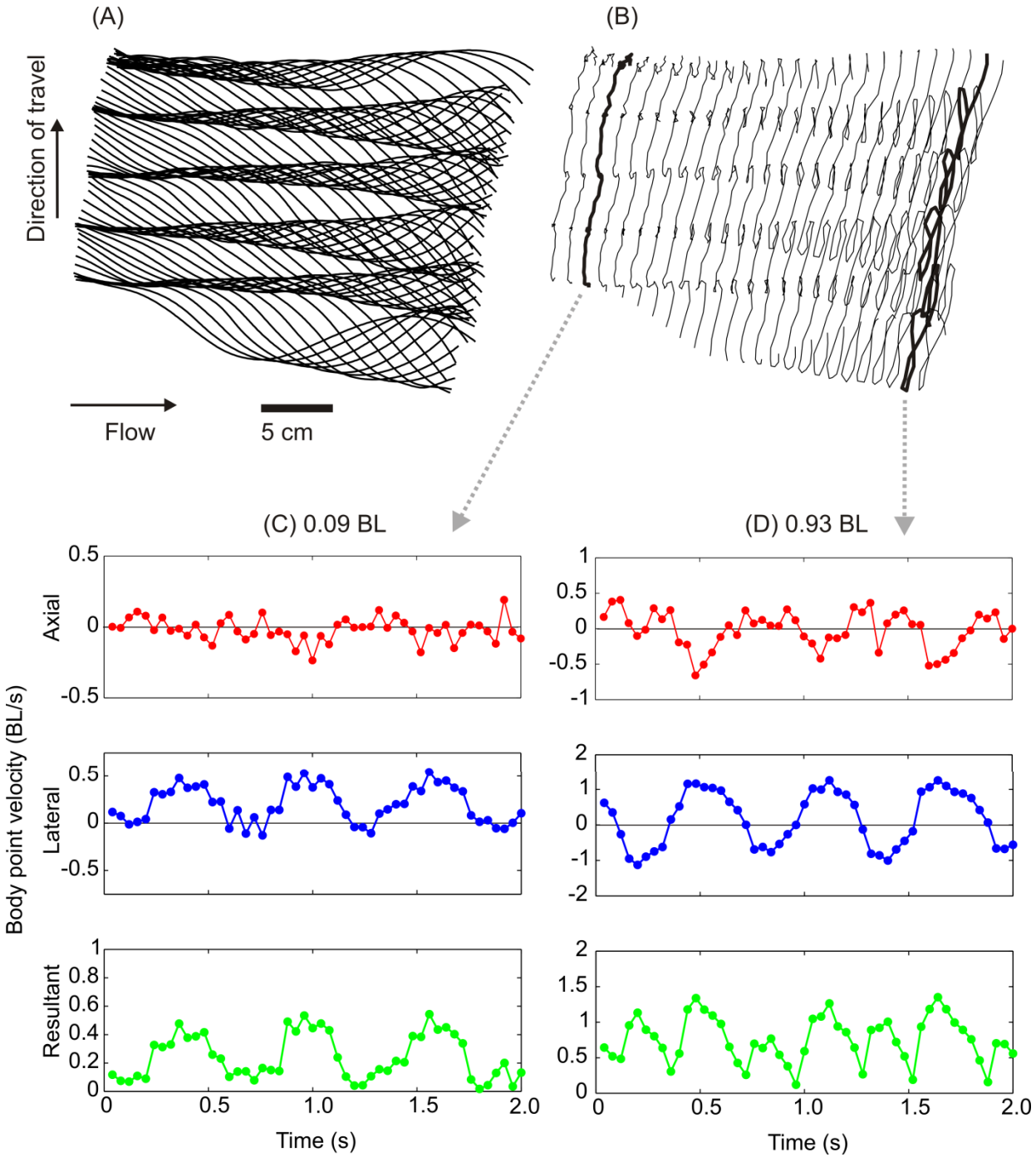

Figure 2.8 (Continued)

similar pattern where one undulation cycle is represented by one peak in velocity as the body point moves laterally (Figure 2.8C, bottom panel). In contrast, lateral velocity near the tail tip (0.93 BL) never sits at zero (Figure 2.8D, middle panel) and resultant velocity peaks twice during a single undulation cycle (Figure 2.8D, bottom panel), both patterns reflecting the motion of the posterior body back and forth.

Greater oncoming flow speeds were correlated with lower tail beat amplitudes (TBA) in lateral maneuvers (Figure 2.9A; Table 2.2). Similarly, flow speed had a significant effect on amplitude along the body (Table 2.2), which tended to decrease as flow speed increased (Figure 2.10B). While the repeated measures model failed to detect a significant effect of longitudinal position (LP) on undulatory amplitude, the distinct amplitude envelope of a hagfish body performing a lateral maneuver warrants describing. The anterior 40% of the body undulates at a relatively constant, low amplitude (<50% of maximum amplitude near the tail tip), while the posterior 60% of the body undulates with increasingly large amplitude before reducing slightly at the tail (Figure 2.10A).

Tail beat frequency (TBF) was positively correlated with flow speed (Figure 2.9B), but there were no significant effects of speed or longitudinal position on undulatory frequency along the body (Table 2.2). Tail tip speed, which is proportional to the product of TBA and TBF, remained relatively constant with greater flow speeds (Figure 2.9C), as did the nose:tail tip amplitude ratio (Figure 2.9E). Both the Strouhal number (*St*) (Figure 2.9D) and the angle of the hagfish body relative to the oncoming flow (Figure 2.9F) tended to decrease with higher flow speeds during lateral maneuvers, although neither correlation was significant.

Undulatory wave speed and wavelength varied considerably along the length of the hagfish body (Figure 2.11). Both longitudinal position and LP x flow speed were significant

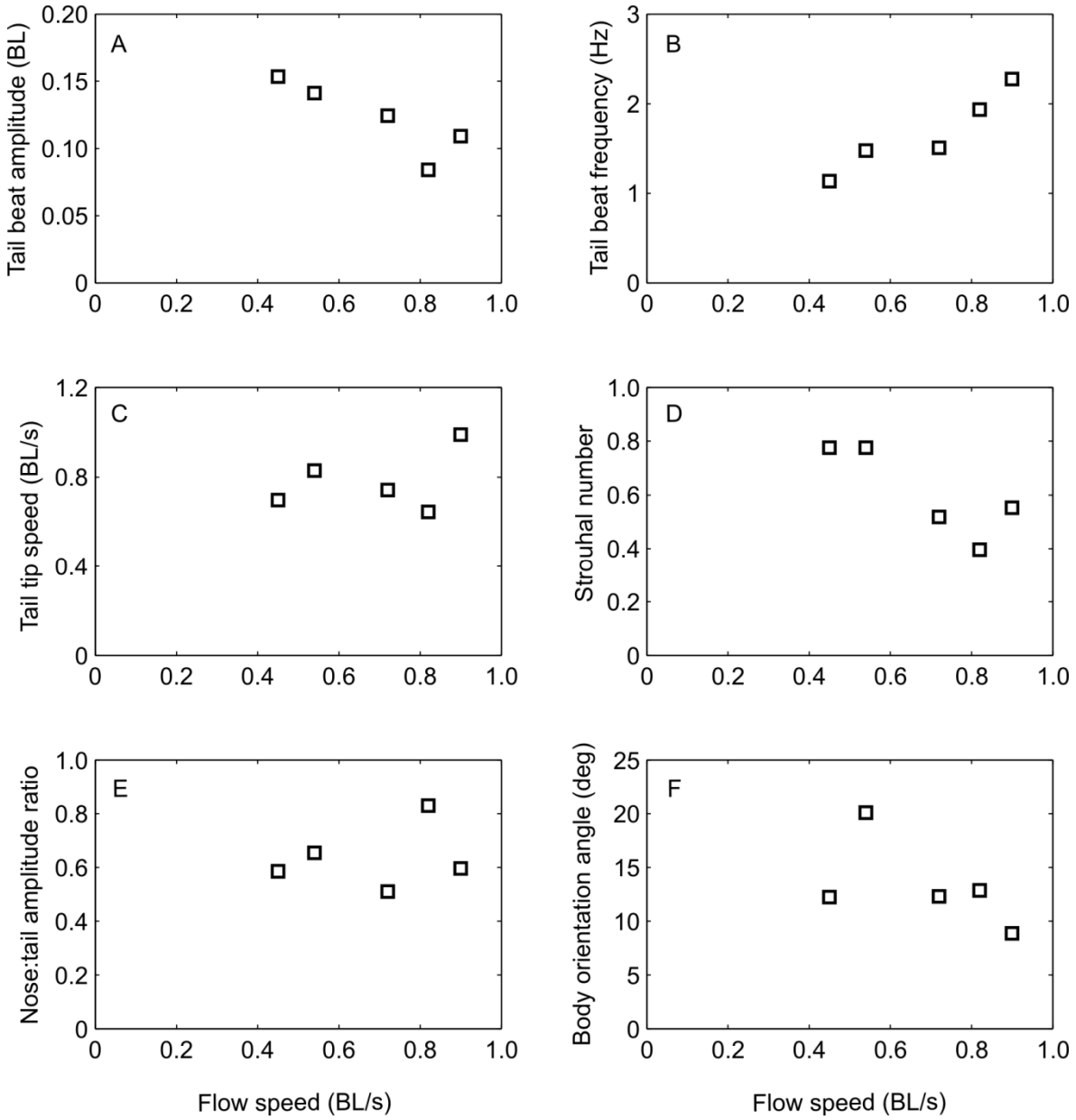

Figure 2.9. Relationships between single-measure kinematics and oncoming flow speed in *E. stoutii* performing lateral maneuvers. (A) Tail beat amplitude decreased with flow speed over the range of speeds recorded here (see Table 2.2). (B) Tail beat frequency increased with flow speed. (C-F) Tail tip speed, Strouhal number (*St*), nose:tail tip amplitude ratio, and body orientation angle showed no statistically significant correlation with flow speed, though (D) *St* and (F) the angle of the body relative to oncoming flow tended to decrease as flow speed increased.

Table 2.2. Linear correlation and repeated measures general linear model results for kinematic measurements on *E. stoutii* performing lateral maneuvers.

Kinematic variable with single measure	Linear correlation with flow speed	
	Spearman's ρ	*p*
Tail beat amplitude (BL)	-0.90	**0.037**
Tail beat frequency (Hz)	1.00	**<0.001**
Tail tip speed (BL/s)	0.30	0.624
Nose:tail tip amplitude ratio	0.30	0.624
Strouhal number	-0.70	0.188
Slip (propeller efficiency)	0.60	0.285
Body orientation angle (deg)	-0.30	0.624

Kinematic variable with repeated measures along the body	Repeated measures general linear model					
	Between-individuals effects		Within-individuals effects			
	Flow speed		Longitudinal position (LP)		LP x Flow speed	
	F ratio	*p*	*F* ratio	*p*	*F* ratio	*p*
Undulatory amplitude (BL)	21.23	**0.019**	0.06	0.978	0.45	0.724
Max body segment angle (deg)	5.86	0.094	8.32	**0.015**	2.20	0.185
Undulatory wave frequency (Hz)	7.46	0.072	0.68	0.620	0.08	0.986
Undulatory wave speed (BL/s)	1.16	0.360	34.08	**<0.001**	30.24	**<0.001**
Undulatory wavelength (BL)	36.10	**0.009**	11.70	**<0.001**	7.65	**0.003**

p-values in bold denote significance at the alpha = 0.05 level

Random effects tests indicated that individual had no effect on any variables

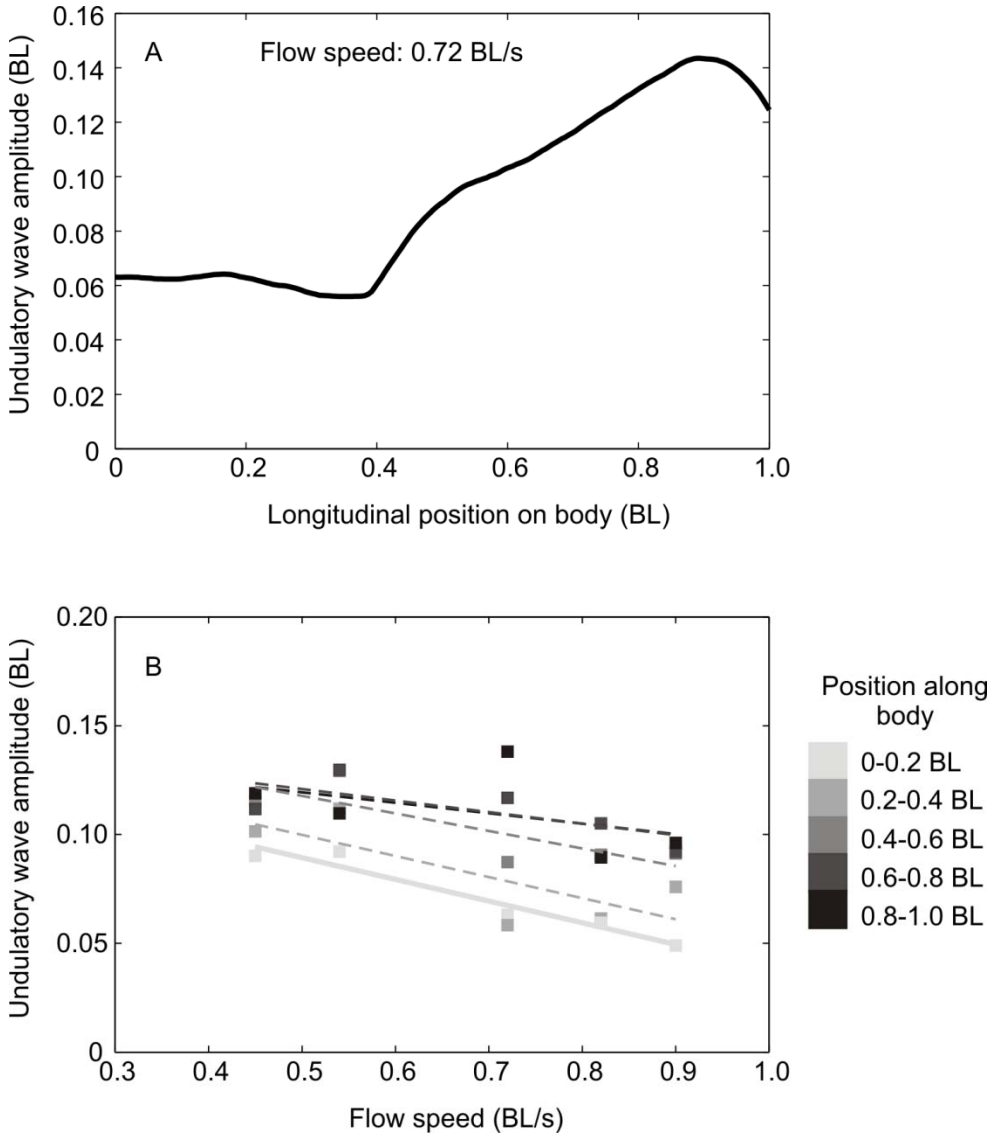

Figure 2.10. Undulatory amplitude as a function of (A) position along the body (representative example) and (B) flow speed during lateral maneuvers in *E. stoutii*. (A) The amplitude envelope along the body is distinct even though a repeated measures model failed to detect a significant effect of longitudinal position on amplitude. (B) Amplitude tended to decrease with increasing flow speed, particularly at the head. Darker shades correspond to more caudal positions along the body. Trend lines are Ordinary Least Squares fits, where solid thick lines represent correlation coefficient magnitudes $r > 0.9$, and dashed lines represent coefficient magnitudes of $r < 0.9$.

Figure 2.11. (A, B) Undulatory wave speed and (C, D) wavelength as a function of position along the body and flow speed during lateral maneuvers in *E. stoutii*. (A, C) Both wave speed and wavelength significantly varied along the body. (B, D) Relationships between wave speed and flow speed and wavelength and flow speed differed at different body segments. Wave speed tended to increase with flow speed at the posterior end (B), while wavelength tended to decrease with flow speed at the anterior end (D). Darker shades correspond to more caudal positions along the body. Trend lines are Ordinary Least Squares fits, where solid thick lines represent correlation coefficient magnitudes $r > 0.9$, and dashed lines represent coefficient magnitudes of $r < 0.9$.

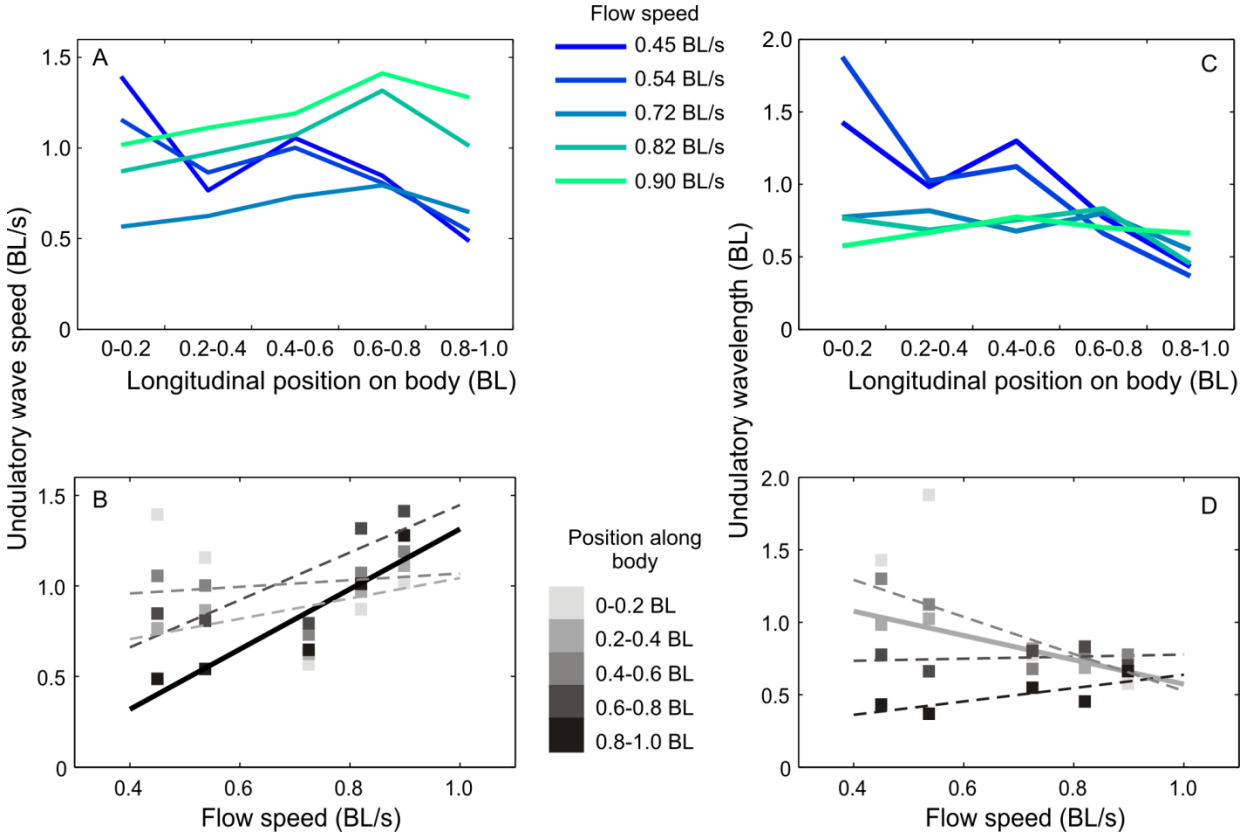

Figure 2.11 (Continued)

effects on wave speed and wavelength (Table 2.2), indicating different patterns of variation in these wave variables along the body and across flow speeds. Wave speed tended to increase with flow speed at the caudal end (Figure 2.11B), while wavelength tended to decrease with flow speed at the anterior end (Figure 2.11D) and also varied with flow speed between individual hagfish. Slip was not significantly correlated with flow speed (Table 2.2) though it generally increased as flow speed increased (Figure 2.12).

The degree of flexion at different body segments varied significantly with longitudinal position (Table 2.2). In general, smaller body angles were observed at higher speeds (Figure 2.13) even though speed was not identified as a significant factor by the statistical model.

Discussion

In this chapter, I quantify the kinematics of the body undulatory wave in hagfishes performing two different unsteady swimming behaviors: linear accelerations and lateral maneuvers. For linear accelerations, which were performed by both *Myxine glutinosa* and *Eptatretus stoutii*, I examine how kinematic variables change along the bodies of individual hagfish throughout decelerating or accelerating swimming cycles. For lateral maneuvers, which were readily performed by only *E. stoutii*, I examine how kinematics change along the body over a range of flow speeds. I describe the mechanisms of linear accelerations and lateral maneuvers in hagfish, and include how the kinematics of these unsteady behaviors compare to those in hagfish steady swimming, as well as in other elongate animals.

Mechanism of linear accelerations

In Chapter 1, I found that hagfish voluntary steady swimming speeds were relatively low

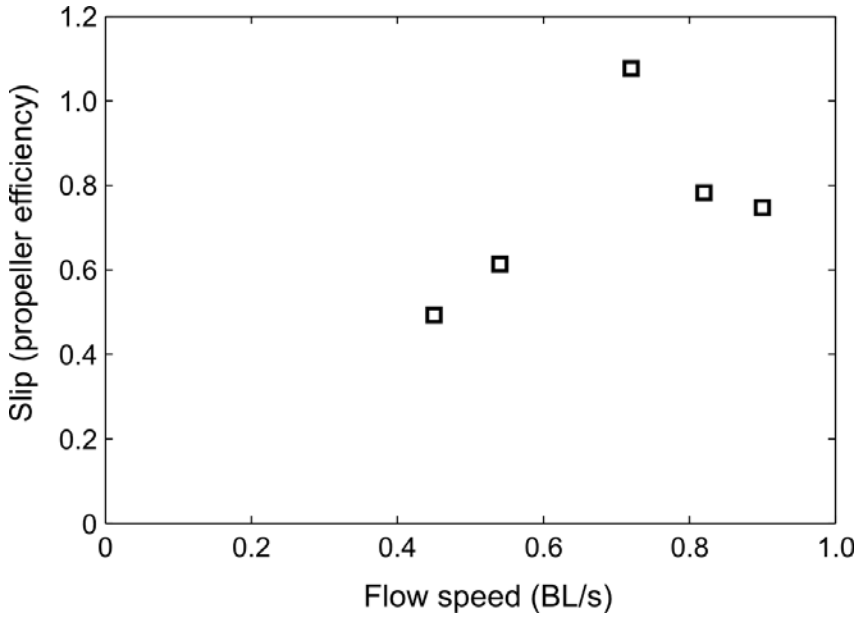

Figure 2.12. Slip generally increased with increasing flow speed during lateral maneuvers, though this trend was not statistically significant.

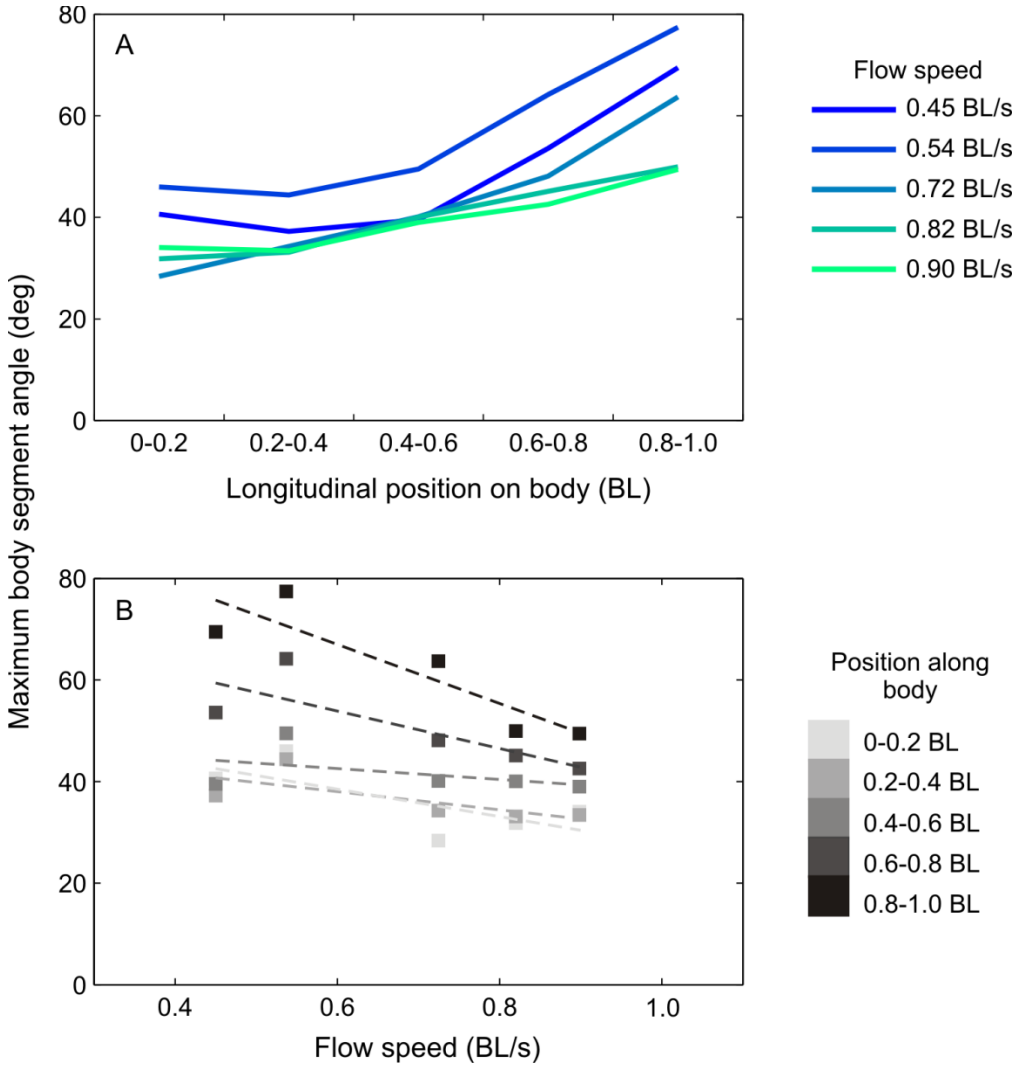

Figure 2.13. Maximum body segment angle as a function of longitudinal position and flow speed during lateral maneuvers in *E. stoutii*. (A) Body segment angles varied along the body, tending to increase toward the caudal end. (B) Body segment angles tended to decrease with increasing flow speed, though flow speed was not a significant factor in the statistical model. Darker shades correspond to more caudal positions along the body. Trend lines are Ordinary Least Squares fits, where dashed lines represent coefficient magnitudes of $r < 0.9$.

compared to other elongate anguilliform swimmers. Similarly, positive linear accelerations by hagfishes were fairly low: the maximum acceleration measured in *E. stoutii* here was 0.1 BL/s^2, while eels have been recorded accelerating at 1.3 BL/s^2 (Tytell, 2004b). Patterns and trends in kinematic changes over a range of accelerations were more apparent in *E. stoutii* than in *M. glutinosa.* Here, I present a mechanism for how hagfish of the species *E. stoutii* accelerate and decelerate by changing the kinematics of their body undulatory wave, and compare kinematics between species when patterns are discernible.

Accelerating in *E. stoutii* generally involves more exaggerated, high amplitude movements that change the shape of the body's undulatory wave as it is swimming. Increasing amplitude (Figure 2.3), flexion (Figure 2.4), and wavelength along the body (Figure 2.6) all result in the hagfish bending into a larger, longer wave. Conversely, slowing down (decelerating) is associated with the anterior body bending less, lower amplitudes along the body, and smaller wavelengths resulting in more waves along the hagfish body. Changes in kinematic variables were often more evident at the head in *E. stoutii.* In addition to undulatory amplitude and body segment angle, wave speed along anterior body segments also grew markedly during accelerations (Figure 2.5A). Increased recruitment of the head during linear accelerations has previously been reported for the American eel *Anguilla rostrata*, which also increases amplitude along the body as it swims faster (Tytell, 2004b). However, head amplitude did not obviously increase at a faster rate than tail amplitude in hagfish, based on the variable relationship between changes in the nose:tail amplitude ratio and acceleration (Figure 2.2E).

The undulatory amplitude of posterior body regions also generally grew as *E. stoutii* accelerated forward (Figures 2.2A, 2.3A, B), though the trend was much less apparent in *M. glutinosa* (Figures 2.2A, 2.3C, D), and not statistically significant in either species. How changes

in other kinematic variables along the posterior body and at the tail tip contributed to accelerations was also less evident. Undulatory wave speed did not appear to be a primary kinematic variable in modulating acceleration, despite its positive relationship with acceleration near the head in *E. stoutii*. Along the rest of the body in both *E. stoutii* and *M. glutinosa*, changes in wave speed were inconsistent (Figure 2.5).

Modulation of tail beat frequency (TBF) over a range of accelerations was counterintuitive, with TBF growing as hagfish decelerated and TBF declining as hagfish accelerated (Figure 2.2B). This pattern can be explained by accounting for initial swimming speeds, however: at fast initial swim speeds, TBF is already high and increases further as the hagfish attempts swim against the fast oncoming flow. But TBF is likely nearing the upper limit of the hagfish's swimming capabilities, so the amount of frequency increase does not add enough thrust, resulting in the hagfish losing position and decelerating. At slow initial swim speeds, TBF is low and can actually decline while the hagfish is still accelerating, possibly because other variables (i.e. amplitude, wavelength) are increasing.

Tail tip speed also does not consistently change during acceleration or deceleration in hagfishes (Figure 2.2C). In eels, however, tail tip speed was found to be a main kinematic variable modulating acceleration (Tytell, 2004b). The importance of tail tip speed appears to be the main difference between hagfishes and eels during acceleration, as the changes in wavelength and amplitude observed here in hagfishes were also predicted to occur in undulating eels (Tytell, 2004b). Changes in slip (Figure 2.7) and Strouhal number (Figure 2.2D) — both simple estimates of efficiency for undulatory locomotion— had no apparent relationship with acceleration. This was likely due to contributing kinematic variables also lacking a clear relationship with acceleration, but also in part because the velocity used in calculating these

indices is steady swimming velocity rather than instantaneous velocity (Tytell, 2004b).

Accelerating versus swimming at different steady speeds

In comparing how hagfish change their body wave motion to accelerate *versus* to swim at a different steady speed, it is reasonable to predict that hagfish would perform similar actions in either case as they simply "speed up." However, the larger and longer undulatory wave that hagfish employ to accelerate contrasts with the smaller and shorter waves used when swimming at increasingly faster steady speeds (Chapter 1). Similarly, the greater involvement of anterior body regions and inconsistent contributions by caudal regions during acceleration differ sharply from the distinct role of the posterior body in controlling changes in steady speed. This diversity in kinematic approaches to speeding up suggests there are complex dynamic relationships between body wave modulation and fluid forces while changing and then maintaining speed (Tytell et al., 2010). Based on the kinematics of hagfish swimming recorded in this and the previous chapter, I propose that hagfish temporarily undulate with larger body waves to power their accelerations, much like other fishes bend their bodies into highly-curved shapes to accelerate during a fast-start (Domenici and Blake, 1997; Webb, 1983). In addition to the experimental work presented here for hagfish and for other body and caudal fin swimmers (Domenici and Blake, 1997; Tytell, 2004b), the particular importance of increased undulation amplitude to drive accelerations has also been demonstrated by mathematical models of flexible undulatory swimmers (McMillen and Holmes, 2006).

Mechanism of lateral maneuvers in hagfish

In Pacific hagfish (*E. stoutii*), the undulatory wave kinematics recorded from lateral maneuvers

and from steady forward swimming were surprisingly similar. Kinematic variables measured at the tail tip and along the body showed similar patterns of variation with flow speed for both types of swimming behavior. As in steady forward swimming, hagfish performing unsteady lateral maneuvers moved their bodies with smaller, shorter undulatory waves as oncoming flow speeds increased (Figures 2.10B, 2.11C, D). Faster flow speeds were also associated with less flexion along the body (Figure 2.13).

To understand how similar patterns of body undulation can give rise to two distinct swimming behaviors, I again focus on the hagfish head. Lateral maneuvers are made unique by the particular pattern of unsteady, unilateral motion of the anterior body and its interaction with the ground: the head first sweeps sideways, then stops and makes contact with the ground, and then sweeps sideways again in the same direction (Figure 2.8). This cycle is repeated as the hagfish translates across the ground, travelling perpendicular to the oncoming water flow. In either steady or accelerated forward swimming, however, the head oscillates from side-to-side without making obvious contact with the ground (Figure 2.1 and Chapter 1).

In contrast to the activity of anterior regions, the motion of the hagfish's posterior body regions differs little among lateral maneuvers, linear accelerations, and steady forward swimming. Posterior regions act as the primary source of propulsive thrust during lateral maneuvers as they execute larger amplitude movements than anterior regions at a given speed (Figures 2.1, 2.8A, B, and Chapter 1). As flow speed increases, tail beat amplitude decreases (Figure 2.9A), while tail beat frequency (Figure 2.9B) and wave speed along caudal regions increase (Figure 2.11B). This asymmetry in activity along the body during a lateral maneuver results in an amplitude envelope that is distinct from that seen in steady swimming (Figure 2.10A). The relatively flat, low amplitude section of the envelope representing the first 40% of

the body likely reflects that portion's direct interaction with the ground.

More interestingly, the differential interaction of body segments with the ground during hagfish lateral maneuvers results in the behavior's resemblance to sidewinding in terrestrial snakes. As with hagfish lateral maneuvers, during sidewinding the snake's overall direction of travel is largely perpendicular to the long axis of the body. Pure sidewinding combines lateral undulatory body motion with vertical body motion such that some segments of the body make static contact with the ground while intervening segments lift off the ground and move in the direction of travel (Gray, 1946; Jayne, 1986; Mosauer, 1930). Hagfish performing lateral maneuvers also use a static point of contact near the head as a pivot around which the rest of the body moves (Figure 2.8A, B). Plots of component velocities over time for such a contact point near the head on a hagfish moving underwater (Figure 2.8C) closely resemble the same plots from a sidewinding snake, *Nerodia fasciata*, on land (Jayne, 1986). Static contact is indicated by a body point's resultant velocity reaching zero, which occurs at the body point near the head but not near the tail in *E. stoutii* (Figure 2.8C, D).

Terrestrial sidewinding has been described in several snake species (Gray, 1946; Jayne, 1986; Mosauer, 1930) that all display specific kinematic features when using this locomotory mode. Based on data from this study on hagfish, certain features are either lacking or currently difficult to identify in hagfish performing lateral maneuvers. During snake sidewinding, there are typically two or three static contact points spread out along the body at any given time in an activity cycle, and these contact points travel down the body as the snake progresses (Gray, 1946; Mosauer, 1930). Tracks made in sand as successive body segments lay down are at an oblique angle to the direction of travel (Gray, 1946; Jayne, 1986). In contrast, during a hagfish lateral maneuver the portion of the body that contacts the ground appears to remain in one

location near the head. As a result, its tracks would be parallel to the direction of travel (Figure 2.8B). The vertical lifting of the body between static contact points also distinguishes snake sidewinding (Jayne, 1986; Mosauer, 1930). For hagfish lateral maneuvers, measured kinematics and observation of lateral view videos both suggest that the posterior half of the body is always lifted above the ground as it undulates and exerts forces on the water. Buoyant forces likely aid in lifting that may allow the posterior body to direct fluid forces to increase or decrease the anterior body's contact with the ground.

Higher resolution video from multiple angles and detailed analysis of the three-dimensional kinematics of lateral maneuvers in hagfish will help in quantitatively comparing this behavior to true sidewinding. This comparison would be valuable in furthering our understanding of diversity in aquatic locomotion, as to my knowledge, sidewinding-like locomotory behavior has not been previously reported for an aquatic animal. The precise function of hagfish lateral maneuvers has also yet to be understood. Observation of recorded swimming sequences suggests that hagfish used lateral maneuvering to seek walls for assisted swimming against oncoming water flow. Additional questions include whether water flow is needed to elicit lateral maneuvers, and whether all hagfish species are capable of performing this maneuver.

Masters of maneuvering

Many fishes possess discrete, deformable fins that they use to maneuver throughout the water column (Webb, 2004). Hagfishes are also highly maneuverable, but their maneuverability appears to arise from a whole-body dexterity. As was proposed for hagfish swimming steadily (Chapter 1), the structural flexibility of the hagfish body may lead to multiple ways in which the

body's undulatory wave can change to modulate unsteady swimming. Body surfaces may have more degrees of freedom to act as control surfaces during maneuvers (Webb, 1997). Differential activity along the body also appears to contribute to hagfish maneuverability. The kinematics of steady swimming conveyed the importance of the hagfish tail as a propulsor, but the unsteady data presented here suggest the importance of the head in maneuvering. For hagfish, the relative uniformity of the elongate body and lack of discrete fins as control surfaces for locomotion might be compensated for in part by the versatility in how different parts of the body function.

List of symbols and abbreviations

BL Body length of the fish

COM Center of mass

TBA Tail beat amplitude

TBF Tail beat frequency

St Strouhal number

LP Longitudinal position along the fish body

r Linear coefficient of correlation

Acknowledgements

I sincerely thank Timothy Winegard for his time and patience while transporting hagfish to Harvard University and assisting with data collection. I also thank Douglas Fudge and Timothy for collecting the live hagfish. George Lauder, Bruce Jayne, and members of the Lauder Lab provided helpful comments and stimulating discussion about this research. Special thanks also to Chuck Witt for providing invaluable Matlab code. This work was funded by NSF grant EFRI-

0938043 to George Lauder, the Harvard University OEB Department, and an NSERC Canada Graduate Scholarship to Jeanette Lim.

References

Adam, H. (1960). Different types of body movement in the hagfish, *Myxine glutinosa* L. *Nature* **188**, 595-596.

Campbell, B. (1940). Integration of locomotor behavior patterns of the hagfish. *J. Neurophysiol.* **3**, 323-328.

Carlson, R. L. and Lauder, G. V. (2011). Escaping the flow: boundary layer use by the darter *Etheostoma tetrazonum* (Percidae) during benthic station holding. *J. Exp. Biol.* **214**, 1181-1193.

D'Août, K. and Aerts, P. (1999). A kinematic comparison of forward and backward swimming in the eel *Anguilla anguilla*. *J. Exp. Biol.* **202**, 1511-1521.

Danos, N. and Lauder, G. V. (2007). The ontogeny of fin function during routine turns in zebrafish *Danio rerio*. *J. Exp. Biol.* **210**, 3374-3386.

Domenici, P. and Blake, R. W. (1997). The kinematics and performance of fish fast-start swimming. *J. Exp. Biol.* **200**, 1165-1178.

Drucker, E. G. and Lauder, G. V. (2001). Wake dynamics and fluid forces of turning maneuvers in sunfish. *J. Exp. Biol.* **204**, 431-442.

Gillis, G. B. (1997). Anguilliform locomotion in an elongate salamander (*Siren intermedia*): effects of speed on axial undulatory movements. *J. Exp. Biol.* **200**, 767-784.

Gray, J. (1946). The mechanism of locomotion in snakes. *J. Exp. Biol.* **23**, 101-120.

Hart, J. L. (1973). Pacific fishes of Canada. *Fish. Res. Board Can. Bull.* **180**, 1-740.

Jayne, B. C. (1986). Kinematics of terrestrial snake locomotion. *Copeia* **1986**, 915-927.

Koob, T. J. and Long, J. H., Jr. (2000). The vertebrate body axis: evolution and mechanical function. *Amer. Zool.* **40**, 1-18.

Liao, J. C. and Lauder, G. V. (2000). Function of the heterocercal tail in the white sturgeon: flow visualization during steady swimming and vertical maneuvering. *J. Exp. Biol.* **203**, 3585-3594.

Lighthill, M. J. (1970). Aquatic animal propulsion of high hydromechanical efficiency. *J. Fluid Mech.* **44**, 265-301.

Long, J. H., Jr., Koob-Emunds, M., Sinwell, B. and Koob, T. J. (2002). The notochord of hagfish *Myxine glutinosa*: visco-elastic properties and mechanical functions during steady swimming. *J. Exp. Biol.* **205**, 3819-3831.

Long, J. H., Shepherd, W. and Root, R. G. (1997). Maneuverability and reversible propulsion: how eel-like fish swim forward and backward using traveling body waves. In *Tenth International Symposium on Unmanned Untethered Submersible Technology: proceedings of the special session on bio-engineering research related to autonomous underwater vehicles*, pp. 118-134: Autonomous Undersea Systems Inst.

Martini, F. H. (1998). The ecology of hagfishes. In *The Biology of Hagfishes* (eds. J. M. Jørgensen, J. P. Lomholt, R. E. Weber and H. Malte), pp. 57-77. London: Chapman & Hall.

McMillen, T. and Holmes, P. (2006). An elastic rod model for anguilliform swimming. *J. Math. Biol.* **53**, 843-886.

Mosauer, W. (1930). A note on the sidewinding locomotion of snakes. *Am. Nat.* **64**, 179-183.

Müller, U. K., Stamhuis, E. J. and Videler, J. J. (2000). Hydrodynamics of unsteady fish swimming and the effects of body size: comparing the flow fields of fish larvae and adults. *J. Exp. Biol.* **203**, 193-206.

Schlichting, H. (1979). *Boundary-layer theory*. New York: McGraw-Hill.

Schrank, A. J. and Webb, P. W. (1998). Do body and fin form affect the abilities of fish to stabilize swimming during maneuvers through vertical and horizontal tubes? *Environ. Biol. Fish.* **53**, 365-371.

Shadwick, R. E. and Gemballa, S. (2006). Structure, kinematics, and muscle dynamics in undulatory swimming. In *Fish Biomechanics* (eds. R. E. Shadwick and G. V. Lauder), pp. 241-280. London: Elsevier Inc.

Singh, K. and Pedley, T. J. (2008). The hydrodynamics of flexible-body manoeuvres in swimming fish. *Physica D* **237**, 2234-2239.

Singh, K. and Pedley, T. J. (2012). Modelling lateral manoeuvres in fish. *J. Fluid Mech.* **697**, 1-34.

Sokal, R. R. and Rohlf, F. J. (1981). *Biometry: the principles and practice of statistics in biological research*. San Francisco: W. H. Freeman & Co.

Triantafyllou, G. S., Triantafyllou, M. S. and Grosenbaugh, M. A. (1993). Optimal thrust development in oscillating foils with application to fish propulsion. *J. Fluids Struct.* **7**, 205-224.

Tytell, E. D. (2004a). The hydrodynamics of eel swimming II. Effect of swimming speed. *J. Exp. Biol.* **207**, 3265-3279.

Tytell, E. D. (2004b). Kinematics and hydrodynamics of linear acceleration in eels, *Anguilla rostrata*. *Proc. R. Soc. Lond. B* **271**, 2535-2540.

Tytell, E. D., Hsu, C.-Y., Williams, T. L., Cohen, A. H. and Fauci, L. J. (2010). Interactions between internal forces, body stiffness, and fluid environment in a neuromechanical model of lamprey swimming. *Proc. Nat. Acad. Sci. USA* **107**, 19832-19837.

Tytell, E. D. and Lauder, G. V. (2004). The hydrodynamics of eel swimming I. Wake structure. *J. Exp. Biol.* **207**, 1825-1841.

Vogel, S. (2003). *Comparative Biomechanics: Life's Physical World*. Princeton: Princeton University Press.

Webb, P. W. (1983). Speed, acceleration and manoeuvrability of two teleost fishes. *J. Exp. Biol.* **102**, 115-122.

Webb, P. W. (1997). Designs for stability and maneuverability in aquatic vertebrates: what can we learn? In *Tenth International Symposium on Unmanned Untethered Submersible Technology: proceedings of the special session on bio-engineering research related to autonomous underwater vehicles*, pp. 86-103: Autonomous Undersea Systems Inst.

Webb, P. W. (2004). Maneuverability – General issues. *IEEE J. Oceanic Eng.* **29**, 547-555.

Wilga, C. D. and Lauder, G. V. (2002). Function of the heterocercal tail in sharks: quantitative wake dynamics during steady horizontal swimming and vertical maneuvering. *J. Exp. Biol.* **205**, 2365-2374.

Zintzen, V., Roberts, C. D., Anderson, M. J., Stewart, A. L., Struthers, C. D. and Harvey, E. S. (2011). Hagfish predatory behaviour and slime defence mechanism. *Sci. Rep.* **1**:131 doi: 10.1038/srep00131.

Chapter 3

Hydrodynamics of steady and unsteady swimming in the Pacific hagfish, *Eptatretus stoutii*

Abstract

Experimental and theoretical studies on the hydrodynamics of anguilliform swimming have revealed striking similarities in fluid flow patterns generated by swimmers ranging from live freshwater eels to robotic lamprey models and leeches. Hagfishes share general characteristics in body shape and swimming patterns with these elongate undulatory swimmers, but distinct aspects of the hagfish's reduced morphology and varied kinematics during different swimming behaviors may translate into distinct hydrodynamic patterns as well. To examine how hagfish manipulate their fluid environment to achieve diverse swimming behaviors, I use particle image velocimetry to visualize and quantify flow fields around Pacific hagfish (*Eptatretus stoutii*) performing bouts of steady and unsteady swimming. For all swimming behaviors, formation of wake flow structures begins along the hagfish body as high amplitude undulations draw and propel fluid along the body. During steady swimming, the wake consists of caudo-laterally-directed fluid jets (60 ± 2.4 degrees, mean angle ± SEM) between opposite-sign vortices, suggesting vortex rings shed into the wake. Measured wake variables did not correlate with swim speed, but the consistently angled jets in the hagfish wake differ from laterally-directed jets reported for other anguilliform swimmers. Throughout accelerating tail beats, fluid jets in the hagfish wake oriented more caudally and widened, and the force producing these jets increased. During lateral swimming, where the hagfish body travels perpendicular to its long axis, wake jets were asymmetrically oriented, contributing both forward and lateral thrust over a complete tail beat. The hydrodynamic patterns elucidated here reinforce kinematics-based mechanistic hypotheses on how hagfishes enact their various swimming behaviors.

Introduction

Hagfishes can be broadly categorized as anguilliform-mode swimmers. In the classic description of this swimming mode, animals pass waves of bending down the length of their bodies to propel forward through the water (Breder, 1926; Gillis, 1996; Webb, 1975). Extending focus beyond the body's motion and to the fluid surrounding the animal, experimental and theoretical studies on the hydrodynamics of anguilliform swimming have revealed striking similarities in fluid flow patterns produced by diverse swimmers. Wake flows behind steady swimming American and European eels (Müller et al., 2001; Tytell, 2004a; Tytell and Lauder, 2004), robotic lamprey models (Hultmark et al., 2007; Leftwich et al., 2012), and leeches (Chen et al., 2011), for instance, consist of alternating fluid jets oriented nearly perpendicular to the path of travel. This wake signifies a balance between thrust and drag along the length of the body (Müller et al., 2001; Tytell and Lauder, 2004), rather than separate production of these forces at an oscillating tail fin and more stationary body, respectively (Müller et al., 1997). In addition to their wake flow patterns, these anguilliform swimmers also have in common an elongate, flexible body that changes little in profile along its entire length.

Hagfishes share this general body shape, but they have unique anatomical features that may influence the mechanics of their swimming. Lacking fully developed vertebrae (Ota et al., 2011), adult hagfish retain a flexible cartilaginous notochord that serves as their main propulsive axis (Long et al., 2002). Pronounced or paired fins are absent along the hagfish body, which is cylindrical with moderate lateral compression toward the caudal end (Figure 3.1) (Hart, 1973). Whole-body kinematic analyses of swimming behaviors in two different species of hagfish (Pacific hagfish, *Eptatretus stoutii*, and Atlantic hagfish, *Myxine glutinosa*) provided an initial picture of how hagfishes move their highly bendable bodies to execute different locomotory

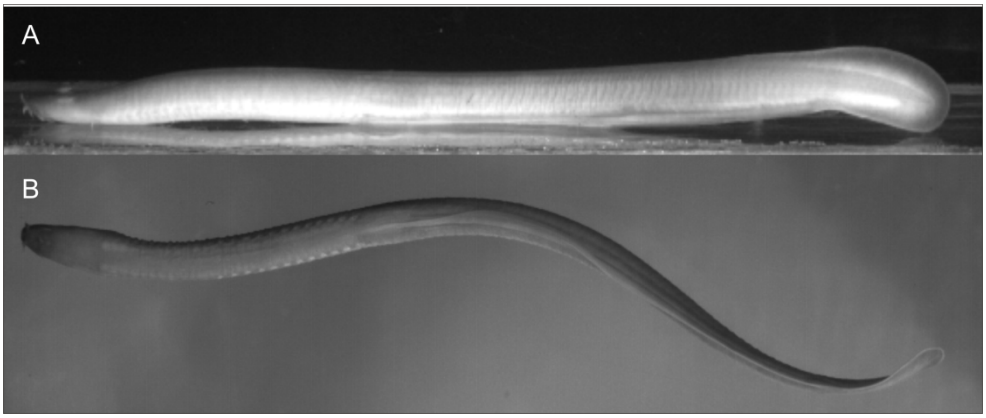

Figure 3.1. (A) Lateral and (B) ventral views of a Pacific hagfish (*Eptatretus stoutii*) swimming in the experimental flow tank.

behaviors (Chapters 1 and 2). During both steady and unsteady swimming, hagfish display an impressive degree of diversity in how they can alter the kinematics of their undulatory wave at specific body regions to modulate swim speed or direction. While performing a lateral maneuver across a bottom substrate, for example, the Pacific hagfish resembled a snake sidewinding on land (Chapter 2) more than the average conjured image of a typical fish shape swimming underwater. Even during steady forward swimming, hagfish body motion patterns often differed from those observed for eels (Tytell, 2004a), after which the "anguilliform" mode was named (Breder, 1926). This variety in the kinematics of hagfish swimming suggests that their body-fluid interactions may not necessarily be typical of other anguilliform swimmers as well.

Using their undulatory kinematics as a basis, I previously proposed mechanistic accounts of how hagfish modulate steady swim speed (Chapter 1), accelerate during linear accelerations, and translate across the substrate during lateral maneuvers (Chapter 2). In this chapter, I (1) examine how hagfish manipulate their fluid environment to achieve these different swimming behaviors by visualizing and quantifying fluid flows produced by Pacific hagfish (*Eptatretus stoutii*) performing bouts of steady and unsteady swimming; (2) integrate kinematics and hydrodynamics to explore whether hydrodynamic patterns of hagfish swimming are congruent with proposed mechanisms of propulsion based on kinematics; and (3) compare hagfish to other elongate anguilliform swimmers in terms of their fluid flow patterns and force production capabilities. An increasing number of theoretical studies have begun to exploit the freedom of a modeled system and examine how the fluid mechanics of undulatory swimming are influenced by prescribed changes in body motion or mechanics (e.g. Ferreira de Sousa and Allen, 2011; Tytell et al., 2010b). The hagfish presents an opportunity to expand on our understanding of locomotor diversity and function through experimental work, as it is a live organism with

documented abilities to execute a rich repertoire of controlled swimming behaviors using a simple body morphology.

Materials and Methods

Experimental animals

Pacific hagfish (*Eptatretus stoutii*, Lockington) were collected in baited traps from Barkley Sound, British Columbia, with assistance from the Bamfield Marine Sciences Centre. The hagfish were transported to an aquarium facility at Harvard University and maintained in a recirculating artificial seawater tank (8 – 9°C, 35‰) on a 12:12 hour light:dark cycle while fed frozen squid monthly. Swimming behaviors were recorded from four individuals ranging from 23.0 – 30.3 cm in body length (BL) (mean BL ± standard deviation, 28.0 ± 3.4 cm). All procedures and experiments were conducted in accordance with Harvard University IACUC guidelines (protocol # 20-03).

Quantifying flow around swimming hagfish

Particle image velocimetry (PIV) was used to visualize and quantify flows around swimming hagfish. Individual hagfish were placed in an 84 x 28 x 28 cm working section of a recirculating, variable-speed flow tank containing artificial seawater (9°C, 35‰) seeded with neutrally buoyant 50 μm plastic beads (Degussa Corp., Piscataway, NJ). A continuous argon-ion laser (10 W, Coherent Inc., Santa Clara, CA) directed through a beveled cylindrical lens produced a 2 mm thick horizontal light sheet that illuminated a slice of the seeded water. The laser sheet was positioned approximately 15 mm above the floor of the flow tank as *E. stoutii* tended to swim at the bottom of the tank. In previous studies, the same flow tank was found to have a boundary

layer thickness of approximately 2 – 7 mm at flow speeds similar to the lowest speeds recorded in the present study (Carlson and Lauder, 2011; Tytell and Lauder, 2004). Because these boundary layer values are smaller than the light sheet height and the body depths of hagfish used in this study, and because the boundary layer thins as flow speed increases (Schlichting, 1979), it was assumed that boundary layer flows had a negligible effect on swimming and hydrodynamics measured here. Hagfish were prompted to swim by slowly increasing the speed of water flow in the tank or by gently prodding the underside of the hagfish's caudal end. Specific swimming behaviors (described below) and the speed at which they were performed by hagfish were voluntary. A digital high-speed video camera (500 frames/s, 1024 x 1024 pixels, Photron USA Inc., San Diego, CA) aimed at a 45 degree-angled mirror below the clear tank bottom filmed ventral views of the hagfish and the plastic particles in the water as they moved through the light sheet.

Filmed swimming sequences that were subsequently analyzed consisted of 2 – 5 consecutive tail beats of a given swimming behavior. DaVis software (v. 7.2.2, LaVision Inc., Goettingen, Germany) was used to calibrate video frames and then quantify fluid velocity and vorticity from particle movement over time. An FFT-based cross-correlation routine processed pairs of video frames in two passes (16 x 16 pixel interrogation areas with 50% overlap) to produce a two-dimensional matrix of velocity vectors. Average free-stream velocity was subtracted from raw vector maps to highlight hagfish-generated flows (as opposed to flows generated by the flow tank impeller), and obvious erroneous vectors were manually deleted to validate the vector map. Images of velocity vector fields presented here display a subset of vectors for visual clarity, but the entire matrix was used in all quantitative analyses. Validated PIV vector maps were imported into Matlab (R2011a, The Mathworks Inc., Natick, MA) where a

custom routine (written by Eric Tytell, Harvard University, 2005) was used to define and measure flow structures in the swimming hagfish wake. Identifiable fluid jets in the wake were measured for their instantaneous mean vector angle, diameter, mean and maximum speed, and mean axial and lateral velocity components (parallel and perpendicular to the free-stream, respectively). A fluid jet typically occurred between two opposite-sign vorticity centers and was therefore assumed to be the central jet of a vortex ring to permit simplified calculations of force production in the wake (Müller et al., 2001; Tytell and Lauder, 2004). The circulation of this vortex ring, representing its strength, was measured as the line integral of the velocity along the jet's main axis through the center of the vortex ring (Stamhuis and Nauwelaerts, 2005; Tytell and Lauder, 2004). Vortex ring impulse (I) was then calculated as:

$$I = \tfrac{1}{4}\pi\rho\Gamma h d$$

where ρ is the fluid density, Γ is the vortex ring circulation, d is the diameter of the vortex ring (approximated as the measured jet diameter), and h is the height of the ring (approximated by the depth of the hagfish body, 1.75 cm) (Tytell and Lauder, 2004). Previous PIV studies on swimming fishes have demonstrated that vortex ring height closely matches caudal fin height (Lauder, 2000), such that vortex rings may actually be more oval-shaped than circular (Tytell and Lauder, 2004). An estimate of the force generating the ring was calculated as the ring impulse divided by the time period between maximum lateral tail excursions (Müller et al., 2001; Tytell and Lauder, 2004), as a sweep of the hagfish tail from one side to the other would typically produce a single vortex ring.

Basic kinematic analysis

Basic tail tip kinematics were also measured from PIV video recordings to confirm that individuals in this study were swimming within the range of kinematics observed in hagfish from previous chapters. Photron Motion Tools software (v.1.3) was used to record the two-dimensional (*x, y*) coordinates of the hagfish tail tip at each maximum lateral excursion. These position data and their corresponding times were used to estimate tail beat amplitude (TBA), tail beat frequency (TBF), tail tip speed, and Strouhal number (*St*). TBA was measured as half the distance between maximum lateral tail excursions within a tail beat cycle; TBF was calculated as the inverse of the period of a tail beat cycle; tail tip speed was calculated as the total distance travelled by the tail tip over a complete tail beat divided by the beat period; and *St*, a dimensionless ratio that indicates the amount of oscillatory motion by a fin or wing that gives rise to forward motion, was calculated as the product between 2·TBA and TBF divided by forward swim speed (Triantafyllou et al., 1993; Tytell et al., 2010a; Vogel, 2003).

Swimming speed and acceleration were measured using position data from a designated location on the hagfish body that was visible in all video frames. Steady swimming was defined as less than a 10% change in swim speed over a whole tail beat cycle. The range of steady swimming speeds over which *E. stoutii* voluntarily swam was 0.33 to 0.78 BL/s. Hagfish were also observed executing unsteady swimming behaviors, though they occurred less frequently than steady swimming. Linear accelerations were one example of unsteady swimming, defined as a greater than 10% change in swim speed while maintaining a direction of travel parallel to the oncoming water flow. Acceleration was measured as the slope of the ordinary least squares regression line fit to swim speed data over time for a complete tail beat, and ranged from -0.12 to 0.12 BL/s^2; however, only one swimming sequence with an acceleration of 0.063 BL/s^2 was

suitable for hydrodynamic analysis of the wake. Lateral swimming was another unsteady behavior recorded, where changes in swim speed in the axial direction are still less than 10%, but the overall direction of travel is perpendicular to the oncoming flow and long axis of the hagfish body. The general term "lateral swimming" is used here to distinguish the behavior from "lateral maneuvers," for which a precise kinematic description was provided in Chapter 2. Hagfish lateral maneuvers were characterized by instances of contact between the anterior hagfish body and the flow tank floor, which could not be observed in PIV videos that often did not capture the whole hagfish body. In this study, hagfish performed lateral swimming bouts at flow speeds of 0.25 and 0.71 BL/s.

Statistical analysis

When available, multiple measurements were averaged within individual hagfish to provide a better estimate of kinematic and hydrodynamic variables. For bouts of steady swimming, kinematic and hydrodynamic data were averaged over multiple complete tail beats. For linear accelerations, the change in kinematic and hydrodynamic quantities over consecutive tail beats was calculated to demonstrate the effect of acceleration during swimming. For lateral swimming, hydrodynamic data were averaged over half tail beats to reveal any differences between left and right lateral tail excursions. When appropriate, data were normalized by dividing by body length, an all data were $\log_{10}$ transformed prior to statistical analysis. A Spearman's non-parametric correlation test was used to detect relationships between kinematics and swim speed, and hydrodynamics and swim speed, for steady forward swimming. As only 2 to 3 instances of each unsteady swimming behavior were observed, kinematics and hydrodynamics could not be related to swim speed or acceleration. Rather, general descriptions and quantities characterizing each

behavior are given. All statistical analyses were performed with JMP Pro 10 (SAS Institute, Inc., Cary, NC).

Results

Basic kinematics of steady and unsteady swimming

For steady swimming *E. stoutii*, tail tip speed was the only kinematic variable measured that significantly correlated with swim speed, increasing as swim speed increased (Figure 3.2, Table 3.1). The other tail tip variables measured (tail beat amplitude (TBA), tail beat frequency (TBF), and Strouhal number (*St*)) showed a high degree of inter-individual variability and did not vary with swim speed consistently over the range of speeds observed in this study, but were within the range of steady swimming kinematics reported for *E. stoutii* in Chapter 1. Similarly, hagfish performing bouts of lateral swimming had tail tip kinematics similar to those observed during lateral maneuvers (Chapter 2) and steady swimming within the range of swim speeds recorded. Finally, changes in kinematic variables as hagfish accelerated were consistent with the major kinematic trends identified in Chapter 2 for similar initial swim speeds. In brief, TBA and TBF increase throughout an acceleration. Tail tip speed and Strouhal number are both proportional to TBA and TBF, and as a result, both increase as well.

Hydrodynamics of steady swimming

Flow visualization around the posterior half of a steadily swimming hagfish reveals that formation of wake flow structures begins along the body. As the hagfish undulates, fluid is drawn into the concave side of a large-amplitude body bend (Figure 3.3, region A; Figure 3.4, t = 0 s, region C) and travels with the bend along the body toward the tail tip before forming a fluid

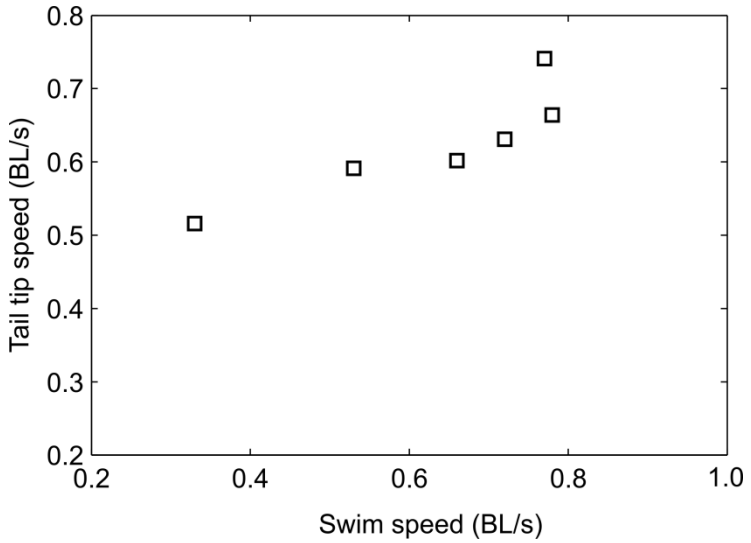

Figure 3.2. Average tail tip speed was the only kinematic variable that correlated significantly with swim speed during steady swimming in *E. stoutii* (see Table 3.1).

Table 3.1. Non-parametric linear correlation results between kinematics and swim speed in Pacific hagfish (*Eptatretus stoutii*) during steady forward swimming. Means and standard error of the mean (SEM) are calculated from data across all swim speeds. Swim speed range = 0.33 – 0.78 BL/s, mean swim speed = 0.63 BL/s.

	Linear correlation with swim speed		**Mean across swim speeds ± SEM**
Kinematic variable	Spearman's ρ	*p*	
Tail beat amplitude (BL)	0.26	0.623	0.12 ± 0.01
Tail beat frequency (Hz)	0.09	0.872	1.38 ± 0.13
Tail tip speed (BL/s)	0.94	**0.005**	0.62 ± 0.03
Strouhal number	-0.49	0.329	0.54 ± 0.07

p- values in bold denote significance at the alpha = 0.05 level

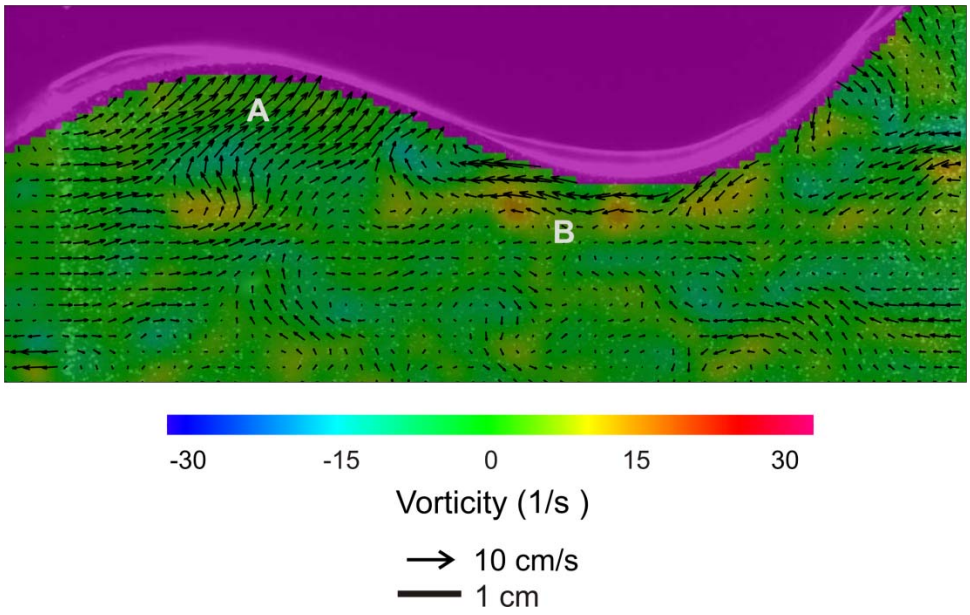

Figure 3.3. Ventral view of a typical flow field around the body of a steady swimming Pacific hagfish (BL = 30.3 cm, swim speed = 0.53 BL/s). Fluid velocity vectors are represented by black arrows, and the vorticity field is color-coded. Only every second vector is shown for clarity. Water flow is from left to right and the freestream velocity has been subtracted from the flow. The hagfish body and area to its right where laser light did not reach have been masked. Fluid is entrained along the concave bend of the anterior body (A) while flows that point upstream indicate drag incurred by the convex side of a body bend (B).

Figure 3.4. Representative time-series of ventral-view flows generated by a half-tail beat around the posterior body and in the wake of a steady swimming Pacific hagfish (BL = 23.0 cm, swim speed 0.33 BL/s). Fluid velocity vectors are represented by black arrows, and the vorticity field is color-coded. Only every second vector is shown for clarity. Water flow is from left to right and the freestream velocity has been subtracted from the flow. Large open arrows represent overall fluid jet direction. At t = 0 s, the tail tip is at its left-most excursion and has generated an angled jet (A) and region of negative vorticity at its tip (B). Fluid is drawn into the more anterior bend of the hagfish body (C). As the tail moves to the hagfish's right side, the negative vorticity at the tip is stretched (t = 0.11 s, B) before being shed into the wake (t = 0.22 s, B). At the same time, fluid drawn into the body bend (C) continues to travel caudally as the undulatory wave passes down the body, eventually forming a second angled jet as the tail reaches its right excursion (t = 0.33 s, C). As this second jet is shed into the wake, the negative vorticity first seen at t = 0 s has divided into two regions (t = 0.44 s, B1 and B2) that can be regarded as the two same-sign vortices shed per half-tail beat.

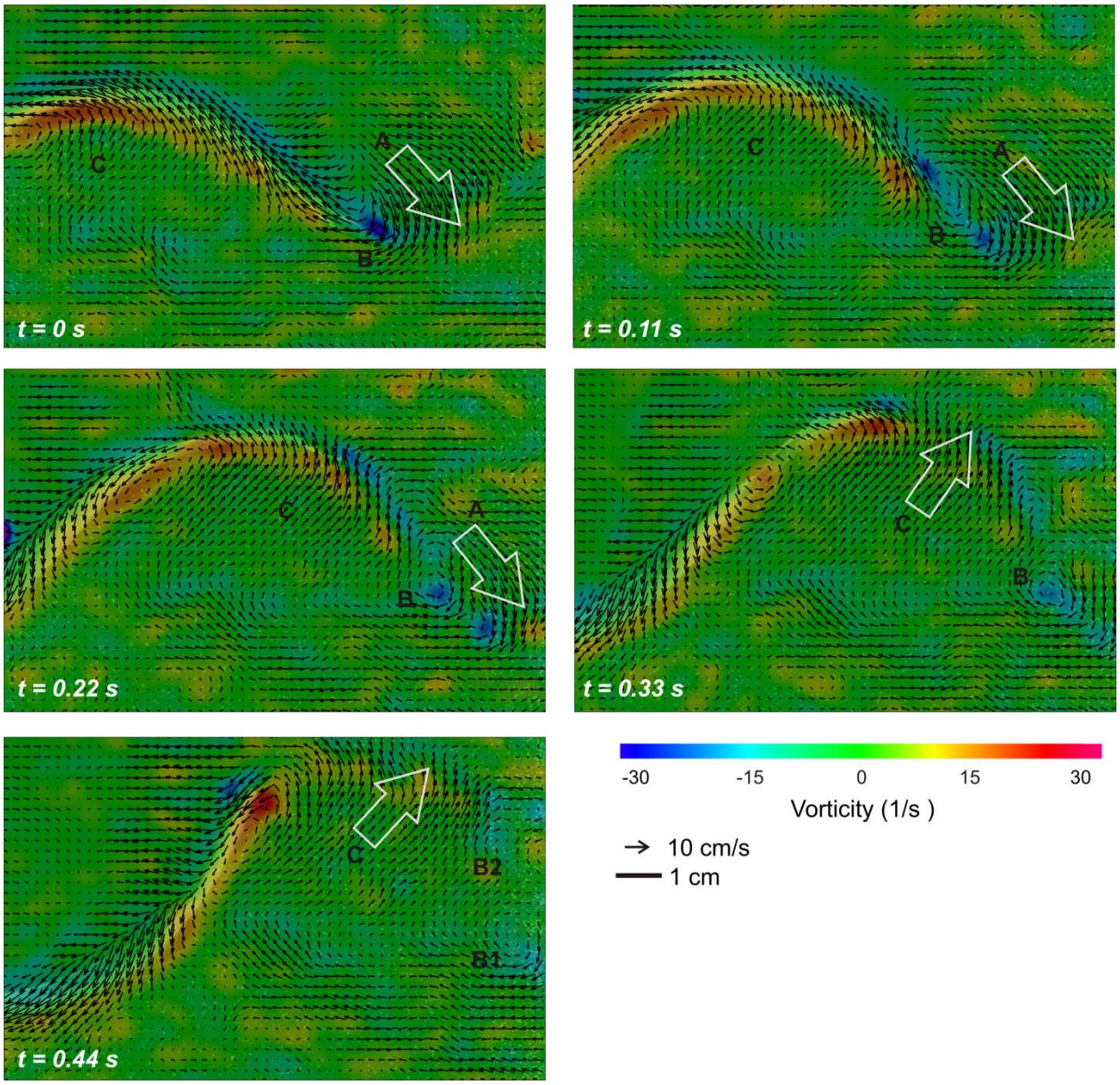

Figure 3.4 (Continued)

jet in the wake. The wake consists of caudo-laterally-directed jets with a mean angle of 60 degrees (± 2.4 degrees, SEM; Table 3.2) relative to the direction of travel (Figure 3.4, open white arrows). Two opposite-sign vortices on either side of the fluid jet are shed as the hagfish tail reaches its maximum lateral excursion, with the vortex core closest to the tail tip (labeled B in Figure 3.4, t = 0 s) being a stop-start vortex shed as the tail reverses direction. The tail tip continues to interact with this vortex as it sweeps to the other side, stretching the vortex across the span of the wake (Figure 3.4, t = 0.11 – 0.22 s). As the tail reaches its other maximum lateral excursion, the stretched vortex typically separates into two same-sign vortices (Figure 3.4, t = 0.44 s, B1 and B2), the second of which belongs to a newly formed fluid jet on the opposite side as the previous jet. The result of this undulatory swimming pattern is a wake consisting of two pairs of vortices per complete tail beat cycle, termed a "2P" wake (where "P" indicates pairs of vortices) (Hultmark et al., 2007).

This general wake pattern occurred for all swim speeds observed in the present study. Furthermore, hydrodynamic variables quantified from the hagfish wake did not significantly correlate with swimming speed for the range of speeds recorded here (Table 3.2). Figure 3.5 illustrates the high variability in fluid jet measurements, and Table 3.2 reports the means and standard error of the mean across all swim speeds for each hydrodynamic variable given the lack of an apparent speed effect.

Hydrodynamics of unsteady swimming

While only one swimming bout featuring a linear acceleration was suitable for a detailed hydrodynamic analysis, a brief description of the wake is still given here as a preliminary result. The general wake structure did not obviously differ from that observed for steady forward

Table 3.2. Non-parametric linear correlation results between jet wake hydrodynamics and swim speed in Pacific hagfish during steady forward swimming. Means and standard error of the mean (SEM) are calculated from data across all swim speeds. Swim speed range = 0.33 – 0.78 BL/s, mean swim speed = 0.63 BL/s.

	Linear correlation with swim speed		**Mean across swim speeds ± SEM**
Hydrodynamic variable	Spearman's ρ	*p*	
Jet angle (deg)	0.54	0.266	60.6 ± 2.4
Jet diameter (BL)	-0.26	0.623	0.18 ± 0.01
Max jet speed (BL/s)	0.20	0.704	0.42 ± 0.02
Mean jet speed (BL/s)	0.14	0.787	0.22 ± 0.01
Mean jet axial velocity (BL/s)	-0.31	0.544	0.09 ± 0.01
Mean jet lateral velocity (BL/s)	0.66	0.156	0.17 ± 0.01
Circulation (cm^2/s)	0.49	0.329	31.23 ± 1.53
Impulse (mN s)	0.09	0.872	2.11 ± 0.21
Force (mN)	0.20	0.704	7.08 ± 1.05

p-values in bold denote significance at the alpha = 0.05 level

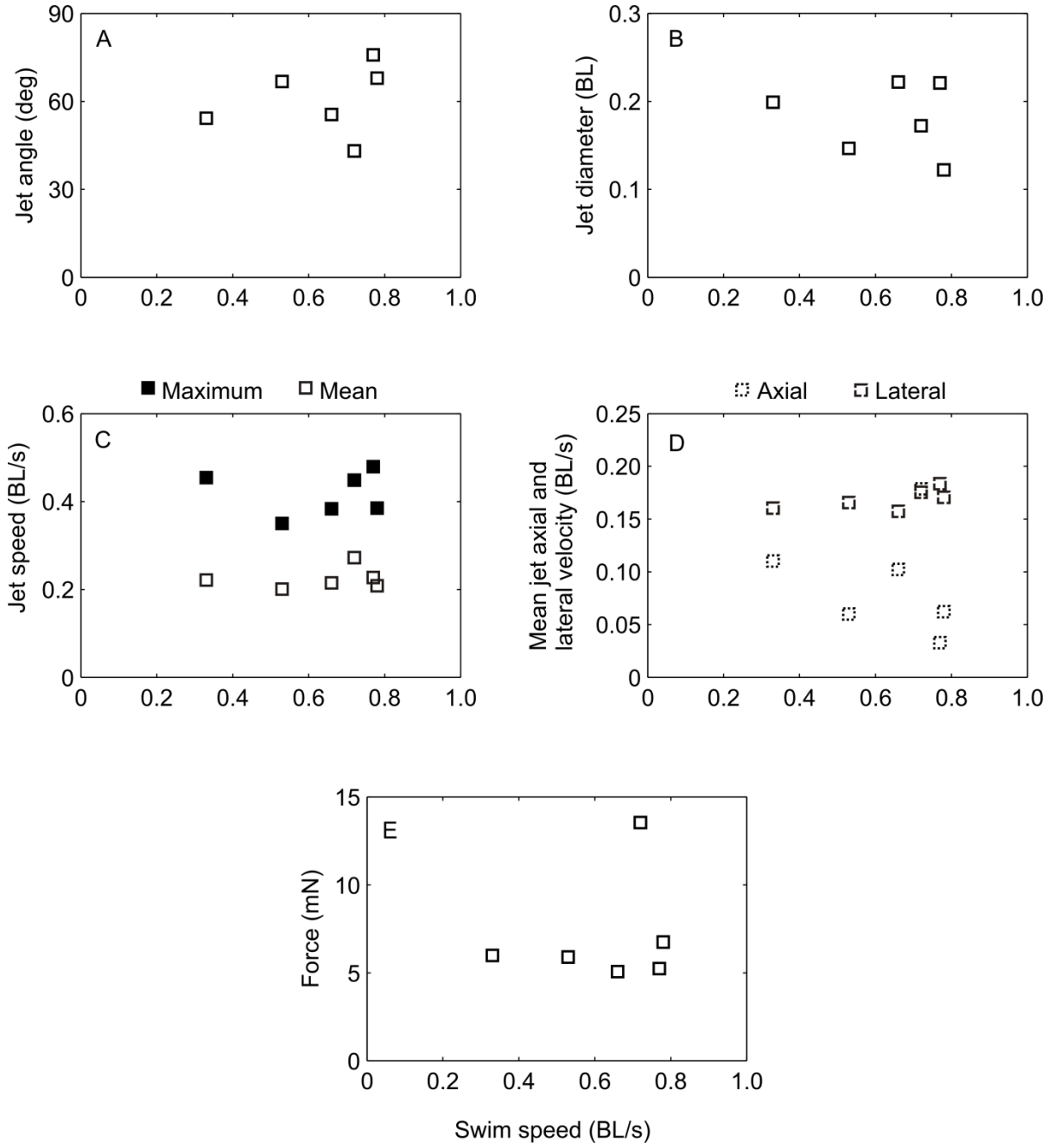

Figure 3.5. Relationships between hydrodynamic variables recorded in the wake and swim speed in steady forward swimming Pacific hagfish. None of the variables quantified significantly correlated with swim speed for the range of speeds recorded here (see Table 3.2).

swimming. While the magnitude of the acceleration was modest for a hagfish (0.063 BL/s^2 from an initial swim speed of 0.41 BL/s), changes in the fluid jets over the course of consecutive tail beats could still be quantified. As the hagfish accelerated, fluid jets originating at the tail oriented more caudally as jet angle declined and jet axial velocity increased (Table 3.3). Fluid jets also widened throughout accelerating tail beats, and the strength and force of presumptive vortex rings associated with the jets increased (Table 3.3).

Lateral swimming, in which the hagfish body axis is parallel to the oncoming flow while it travels laterally across the bottom of the flow tank, was characterized by asymmetry in the orientation of the wake. Fluid jets produced by the tail were angled differently on either side of the hagfish depending on its overall direction of travel. A representative time-series of velocity and vorticity fields around a hagfish swimming laterally toward its right show that wake jets on the left side are oriented more laterally (Figure 3.6, t = 0 s, arrow A), while jets on the right side are oriented more caudally (Figure 3.6, t = 0.24 s, arrow C). Figure 3.6 (t = 0.96 s) shows this asymmetrical arrangement for four separate fluid jets resulting from four side-to-side tail excursions during a rightward lateral swimming bout. When the hagfish swims toward its left, the arrangement reverses and jets on the right side are oriented more laterally than jets on the left side (Figure 3.7A, open bars). While the mean axial and lateral velocity components of the jet reflect this difference in jet angle (Figure 3.7D), the other hydrodynamic variables measured do not show the same pattern of variation with direction of travel (Figure 3.7B, C, E). Overall, the formation and structure of the hagfish wake during lateral swimming resemble the 2P wake observed during steady forward swimming. The hagfish's undulating body moves fluid toward the tail tip where it is shed as a jet with opposite-sign vortices on either side (Figure 3.6, t = 0 – 0.24 s). The side-to-side motion of the tail tip creates distinct bands of vorticity that separate into

Table 3.3. Amount of change in hydrodynamic variables measured in the jet wake relative to the start of a linear acceleration by a Pacific hagfish (initial swim speed = 0.41 BL/s, acceleration = 0.063 BL/s^2). A positive change indicates that the variable grew during the acceleration, while a negative change indicates that the variable declined.

Hydrodynamic variable	Change during acceleration
Jet angle (deg)	-20.4
Jet diameter (BL)	0.051
Max jet speed (BL/s)	0.015
Mean jet speed (BL/s)	-0.001
Mean jet axial velocity (BL/s)	0.057
Mean jet lateral velocity (BL/s)	-0.036
Circulation (cm^2/s)	3.79
Impulse (mN s)	1.15
Force (mN)	12.32

Figure 3.6. Representative time-series of ventral-view flows generated around the posterior body and in the wake of a Pacific hagfish (BL = 28.6 cm, swim speed 0.25 BL/s) swimming laterally toward its right (top of figure panels). Fluid velocity vectors are represented by black arrows, and the vorticity field is color-coded. Only every second vector is shown for clarity. Water flow is from left to right and the freestream velocity has been subtracted from the flow. Large open arrows represent overall fluid jet direction. At t = 0 s, the tail tip is shedding a fluid jet (A) directed laterally to its left. As the tail moves to the right (t = 0.24 s), positive vorticity generated along the body (B) travels to the tail tip and a second jet with a rearward component forms (C). The positive vorticity stretches as the tail tip moves to the hagfish's left (t = 0.48 s, B), which produces a third laterally-directed jet (t = 0.72 s, D). The negative band of vorticity that forms as the tail moves right again (t = 0.72 s, E) breaks up into two same-sign vortices (t = 0.96 s, E1 and E2). The first vortex (E1) is associated with jet (D) and the second vortex (E2) is associated with the forming caudally-directed jet (F).

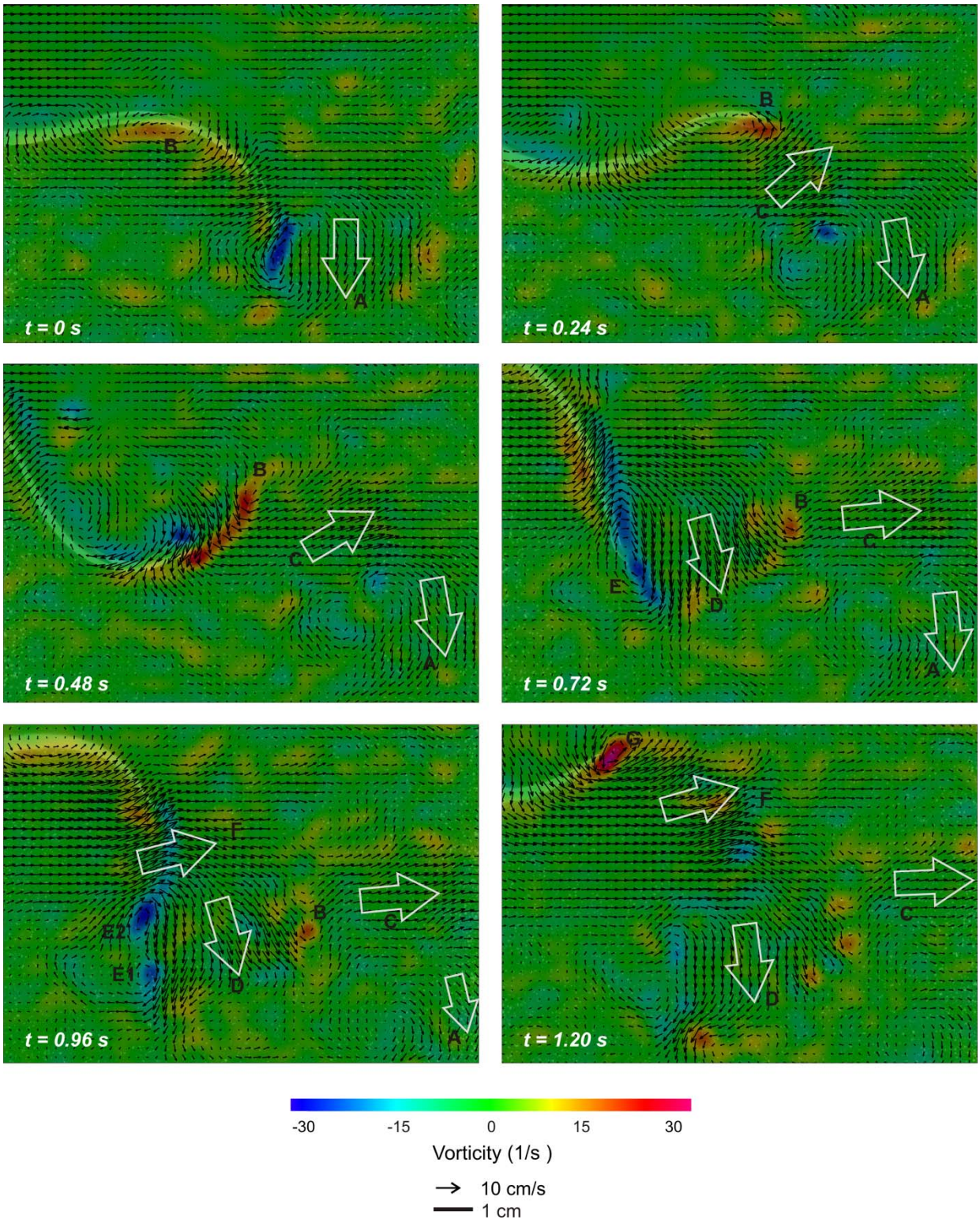

Figure 3.6 (Continued)

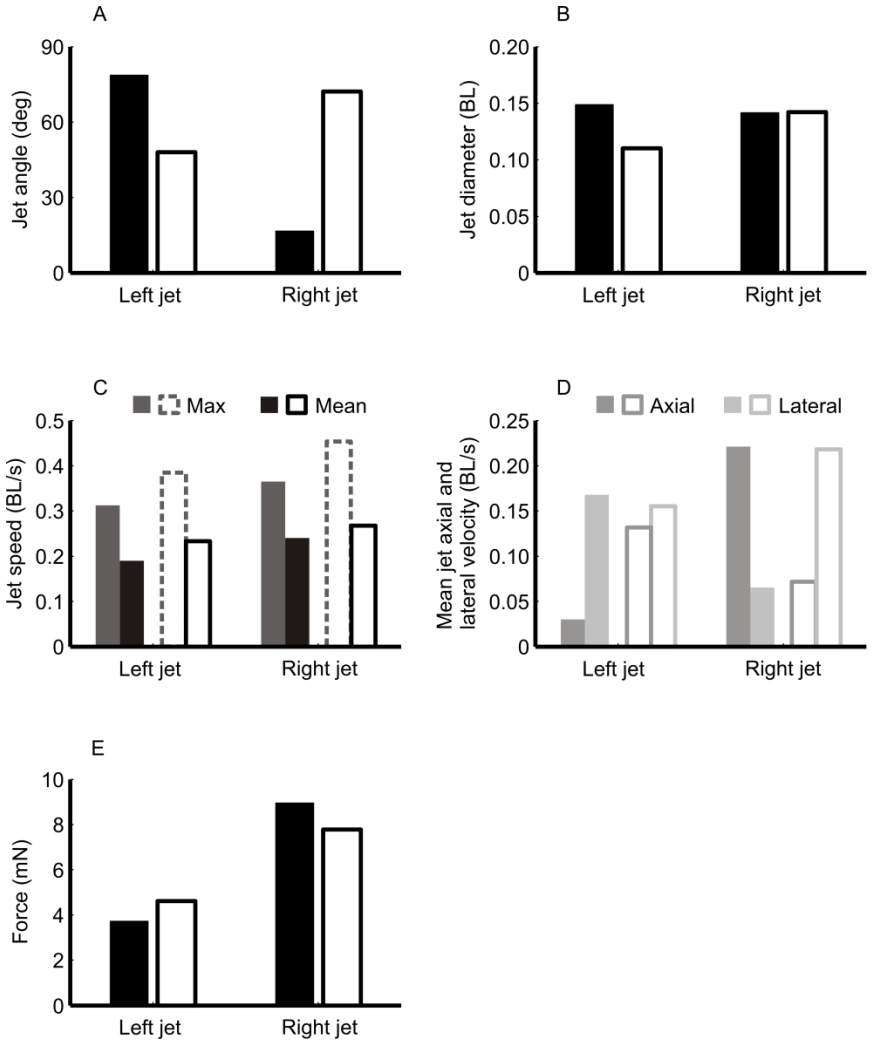

Figure 3.7. Hydrodynamic variables measured from the fluid jet wake during lateral swimming by Pacific hagfish. The solid bars represent a sequence where the hagfish is translating to the right at 0.25 BL/s, while the open bars represent a sequence where the hagfish is translating to the left at 0.71 BL/s. Plotted data are means for fluid jets produced at the left-most excursion ("left jet") and jets at the right-most excursion ("right jet"). (A) When a hagfish swims toward its right, jets on the left side are oriented more laterally than jets on the ride side. This arrangement reverses when the hagfish swims toward its left. This difference in jet angle is reflected in the axial and lateral velocity components of the jets (D), while the other variables measured do not show a consistent pattern of variation with direction of translation.

multiple same-sign vortices associated with different fluid jets (Figure 3.6, $t = 0.72 – 0.96$ s).

Discussion

The present study visualizes and quantifies the fluid flows produced by the Pacific hagfish (*Eptatretus stoutii*) during undulatory swimming. Swimming behaviors include steady swimming over a range of voluntary swim speeds, and specific instances of unsteady maneuvers (lateral swimming and linear acceleration). I describe the general structure of the hagfish wake for these swimming behaviors, and compare the flow field characteristics to those reported for other swimmers, particularly similarly-shaped eels of the genus *Anguilla*. I also relate the hydrodynamics of hagfish undulatory swimming to the whole-body kinematics measured in Chapters 1 and 2.

Wake morphology of steady swimming hagfish

Hagfish steady swimming is characterized by large amplitude, whole-body undulatory waves, and flows generated by the wave along the body directly contribute to the wake behind the hagfish. Fluid drawn into a concave bend on one side of the body is propagated toward the tail tip by the undulating wave and forms a wake jet between a pair of vortices on the contralateral side (Figure 3.4). A complete tail beat cycle results in two fluid jets on either side of the body and a characteristic 2P wake, in which two pairs of vortices are shed per tail beat cycle (Hultmark et al., 2007).

The same general organization of vortices has previously been found in the wakes of other elongate anguilliform swimmers, including American eels (*Anguilla rostrata*, (Tytell, 2004a; Tytell and Lauder, 2004)), European eels (*Anguilla anguilla*, (Müller et al., 2001)), and a

robotic elongate swimmer modelled after swimming lamprey (*Ichthyomyzon unicuspis*, (Hultmark et al., 2007)). The formation of the 2P wake configuration also appears to be similar among these anguilliform swimmers. From the band of vorticity that forms across the wake as the tail tip moves from one lateral maximum to the other, at least two separate same-sign vortices arise and contribute to fluid jets on opposite sides of the body (Figure 3.4). These vortices in the hagfish wake are equivalent to the primary and secondary vortices observed for swimming eels (Tytell and Lauder, 2004). Assuming that hagfish and eel wakes both consist of unlinked vortex rings (Müller et al., 2001; Tytell and Lauder, 2004), the primary vortex of one half tail beat and the secondary vortex of the previous half tail beat constitute the two counter-rotating vortices belonging to a single vortex ring. Over the course of a whole tail beat cycle, two vortex rings are produced and shed on opposite sides of the body.

Broadly in contrast to elongate anguilliform swimmers, carangiform swimmers typically produce a 2S wake, where two single counter-rotating vortices are shed per tail beat cycle and may represent a cross-section through linked vortex rings with angled jets (Lauder, 2000; Müller et al., 1997). Most of this difference in overall wake structure is thought to arise from differences in Strouhal number, which relates tail beat amplitude and frequency to forward swim speed (Tytell et al., 2010a), but also partly from differences in body morphology (Müller et al., 2001). For carangiform swimmers with a body that tapers to a narrow peduncle and a discrete caudal fin, it has been hypothesized that the body tends to incur drag while the caudal fin generates thrust visible in the wake as downstream flows (Müller et al., 1997). For anguilliform swimmers with elongate and relatively uniform body profiles, however, it is thought that thrust and drag are produced and balanced along the entire length of the body during steady swimming (Müller et al., 2001; Tytell and Lauder, 2004). Experimental evidence for this explanation comes from

steadily swimming eels that produce wakes consisting of laterally-directed fluid jets with little downstream momentum visible as rearward flows (Müller et al., 2001; Tytell, 2004a; Tytell and Lauder, 2004).

Hagfish and eels share similar body morphologies and overall wake structure, but interestingly, the hagfish wake differs in its orientation. In the wakes of American and European eels, jet angles are consistently 87 to 90 degrees relative to the direction of travel (Müller et al., 2001; Tytell, 2004a; Tytell and Lauder, 2004). Fluid jets in the wake of steady swimming Pacific hagfish, however, are directed caudo-laterally with a mean angle of approximately 61 degrees (Figure 3.4, Table 3.2), which is closer to jet angles reported for chub mackerel (*Scomber japonicus*) swimming steadily in the carangiform mode (Nauen and Lauder, 2002). Thrust visible in the hagfish wake as the fluid jet's downstream component suggests there is some division of drag and thrust along the elongate body of a steadily swimming hagfish. One potential reason for this difference in wake orientation between eels and hagfish may be differences in undulatory kinematics along the body. Flexion at the caudal end could differ enough to alter wake orientation, but differences in motion of the anterior body may affect downstream flows as well. Hagfish typically swim with large side-to-side head movements even at slow swimming speeds (Chapter 1), while eels keep their heads relatively still and undulate more posterior portions of their bodies during slow steady swimming (Gillis, 1998; Tytell, 2004a). The high amplitude bends that the hagfish anterior body undergoes appear to help entrain (Figure 3.3, region A) and transport fluid along the body for shedding at the tail, but they may also incur drag by increasing the body's projected area. Upstream-directed flows visible at the convex side of a body bend (Figure 3.3, region B) suggest that drag does exceed thrust at these regions.

Quantified hydrodynamics of steady swimming

The general structure of the hagfish wake described above remains the same over the range of swim speeds measured in this study, and interestingly, quantified variables from the jet wake also appear to be independent of swim speed (Figure 3.5). For steady swimming American eels, the wake retains the same organization of lateral jets over a four-fold increase in swimming speed, but the speed of the jets increases as swim speed increases (Tytell, 2004a). Wake jet speed does reach an upper limit for the eel, but not until swim speeds faster than 1.5 BL/s, well above the entire range over which hagfish swam in the present study. Complicating the interpretation of how swimming speed affects hydrodynamics in hagfish are the variable tail tip kinematics observed here. Tail tip speed appeared to be the only kinematic variable that correlated positively with swim speed (Figure 3.2), a result that differs from the kinematic analysis of Chapter 1 where tail tip speed remained relatively constant while tail beat frequency (TBF) increased and tail beat amplitude (TBA) decreased for steady swimming *E. stoutii*. Results from the present study do match those reported for eels, however, which also show a strong correlation between swim speed and tail tip speed, and little correlation of swim speed with TBF and TBA (Tytell, 2004a). This kinematic variability in the hagfish is also consistent with the hypothesis proposed in Chapter 1 that hagfish are capable of modulating swim speeds in a variety of ways.

Another potential explanation for the lack of apparent relationships between hydrodynamic variables and swim speed in hagfish is that the two-fold increase in swim speed was insufficient for revealing changes in the wake. Future studies of hagfish swimming hydrodynamics should attempt to elicit a wider range of swim speeds and simultaneously examine whole-body kinematics to gain a clearer picture of how kinematics and hydrodynamics interact during swimming. A third potential explanation, unrelated to the variability that arises

from working with live animals, is that wake variables are not expected to obviously change with swimming speed because changes in thrust and drag production would occur mostly along the body. Flows that are visible and can be measured in the wake may not entirely contribute to forward propulsion (Tytell and Lauder, 2004).

Nevertheless, the hydrodynamics of hagfish swimming have not been previously quantified to any extent, and data from the present study can be used to place hagfish in a context with other elongate undulatory swimmers in terms of force production capabilities. The mean caudo-lateral force associated with fluid jets in the wake of Pacific hagfish swimming between 0.33 and 0.78 BL/s was 7 mN, with one individual producing 13 mN of force while swimming at 0.72 BL/s (Table 3.2, Figure 3.5E). The hagfish jet's mean force is on the order of lateral jet forces measured in wakes of similarly sized American eels (1 – 6 mN) swimming between 0.55 and 1.88 BL/s (Tytell, 2004a), and juvenile European eels (1 mN) swimming at 1.5 BL/s (Müller et al., 2001). Similarly, typical jet speeds normalized for body length are comparable among the three species (0.2 – 0.3 BL/s) (Table 3.2) (Müller et al., 2001; Tytell, 2004a). That hagfish are generating jet speeds and forces of the same or greater magnitude than eels, but are swimming forward at slower speeds, likely indicates that hagfish are wasting more energy in producing their wakes during steady swimming. A direct comparison of swimming energetics in eels and hagfish under the same environmental conditions and swim speeds would help clarify how these species differ in swimming efficiency.

Maneuvers and the hagfish body as a control surface

For the instance of linear acceleration in *E. stoutii* that was analyzed in detail here, the changes in tail tip kinematics were consistent with those reported previously in Chapter 2. Based on the

whole-body kinematic analysis from that study, I proposed that hagfish undulated their bodies with larger-amplitude, longer-wavelength body waves to power their accelerations through water. Though caution should be taken in extending the current results because whole-body kinematics could not be observed here, that mechanistic hypothesis is supported by the hydrodynamic analysis undertaken here. The diameter of fluid jets in the wake has been shown to correlate positively with body wavelength in accelerating American eels (Tytell, 2004a). For the hagfish observed here, jet diameter grew by 0.05 BL throughout accelerating tail beats (Table 3.3), which represents a 30% increase from the initial diameter (data not shown). Because the impulse and force associated with these jets is proportional to the size of the jet, these quantities also increased during acceleration (Table 3.3). Interestingly, the change in mean jet velocity was small and likely did not contribute to the increase in force production. The jet angle, however, rotated 20 degrees (from approximately 65 to 44 degrees) such that a greater proportion of force was directed downstream. As in linearly accelerating American eels, this indicates the production of net thrust in the wake (Tytell, 2004b).

Reorientation of wake flows was also observed for hagfish performing lateral swimming. For these swimming bouts, asymmetrically oriented wake jets appear to directly steer the unsteady maneuver (Figure 3.6). Over one half of a tail beat cycle, the hagfish tail angles its fluid jets laterally and opposite to the direction of overall travel, providing force to translate the body across the substrate. Over the other half of the cycle, the tail angles its jets more caudally, generating forward thrust against oncoming flow (Figures 3.6, 3.7A). In contrast to steady forward swimming where laterally-directed flows from consecutive half tail beats cancel each other out on average (Tytell and Lauder, 2004), these asymmetrical flows sum and contribute to the hagfish's trajectory. This jet angle asymmetry weakened at the faster flow speed (Figure

3.7A, open bars), possibly reflecting decreased flexion along the body at higher flow speeds observed in Chapter 2. Nonetheless, the jet's angle appears to matter more than the magnitude of force in directing lateral swimming, as force did not show a consistent pattern of left/right variation with direction of travel for the swimming sequences observed (Figure 3.7E).

The importance of the hagfish tail's activity in this unsteady behavior is consistent with findings from the kinematic analysis of hagfish lateral maneuvers in Chapter 2. During lateral maneuvers, the unidirectional and saltatory motion of the anterior body across the substrate may produce less thrust than typical undulations, leaving posterior body regions to be the primary sources of thrust. This chapter's hydrodynamic analysis, however, demonstrates that the hagfish posterior body contributes substantially to steering as well. Other aquatic swimmers are also known to use asymmetry to direct fluid flows during unsteady maneuvers. Differential force production by left and right pectoral fins enables turning in bluegill sunfish (*Lepomis macrochirus* (Drucker and Lauder, 2001)), and the heterocercal caudal fin of white sturgeons (*Acipenser transmontanus*) adjusts jet flow angle to change vertical position in the water column while swimming forward (Liao and Lauder, 2000). Impressively, the hagfish achieves its maneuverability without the use of paired or discrete fins. The flow visualizations presented here support the idea that a relatively uniform and elongate body can exploit its flexibility and implement specific body regions as maneuverable control surfaces during swimming (Chapter 2).

List of symbols and abbreviations

BL Body length of the fish

I Vortex ring impulse

ρ Fluid density

Γ Vortex ring circulation

h Vortex ring height

d Vortex ring diameter

TBA Tail beat amplitude

TBF Tail beat frequency

St Strouhal number

Spearman's ρ Non-parametric coefficient of correlation

SEM Standard error of the mean

t Time

Acknowledgements

I sincerely thank Douglas Fudge and Timothy Winegard for collecting the hagfish, and Timothy for transporting the hagfish to Harvard facilities. I am especially grateful to George Lauder for his support during experiments and constructive comments during analysis, and members of the Lauder Lab for helpful discussions about this work. Special thanks also to Eric Tytell for providing invaluable Matlab code. Funding for this project was provided by NSF grant EFRI-0938043 to George Lauder, the Harvard University OEB Department, and a Robert A. Chapman Memorial Scholarship granted to Jeanette Lim.

References

Breder, C. M. (1926). The locomotion of fishes. *Zoologica* **4**, 159-297.

Carlson, R. L. and Lauder, G. V. (2011). Escaping the flow: boundary layer use by the darter *Etheostoma tetrazonum* (Percidae) during benthic station holding. *J. Exp. Biol.* **214**, 1181-1193.

Chen, J., Friesen, W. O. and Iwasaki, T. (2011). Mechanisms underlying rhythmic locomotion: body-fluid interaction in undulatory swimming. *J. Exp. Biol.* **214**, 561-274.

Drucker, E. G. and Lauder, G. V. (2001). Wake dynamics and fluid forces of turning maneuvers in sunfish. *J. Exp. Biol.* **204**, 431-442.

Ferreira de Sousa, P. J. S. A. and Allen, J. J. (2011). Thrust efficiency of harmonically oscillating flexible flat plates. *J. Fluid Mech.* **674**, 43-66.

Gillis, G. B. (1996). Undulatory locomotion in elongate aquatic vertebrates: Anguilliform swimming since Sir James Gray. *Amer. Zool.* **36**, 656-665.

Gillis, G. B. (1998). Environmental effects on undulatory locomotion in the American eel *Anguilla rostrata*: kinematics in water and on land. *J. Exp. Biol.* **201**, 949-961.

Hart, J. L. (1973). Pacific fishes of Canada. *Fish. Res. Board Can. Bull.* **180**, 1-740.

Hultmark, M., Leftwich, M. and Smits, A. J. (2007). Flowfield measurements in the wake of a robotic lamprey. *Exp. Fluids* **43**, 683-690.

Lauder, G. V. (2000). Function of the caudal fin during locomotion in fishes: kinematics, flow visualization, and evolutionary patterns. *Amer. Zool.* **40**, 101-122.

Leftwich, M. C., Tytell, E. D., Cohen, A. H. and Smits, A. J. (2012). Wake structures behind a swimming robotic lamprey with a passively flexible tail. *J. Exp. Biol.* **215**, 416-425.

Liao, J. C. and Lauder, G. V. (2000). Function of the heterocercal tail in the white sturgeon: flow visualization during steady swimming and vertical maneuvering. *J. Exp. Biol.* **203**, 3585-3594.

Long, J. H., Jr., Koob-Emunds, M., Sinwell, B. and Koob, T. J. (2002). The notochord of hagfish *Myxine glutinosa*: visco-elastic properties and mechanical functions during steady swimming. *J. Exp. Biol.* **205**, 3819-3831.

Müller, U. K., Smit, J., Stamhuis, E. J. and videler, J. J. (2001). How the body contributes to the wake in undulatory fish swimming: flow fields of a swimming eel (*Anguilla anguilla*). *J. Exp. Biol.* **204**, 2715-2762.

Müller, U. K., van den Heuvel, B. L. E., Stamhuis, E. J. and Videler, J. J. (1997). Fish foot prints: morphology and energetics of the wake behind a continuously swimming mullet (*Chelon labrosus* Risso). *J. Exp. Biol.* **200**, 2893-2906.

Nauen, J. C. and Lauder, G. V. (2002). Hydrodynamics of caudal fin locomotion by chub mackerel, *Scomber japonicus* (Scombridae). *J. Exp. Biol.* **205**, 1709-1724.

Ota, K. G., Fujimoto, S., Oisi, Y. and Kuratani, S. (2011). Identification of vertebra-like elements and their possible differentiation from sclerotomes in the hagfish. *Nat. Commun.* **2**:373 doi: 10.1038/ncomms1355.

Schlichting, H. (1979). *Boundary-layer theory*. New York: McGraw-Hill.

Stamhuis, E. J. and Nauwelaerts, S. (2005). Propulsive force calculations in swimming frogs II. Application of a vortex ring model to DPIV data. *J. Exp. Biol.* **208**, 1445-1451.

Triantafyllou, G. S., Triantafyllou, M. S. and Grosenbaugh, M. A. (1993). Optimal thrust development in oscillating foils with application to fish propulsion. *J. Fluids Struct.* **7**, 205-224.

Tytell, E. D. (2004a). The hydrodynamics of eel swimming II. Effect of swimming speed. *J. Exp. Biol.* **207**, 3265-3279.

Tytell, E. D. (2004b). Kinematics and hydrodynamics of linear acceleration in eels, *Anguilla rostrata*. *Proc. R. Soc. Lond. B* **271**, 2535-2540.

Tytell, E. D., Borazjani, I., Sotiropoulos, F., Baker, T. V., Anderson, E. J. and Lauder, G. V. (2010a). Disentangling the functional roles of morphology and motion in the swimming fish. *Integr. Comp. Biol.* **50**, 1140-1154.

Tytell, E. D., Hsu, C.-Y., Williams, T. L., Cohen, A. H. and Fauci, L. J. (2010b). Interactions between internal forces, body stiffness, and fluid environment in a neuromechanical model of lamprey swimming. *Proc. Nat. Acad. Sci. USA* **107**, 19832-19837.

Tytell, E. D. and Lauder, G. V. (2004). The hydrodynamics of eel swimming I. Wake structure. *J. Exp. Biol.* **207**, 1825-1841.

Vogel, S. (2003). *Comparative Biomechanics: Life's Physical World*. Princeton: Princeton University Press.

Webb, P. W. (1975). Hydrodynamics and energetics of fish propulsion. *Bull. Fish. Res. Bd. Can.* **190**, 1-158.

Chapter 4

Flexible fish-like robotic models reveal functional relationships between body stiffness, kinematics, and hydrodynamics in undulatory swimming

Abstract

Swimming performance is influenced by dynamic interactions between a body's motion, internal mechanical properties, and reaction to external fluid forces. Elucidating the individual effects of these factors on swimming is difficult in live fishes, but attainable with physical fish-like models. Models can be manipulated to approximate fish forms and kinematics, perform specific behaviors on cue, and explore parameter space unused by live fishes. Using simple physical models actuated in a flow tank by external programmable motors, the present study contributes to a growing body of model-based research on locomotory mechanisms in flexible bodies. Specifically, the work here aims to provide insights into mechanisms of locomotion in live elongate anguilliform swimmers such as hagfish. In part one of this study, rectangular plastic foils with flexural stiffnesses spanning $10^{-7} – 10^{-3}$ Nm^2 served as two-dimensional representations of elongate swimmers. Foil swimming speed increased with stiffness, driving frequency, or driving amplitude, though the effect of changing input kinematics was dependent on foil stiffness and frequency. Foils that approximated real hagfish in flexural stiffness and kinematics also resembled hagfish in the wake structure produced. In part two of this study, flexible rod and bar models served as more accurate three-dimensional representations of an elongate swimmer. Thrust production and wake structure varied with driving frequency, but changed little with model shape. I discuss the performance of the physical models in relation to known characteristics of hagfish swimming, and consider lessons we can learn from passively undulating models to better understand locomotion by live anguilliform swimmers.

Introduction

While subject to the same set of fundamental mechanical principles, different fishes display an enormous array of locomotory behaviors. Understanding the mechanisms that give rise to this diversity involves studying how a body's motion, mechanical properties, and reaction to external fluid forces all interact to produce a particular swimming behavior (Alben, 2008; Tytell et al., 2010). Technological advances in experimental robotics, modeling, and flow visualization have made this task easier (Lauder et al., 2007). In a laboratory setting, live fish may not perform specific behaviors with enough inter-individual variation to reveal relationships between specific body characteristics, such as stiffness or kinematics, and swim performance. Physical models, however, can be made to perform specific behaviors repeatedly and on cue. Furthermore, their morphology and motion patterns can be manipulated not only to replicate swimming in live fishes but also to extend beyond known physiological limits and explore unused parameter space.

Model-based research on flexible objects moving through fluid has particular relevance in understanding mechanisms of propulsion in fishes that pass waves of bending along their bodies to swim. Several theoretical and computational studies have explored how the swimming performance of undulating flexible membranes or fish-like elongate swimmers depends on complex relationships between internal muscle activation, body stiffness, body kinematics, and dynamic fluid forces (i.e. Alben, 2008; Alben et al., 2012; Ferreira de Sousa and Allen, 2011; McMillen and Holmes, 2006; Prempraneerach et al., 2003). Other workers have used an integrated experimental approach combining live animal studies with physical modeling to examine mechanisms of undulatory propulsion. Root and his colleagues (Root et al., 1999) quantified propulsive wave characteristics in simple physical models with varying stiffnesses for comparison with live, free-swimming lamprey (*Petromyzon marinus*), but the models were

actuated at a single frequency of 12 Hz, much higher than undulation frequencies commonly observed in elongate anguilliform swimmers (i.e. hagfish (Long et al., 2002), eels (Gillis, 1998; Tytell, 2004), and swimming snakes (Jayne, 1985; Munk, 2008)). Leftwich et al. (Leftwich et al., 2012) used a lamprey-like robotic swimmer to study how thrust production and wake morphology change with tail stiffness during anguilliform swimming. This model swam at relatively low frequencies (0.1 to 0.65 Hz), and was actuated over a large portion of its length, so that only the tail could passively flex. Using flexible physical models of pumpkinseed sunfish (*Lepomis gibbosus*), McHenry et al. (McHenry et al., 1995) quantified relationships between body stiffness and undulatory kinematics, and their separate effects on swimming speed. Pumpkinseed sunfish have a more perch-like body, however, and tend to swim with smaller body amplitudes than elongate anguilliform swimmers (Chapter 1; Gillis, 1996).

The present study expands on this body of experimental research, employing simple physical models to specifically examine undulatory swimming mechanisms in elongate anguilliform swimmers, particularly hagfishes. Hagfishes are exceptionally flexible, due in large part to lacking a complete vertebral column but retaining a flexible notochord in adulthood (Long et al., 2002; Ota et al., 2011). They are also relatively simple morphologically. Discrete fins are absent along their bodies, which are mostly cylindrical with some lateral compression toward the caudal end (Hart, 1973). Given their relatively uniform external morphology, hagfishes can be particularly well-approximated by simple physical models. From previous experimental work, we also know that hagfishes are broadly categorized as undulatory anguilliform swimmers (Long et al., 2002), but can display a diversity of steady and unsteady swimming behaviors (Chapters 1 – 3). Even for a behavior as basic as steady swimming, hagfishes are likely capable of using a variety of mechanisms to control swim speed (Chapter 1;

Long et al., 2002).

Here, I use simple physical fish-like models to examine functional relationships between body flexural stiffness, shape, kinematics, hydrodynamics, and swim performance in undulatory swimming. The models are actuated at their anterior end (leading edge) only, removing the effect of active muscular contraction along the length of a live swimming fish's body (Alben, 2008; Tytell et al., 2010). Any undulatory "body" waves present on these models are passively propagated down the model as they interact with surrounding fluid. By comparing model undulatory waves and hydrodynamics with those from live swimming hagfish, I form hypotheses on which elements of undulatory swimming are actively controlled and which arise passively from the balance between internal and external forces on a body. It is informative to note which features of undulatory motion are possible without active input along the whole length of the body, as a fish that exploits passively propagating waves can benefit from energy savings conferred by little need for complex muscular control and extra muscular work along the body (Alben, 2008). In addition, using physical models to systematically control and quantify how various factors independently influence swim performance offers insight into how hagfish might control their body undulatory behavior while swimming.

Materials and Methods

Simple fish models and robotic controller

Two different categories of physical models, each with multiple models within the category, were used to examine undulatory swimming by flexible bodies. The first general type of model consisted of a rectangular piece of thin, flexible plastic shim stock (ARTUS Corp., Englewood, NJ) with the long axis oriented horizontally (19 cm long x 6.8 cm high; Figure 4.1A). This type

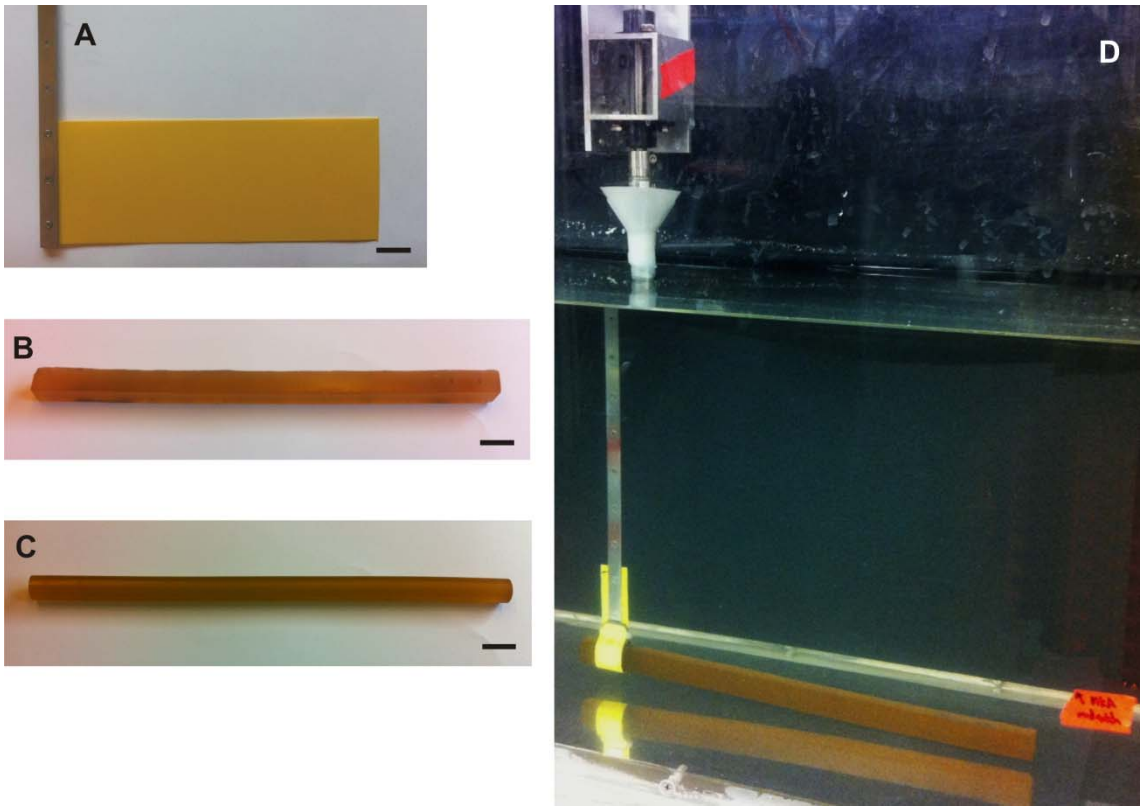

Figure 4.1. Simple physical models approximating elongate anguilliform swimmers. (A) Rectangular plastic foil with a metal shaft attached directly to its leading edge. (B) A polyurethane bar with a square cross-section. (C) A polyurethane rod with a circular cross-section. (D) The polyurethane bar in the variable-speed flow tank, attached to a robotic control device *via* a metal shaft and holster encircling the model. All scale bars are 2 cm.

of model, which I refer to as a "foil," served as a highly simplified and effectively two-dimensional representation of an elongate undulatory swimmer. Three different thicknesses of shim were used to obtain a span of flexural stiffness (*EI*, where *E* is Young's modulus and *I* is the second moment of area) in the models (herein referred to as low, intermediate, and high stiffness, Table 4.1), with the intermediate foil selected to match values of whole-body flexural stiffness previously reported for Atlantic hagfish (*Myxine glutinosa*, 3×10^{-4} Nm^2, (Long et al., 2002)) and the American eel (*Anguilla rostrata*, $1 - 2 \times 10^{-4}$ Nm^2, (Long, 1998)).

The second category of physical models was chosen to more closely approximate the three-dimensional morphology of an elongate swimmer. These models were polyurethane bars (square cross-section) and rods (circular cross-section) (40A durometer, McMaster-Carr, Robbinsville, NJ) with identical diameter and length (1.59 x 30 cm; Figure 4.1B, C). As many elongate anguilliform swimmers have bodies that are cylindrical in anterior regions and laterally compressed in posterior regions (i.e. hagfish (Hart, 1973), freshwater eels (Scott and Scott, 1988)), these models represent opposite simplified extremes in elongate body shape. Due to their identical heights, the rod and bar models have the same lateral projected area but they differ in flexural stiffness (rod: 5.9×10^{-3} Nm^2; bar: 9.4×10^{-3} Nm^2).

A custom-built robotic device was used to actuate each physical model in a variable-speed flow tank filled with freshwater (84 x 28 x 28 cm working section). A detailed description of this robotic apparatus is provided by Lauder and colleagues (Lauder et al., 2007; Lauder et al., 2011), and a brief description is given here. Heave and pitch motors are attached to a carriage that rides on low-friction air bearings above the flow tank, allowing upstream and downstream movement of the motors and carriage. A custom LabView (v. 8, National Instruments, Austin, TX) interface is used to control the motors, which are attached to the physical model submerged

Table 4.1. Properties of the rectangular plastic foils used as fish-like models of undulatory swimmers.

Relative stiffness of rectangular foils	Thickness (mm)	Young's modulus (MPa)	Flexural stiffness (Nm^2)
Low	0.03	3100	4.78×10^{-7}
Intermediate	0.21	2250	1.19×10^{-4}
High	0.55	1240	1.18×10^{-3}

in the water via a metal shaft (Figure 4.1B). Rectangular foils were clamped directly in the shaft along the foil's leading edge and positioned at an intermediate height in the tank. Polyurethane rods/bars were attached to the shaft via a metal holster wrapped around the model approximately 1 cm behind the leading edge, and were positioned approximately 1.5 cm above the bottom of the flow tank. This placement was chosen to approximate the bottom-swimming commonly observed in hagfish (Chapters 1 – 3) and eels (Tytell and Lauder, 2004). The boundary layer for this flow tank was found to be 0.2 to 0.7 cm thick at flow speeds comparable to the highest speeds used in the present study (Carlson and Lauder, 2011; Tytell and Lauder, 2004). Because boundary layers become thicker as flow speeds decrease (Schlichting, 1979), it is possible that boundary layer flows influenced the model's swimming; however, because the main focus of this study is on comparisons between physical models, the potential effect of the boundary layer is not considered here as rod and bar models experienced the same flow conditions.

Kinematics and force measurements

The prescribed leading edge kinematics of the model swimmers were chosen to encompass typical physiological kinematic values and Reynolds numbers for steady swimming hagfish (Chapter 1). Rectangular foils were actuated at heave amplitudes (defined as half the maximum lateral excursion) of 0.5, 1.0, 1.5, 2.5, and 3.5 cm, and at frequencies of 0.5, 1.5, 2.5, 3.5, and 4.5 Hz. At each combination of heave amplitude and frequency, self-propelled swim speed (SPS) and cost of transport (COT) were measured as swim performance metrics. Self-propelled speed is measured by adjusting the flow tank speed to match the model's swimming speed such that the model swims at an equilibrium position in the water while being able to freely move along the air bearings. The flow speed at which the model holds station in the oncoming flow is the SPS at

the given heave and frequency parameters (Lauder et al., 2007). At each swimming model's SPS, force and torque measurements were obtained in three orthogonal planes using a six-axis force transducer (Nano 17 for low stiffness foil, Nano 17E for intermediate and high stiffness foils, ATI Industrial Automation., Apex, NC) attached to the model's leading edge shaft. Force and torque data were phase averaged and imported into LabChart software (v. 7.3.3 ADInstruments, Colorado Springs, CO) where they were combined with data on foil position collected by the robotic control apparatus. These data were used to calculate power (force x velocity) and total work per cycle (integral of power with respect to time) exerted by the motors on the foil. Cost of transport (work per unit distance) was calculated as work per cycle multiplied by driving frequency and divided by SPS. No measurements were made above 2.5 Hz at a heave amplitude of 2.5 cm, nor above 1.5 Hz at a heave of 3.5 cm, due to sensitivity limitations in the robotic apparatus and force sensor.

The polyurethane rod and bar were actuated at a heave amplitude of 2 cm and at frequencies of 0.5 to 2.5 Hz (0.5 Hz intervals). A pitch angle of 25 degrees was also added to the leading edge motion to more closely simulate the appearance of hagfish swimming (Chapter 1). Because the bar and rod models interacted with the flow tank bottom, reliable measurements of SPS were unobtainable and net axial force exerted by the model was measured as a swim performance metric instead. Axial movement of the robotic device's carriage was restricted and flow speed was set at three different constant values: 4.3 cm/s, 6.5 cm/s, and 8.9 cm/s (corresponding to 0.14 BL/s, 0.21 BL/s, and 0.29 BL/s, respectively, where BL = body length = length of the model). Models were then actuated over the range of driving frequencies at the constant flow velocity. Any axial force measurement above or below zero would indicate net thrust or drag, respectively, exerted by the bar or rod; an occurrence of zero net axial force,

however, would indicate a SPS at the driving frequency at which it occurs. Similar to the procedure for the rectangular foils, forces and torques were measured with a force transducer (Nano 17E) on the leading edge shaft and were used to calculate mean net axial force exerted by the model, and work per cycle exerted by the motor.

To obtain a visual representation of each physical model's swimming behavior over the range of frequencies and heave amplitudes prescribed, a high-speed video camera (Photron PCI1024 Fastcam, 1024 x 1024 pixels, Photron USA Inc., San Diego, CA) aimed at a 45 degree-angled mirror below the flow tank was used to film ventral views of the swimming models. Rectangular foils were filmed at 500 frames/s, and the polyurethane rod and bar were filmed at 250 frames/s. Two-dimensional (*x, y*) coordinates of the model's position over time were recorded from the video images using a custom Matlab (R2011a, The Mathworks Inc., Natick, MA) program. At intervals of 0.02 to 0.10 seconds (dependent on the model's driving frequency) over the course of a complete undulatory cycle, approximately 10 manually-digitized points along the length of the model were fitted with a cubic spline to produce a smoothed line representing the model midline at multiple instances in the cycle.

Hydrodynamics of physical model swimming

Flow fields around the swimming physical models were visualized and quantified with particle image velocimetry (PIV). Neutrally buoyant 50 μm plastic beads (Degussa Corp., Piscataway, NJ) were added to the water in the flow tank, and a continuous argon-ion laser (10 W, Coherent Inc., Santa Clara, CA) aimed through a beveled cylindrical lens produced a thin horizontal light sheet that was positioned at mid-height on the model. A digital high-speed video camera (500 frames/s, 1024 x 1024 pixels, Photron USA Inc., San Diego, CA) aimed at a 45 degree-angled

mirror below the clear tank bottom filmed ventral views of the acuated models and the plastic particles in the water as they moved through the light sheet. Video images were imported into DaVis software (v. 7.2.2, LaVision Inc., Goettingen, Germany), where they were calibrated and processed via an FFT-based cross-correlation routine (two-pass, 16 x 16 pixel interrogation area with 50% overlap) that analyzed particle movement to produce a two-dimensional array of fluid velocity vectors and vorticity fields. Average free-stream velocity was subtracted from raw vector data to highlight model-generated flows, and obvious erroneous vectors were manually deleted to validate the vector map. Validated PIV vector maps for the polyurethane rod and bar models were analyzed further in a custom Matlab program (written by Eric Tytell, Harvard University, 2005) that was used to define and measure flow structures in the model's wake. Wakes typically consisted of fluid jets between two opposite-sign vorticity centers, which were assumed to collectively represent a cross-section through a vortex ring to allow simplified calculations of wake force production (Müller et al., 2001; Stamhuis and Nauwelaerts, 2005; Tytell and Lauder, 2004). The circulation of this vortex ring was measured as the line integral of the velocity along the jet's main axis through the center of the vortex ring (Stamhuis and Nauwelaerts, 2005; Tytell and Lauder, 2004). Vortex ring impulse (I_r) was then calculated as:

$$I_r = \tfrac{1}{4}\pi\rho\Gamma hd$$

where ρ is the fluid density, Γ is the vortex ring circulation, d is the diameter of the vortex ring (approximated as jet diameter), and h is the height of the ring (approximated as the height of the model) (Tytell and Lauder, 2004). Previous PIV studies on swimming bodies have demonstrated that vortex ring height closely matches the height of the propulsor (Lauder, 2000), such that

vortex rings produced by low profile bodies may actually be more oval-shaped than circular (Tytell and Lauder, 2004). As actuated models typically produced a single vortex ring per half cycle, the force generating the ring was estimated as the ring impulse divided by the time period between maximum lateral excursions (Müller et al., 2001; Tytell and Lauder, 2004). An analysis of variance (ANOVA) was performed in JMP Pro 10 (SAS Institute, Inc., Cary, NC) to test for differences in vortex ring force produced by the polyurethane bar and rod at 0.5 Hz and 1.0 Hz. Axial velocity profiles across the filmed field of view for the rod and bar models were also obtained in DaVis software as another representation of each model's generated flows.

Results

Swimming of self-propelled rectangular foils

Midline tracings from the self-propelling rectangular foils illustrate that differences in flexural stiffness and leading edge kinematics resulted in differences in the shape of the undulatory wave along the foil (Figure 4.2). Generally, as foil flexural stiffness increases at a given combination of heave amplitude and frequency, fewer waves appear along the foil (Figure 4.2, compare midlines within a box). For the most flexible foil, increasing heave amplitude also appears to decrease wavenumber or cause the wave shape to distort (Figure 4.2, middle column of panels). For the stiffer foils, increasing amplitude and driving frequency both appear to induce greater bending in the foil (Figure 4.2, middle row of panels), though within a foil there is little to no change in the undulation amplitude along the length of the foil.

Differences in foil stiffness and kinematics also influenced swimming performance measured as self-propelled speeds (SPS). Stiffer foils generally reached higher SPS at a given combination of heave and frequency, over the range of kinematics tested here (Figure 4.3). For

Figure 4.2. Ventral midline drawings of self-propelled rectangular foils swimming at select combinations of heave amplitude and driving frequency. Approximately one complete tail beat cycle is shown. For each foil, the leading edge is at the left and water flow is from left to right. Within a box, flexural stiffness increases from top to bottom (see Table 4.1 for foil information). The foil in the middle has a flexural stiffness closest to that of a hagfish body (Long et al., 2002). Heave amplitude and driving frequency change across boxes. Low stiffness (high flexibility) was associated with greater bending at a given combination of heave and frequency. The 2 cm scale bar applies to all midline drawings.

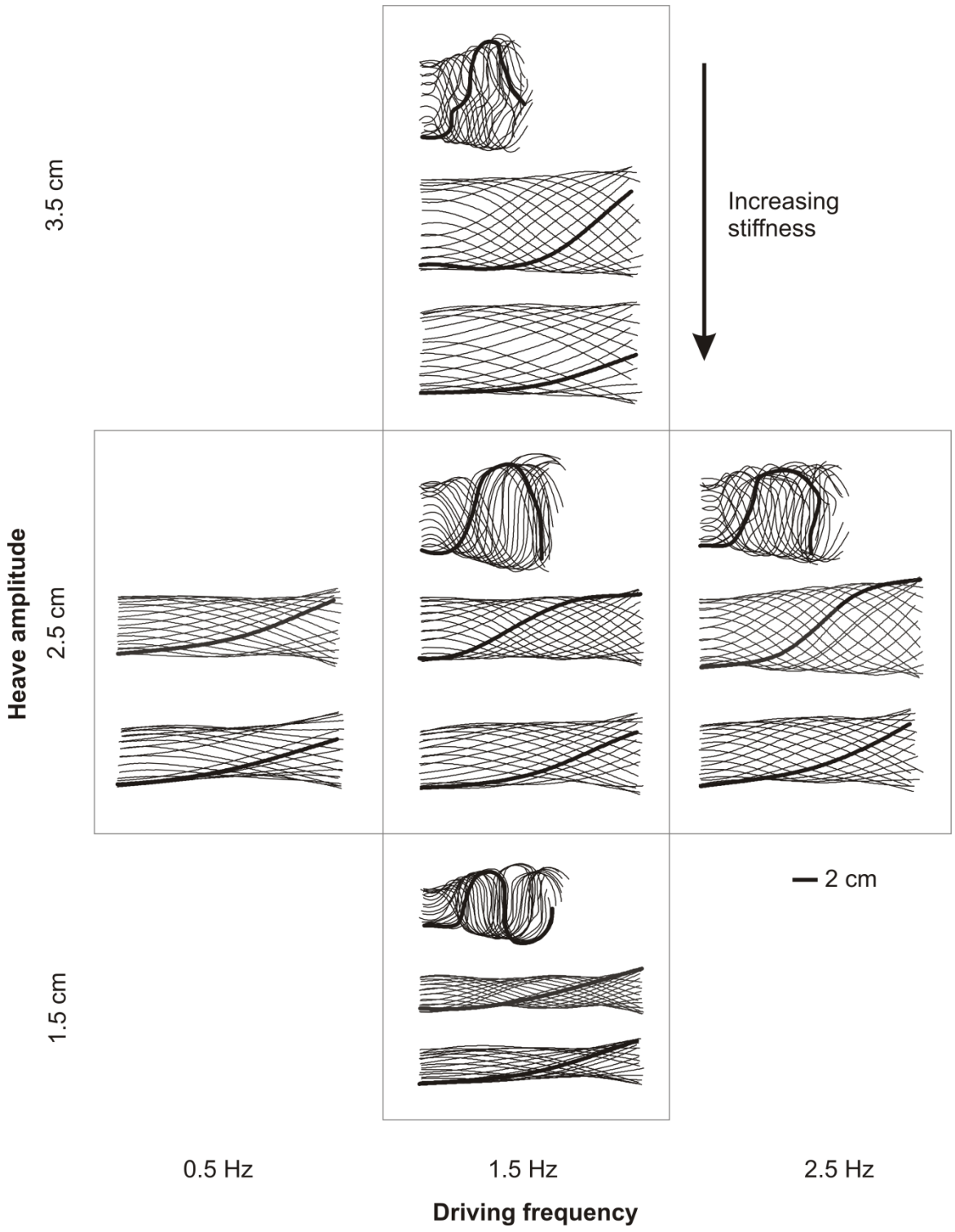

Figure 4.2 (Continued)

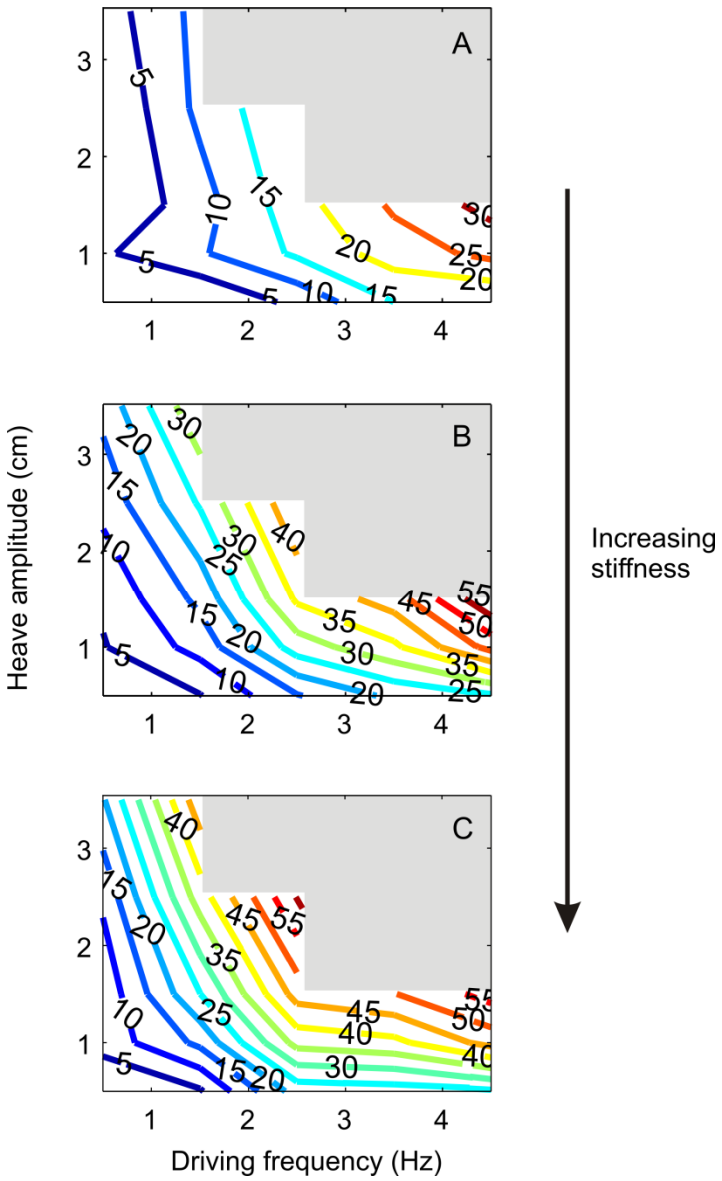

Figure 4.3. Partial contour lines of self-propelled speeds as a function of heave amplitude and driving frequency for rectangular foils with (A) low relative flexural stiffness, (B) intermediate relative flexural stiffness, and (C) high relative flexural stiffness (see Table 4.1 for foil information). Numbers on contour lines are self-propelled speeds in cm/s. Kinematic combinations that could not be tested due to equipment constraints are shaded in gray. Higher flexural stiffness was associated with higher self-propelled speeds.

the most flexible foil, increasing frequency was more effective than increasing heave in enhancing SPS (Figure 4.3A). For the stiffer foils, however, changes in both heave amplitude and frequency affected SPS, with greater heave amplitudes leading to rapidly increasing SPS particularly at high driving frequencies (Figure 4.3B, C). Gains in SPS are also associated with higher costs of transport, which increased with foil stiffness, heave amplitude, and driving frequency (Figure 4.4).

Flow fields generated by the self-propelling models were also visualized to examine relationships between flexural stiffness, kinematics, and hydrodynamics. In every swimming sequence, foils developed an attached leading edge vortex, likely due to the foil shaft's sharp edges and lack of pitching motion. A time-series of particle image velocimetry (PIV) vector maps for the foil of intermediate stiffness oscillating at a heave of 1.5 cm and frequency of 1.5 Hz depicts the development of a 2P wake structure, where two pairs of vortices are shed per cycle (Figure 4.5) (Hultmark et al., 2007; Schnipper et al., 2009). The time-series starts halfway through a cycle, as the foil's leading edge is moving to its left and the trailing edge is moving to its right. The foil has just produced a fluid jet (C) in the wake between two opposite-sign vortices (B and D) (t = 0.1 s, Figure 4.5). The counter-clockwise rotating vortex (D) is associated with an adjacent same-sign vortex, generated from the previous half cycle. As the trailing edge continues moving right, the negative vorticity at the trailing edge stretches across the wake (t = 0.2 s, B) and separates into two adjacent clockwise rotating vortices (t = 0.3 s, B1 and B2). The first vortex (B1) is associated with the first jet (C), while the second vortex (B2) is associated with the newly formed jet (E) on the opposite side (t = 0.4 s). Meanwhile, positive vorticity building along the undulating foil (A) and associated with entrained fluid in the foil's bend has travelled to the trailing edge where it is about to be shed at the end of the cycle (Figure 4.5).

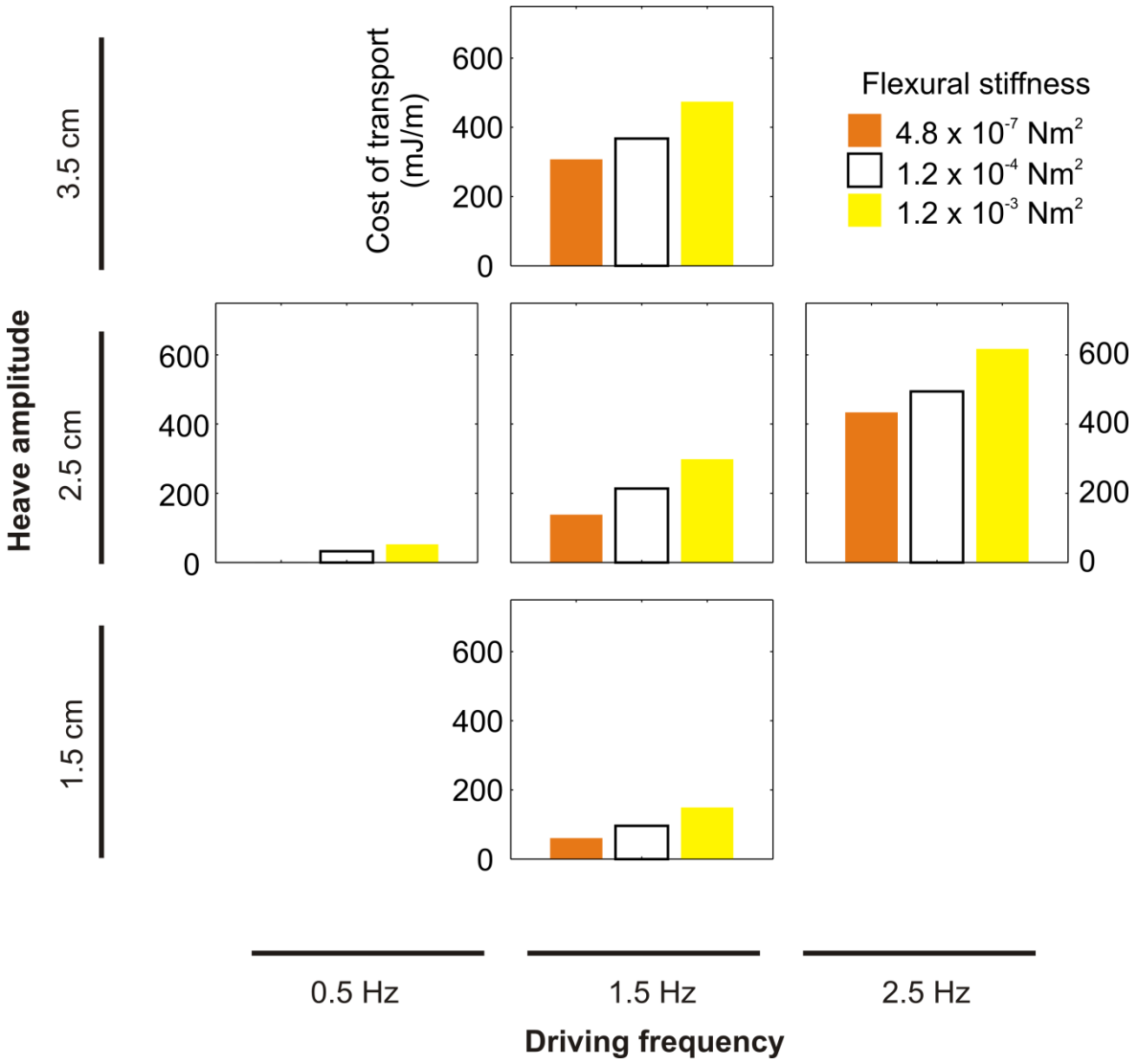

Figure 4.4. Cost of transport for self-propelling rectangular foils with differing flexural stiffness, as a function of heave amplitude and driving frequency. The cost of transport was calculated from the perspective of the heave motor actuating the foils. Increasing flexural stiffness, driving frequency, and heave amplitude all contribute to higher costs of transport.

Figure 4.5. Representative time-series of ventral-view flows around the intermediate relative stiffness rectangular foil self-propelling at 16.3 cm/s. Heave amplitude = 1.5 cm, driving frequency = 1.5 Hz. Fluid velocity vectors are represented by black arrows, and the vorticity field is color-coded. Only every second vector is shown for clarity. Water flow is from left to right and the freestream velocity has been subtracted from the flow. Large open arrows represent overall fluid jet direction. The foil is indicated by the gray line. At this combination of driving amplitude and frequency, the foil generates a 2P wake with distinct vortices. At t = 0 s, the foil has just produced a fluid jet (C) in the wake between two opposite-sign vortices (B and D). The trailing edge moves toward its right, and negative vorticity (in blue) at the trailing edge stretches across the wake (t = 0.2 s, B) before separating into two vortices (t = 0.3 s, B1 and B2). At this point, a second lateral jet (E) is forming on the right side and positive vorticity (in red) that has been building along the bending foil (A) is about to be shed at the trailing edge (t = 0.4 s).

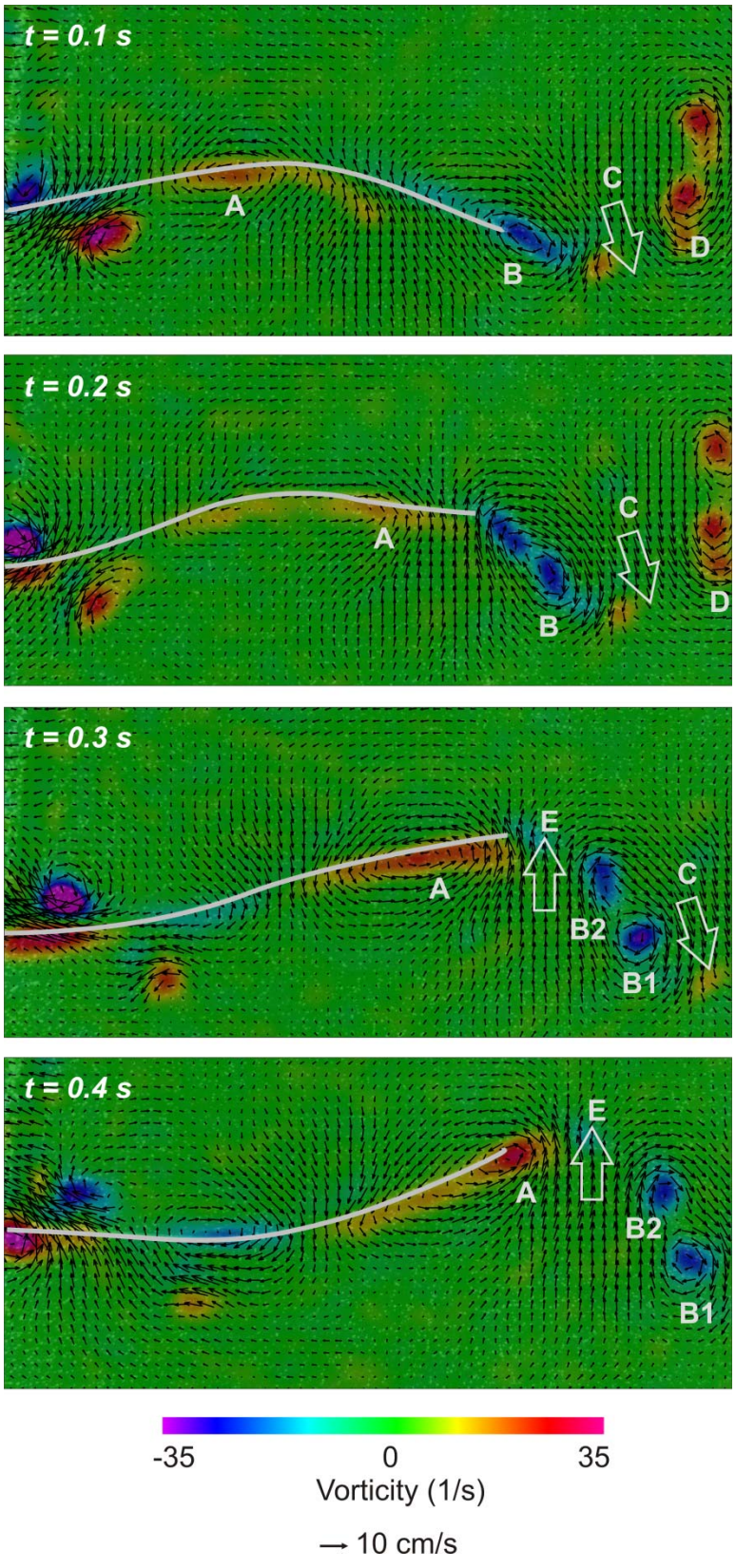

Figure 4.5 (Continued)

Changing the leading edge kinematics influenced wake structure differently depending on the foil flexural stiffness. Keeping driving frequency constant while increasing heave amplitude in the same intermediate stiffness foil, the wake directly behind the trailing edge changes slightly from consisting of distinct pairs of vortices (Figure 4.5) to multiple vortices (Figure 4.6, heave 2.5 cm, middle panel) or a persisting band of vorticity stretched across the widening wake (Figure 4.6, heave 3.5 cm, top panel). Similarly, keeping amplitude constant while increasing frequency produces a long band of vorticity in the wake (Figure 4.6). The increase in passive bending along the foil and different patterns of fluid entrainment into those bends is visible across increasing frequencies as well (Figure 4.6, left panel *vs.* right panel). Wakes produced by the stiffest foil also consisted of long bands of vorticity shed from the trailing edge, but wake structure did not obviously change across different combinations of kinematics. Typical flow fields around this foil consisted of broad regions of entrained fluid and alternating bands of vorticity that persisted in the wake (Figure 4.7).

In contrast, for the most flexible rectangular foil, wake structure can change markedly with changes in heave amplitude or frequency (Figure 4.8). At a heave of 1.5 cm and frequency of 1.5 Hz, the most flexible foil produces a 2S wake, where two single vortices are shed per complete cycle as adjacent same-sign vortices merge into a single vortex (Figure 4.8, bottom panel) (Schnipper et al., 2009). As heave amplitude increases, however, the wake structure becomes less coherent with multiple vortices spread out across the wider wake (Figure 4.8, top panel). At the greatest amplitude, the flows from the large leading edge vortex appear to contribute to the distortion of the undulatory wave along the foil. The wake at the intermediate amplitude (Figure 4.8, left-middle panel) may represent a transition point in wake morphology for this foil, as increasing frequency to 2.5 Hz results in the formation of a 2P wake (Figure 4.8,

Figure 4.6. Ventral views of representative flow fields around the intermediate relative stiffness rectangular foil self-propelling under different heave amplitude and frequency combinations. Fluid velocity vectors are represented by black arrows, and the vorticity field is color-coded. Only every second vector is shown for clarity. Water flow is from left to right and the freestream velocity has been subtracted from the flow. The foil is indicated by the gray line. Note the different scales for velocity vectors and vorticity beneath each image. Wakes at different combinations of heave and frequency generally consist of multiple vortices or stretches of vorticity across the wake.

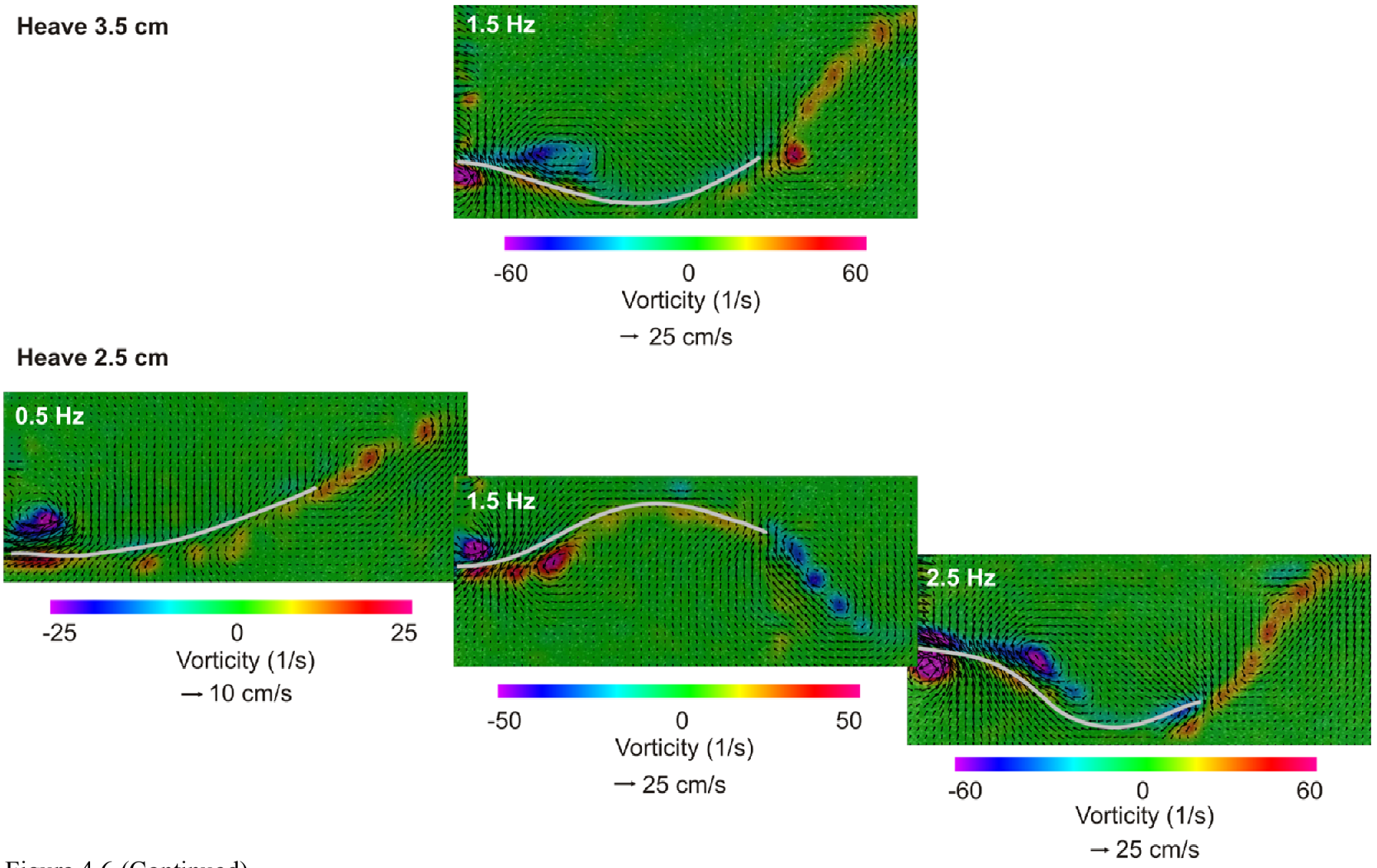

Figure 4.6 (Continued)

Figure 4.7. Representative time-series of ventral-view flows generated by the high relative stiffness rectangular foil self-propelling at 60.3 cm/s. Heave amplitude = 2.5 cm, driving frequency = 2.5 Hz. Fluid velocity vectors are represented by black arrows, and the vorticity field is color-coded. Only every second vector is shown for clarity. Water flow is from left to right and the freestream velocity has been subtracted from the flow. The foil is indicated by the gray line. The area to the right of the foil where laser light did not reach has been masked. Bands of vorticity representing shear layers of fluid persist in the wake during undulatory swimming in this foil.

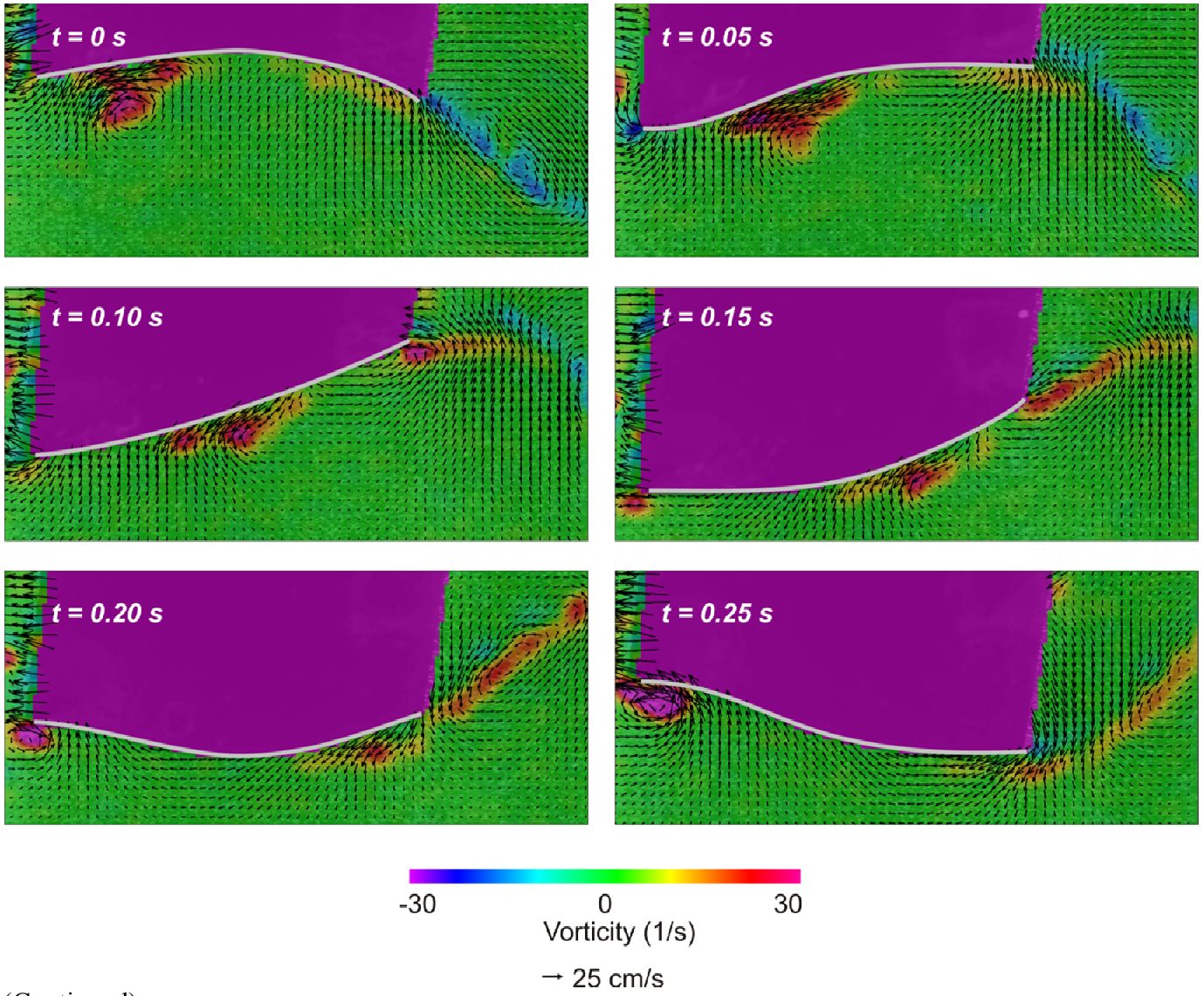

Figure 4.7 (Continued)

Figure 4.8. Ventral views of representative flow fields around the low relative stiffness rectangular foil self-propelling under different heave amplitude and frequency combinations. Fluid velocity vectors are represented by black arrows, and the vorticity field is color-coded. Only every second vector is shown for clarity. Water flow is from left to right and the freestream velocity has been subtracted from the flow. The foil is indicated by the gray line. Note the different scales for velocity vectors and vorticity beneath each image. Wake structure changes with each change in driving frequency or amplitude.

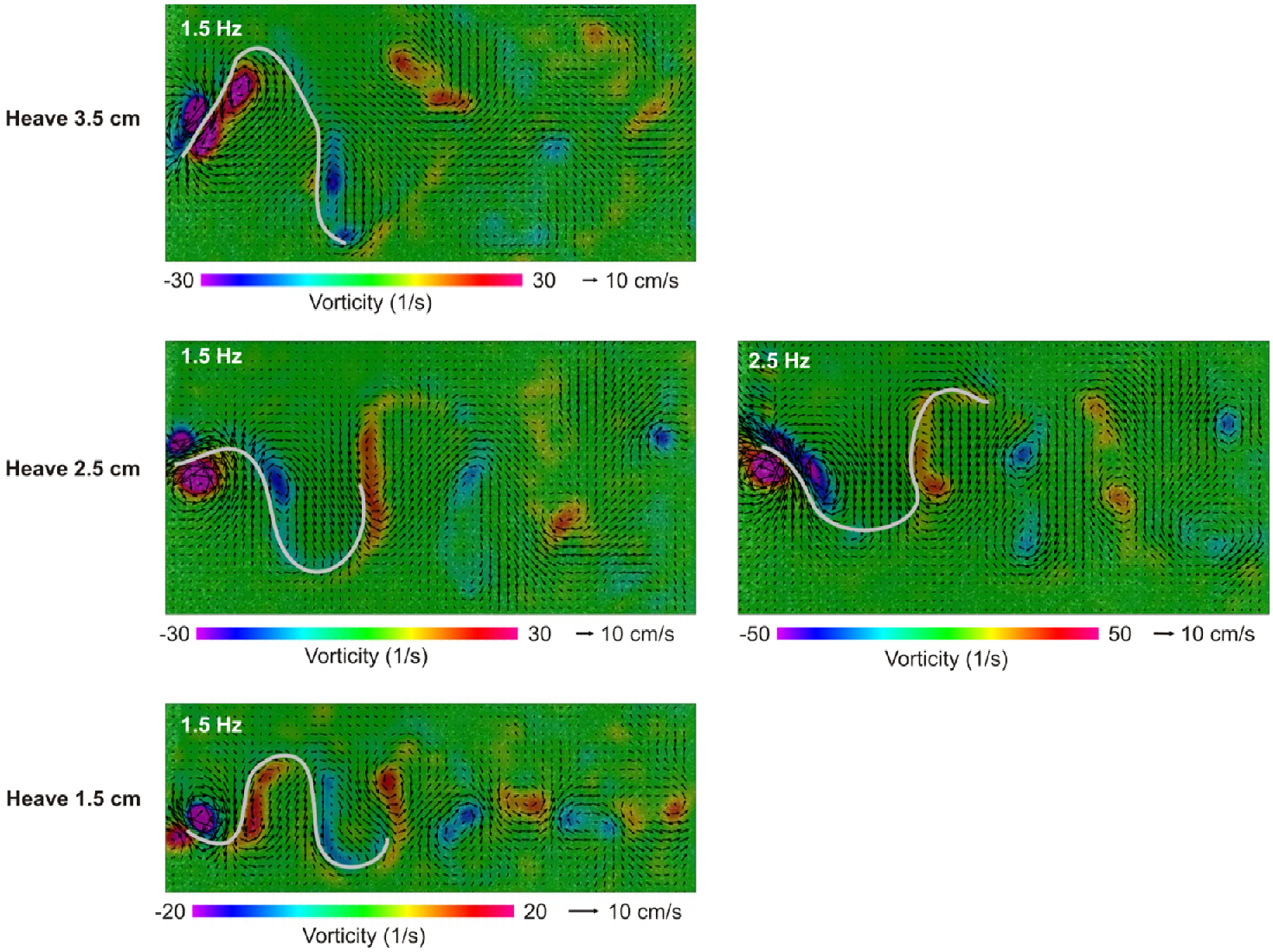

Figure 4.8 (Continued)

right panel).

A more hagfish-like model swimmer

Over the range of driving frequencies tested, few differences arose between the elongate polyurethane rod and bar models. The passive behavior of the undulatory wave along the model changed more with the prescribed kinematics than with the shape of the model (Figure 4.9). As actuation frequency increased, wavelength and trailing edge amplitude decreased for both models. Slightly larger trailing edge amplitudes in the bar were likely due to its greater mass, and therefore inertia, compared to the rod. Net thrust production, measured by the force transducer attached to the model shaft, generally increased with increasing driving frequency and did vary between models at certain frequencies (Figure 4.10A). At low frequencies, the square bar generated more thrust than the round rod. Accordingly, the point of zero net thrust, and therefore a SPS equal to the fixed flow speed (8.9 cm/s), occurred at a lower driving frequency for the bar than the rod. At higher frequencies in the frequency sweep, the rod produced slightly more or roughly equal amounts of net thrust compared to the bar. Meanwhile, the work exerted per cycle to actuate each model was always greater for the bar than the rod, and tended to increase only at higher driving frequencies (Figure 4.10B).

Plotting the axial flow velocity behind each model as an indication of contributed downstream momentum, the square bar generated faster flows than the round rod at 0.5 Hz as well as 2.5 Hz (Figure 4.11). As this result contrasts with the net thrust measurements reported above for 2.5 Hz, the combination of these data suggests greater variability in thrust production by each model at 2.5 Hz, and that the differently shaped models may actually have similar performance at this driving frequency. Wake structure in the plane of oscillation was also similar

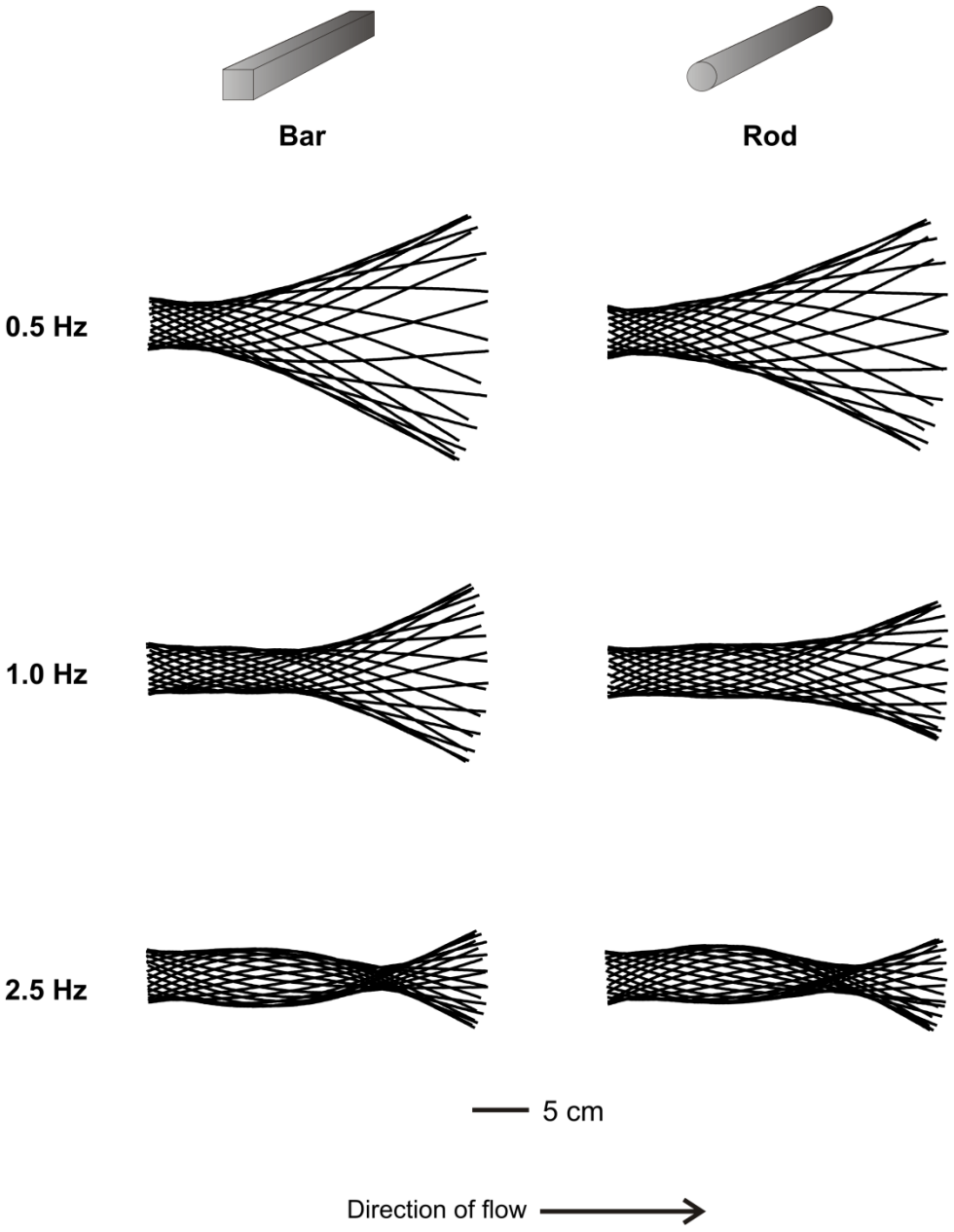

Figure 4.9. Ventral midline drawings of the polyurethane bar and rod models being actuated at select driving frequencies. Heave amplitude = 2 cm, pitch angle = 25 degrees. One complete cycle is shown in each drawing. For each model, the leading edge is at the left and water flow is from left to right. For the both the rod and bar, trailing edge amplitude and wavelength tended to decrease with increasing driving frequency. The 5 cm scale bar applies to all midline drawings.

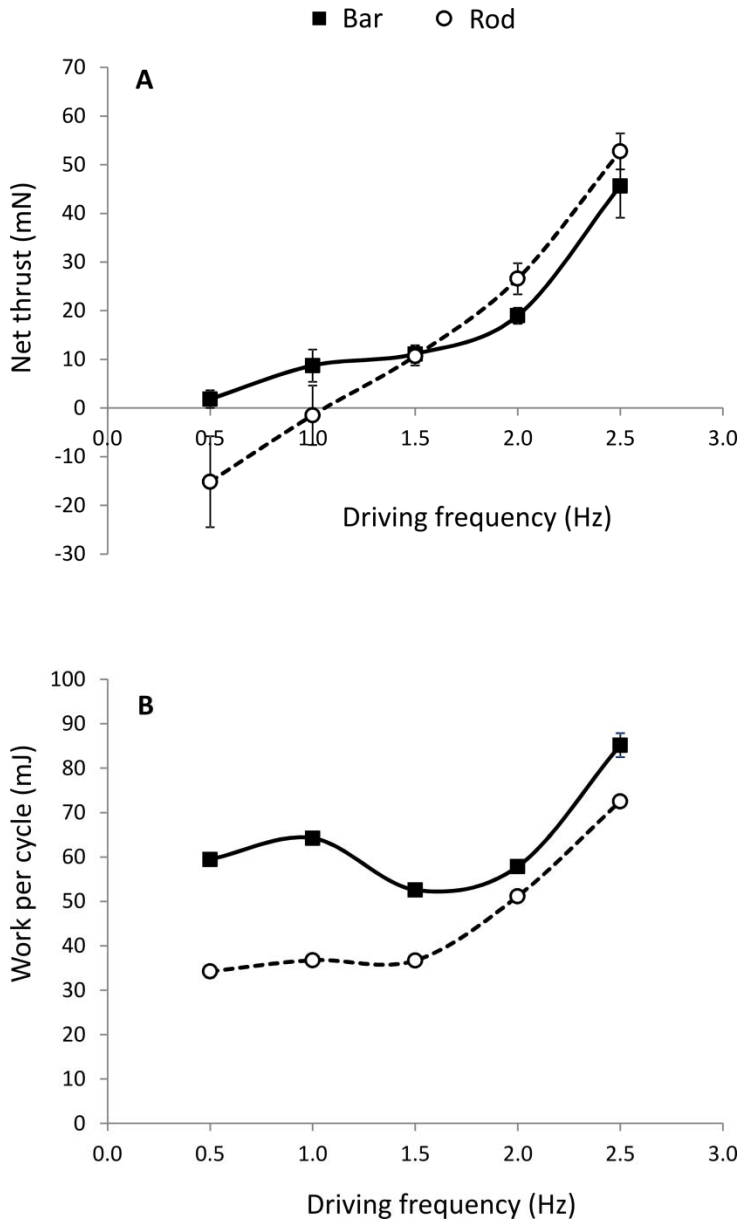

Figure 4.10. (A) Net thrust and (B) work per cycle as a function of driving frequency for the polyurethane bar (solid square symbol) and rod (open circle symbols) models being actuated in a flow tank with a constant flow speed of 8.9 cm/s. Values are averaged over a complete beat cycle, error bars are standard error of the mean. Net thrust (A) generally increases with increasing frequency, but differences between the rod and bar models depend on the driving frequency. Work per cycle (B) is always higher in the bar than the rod regardless of driving frequency.

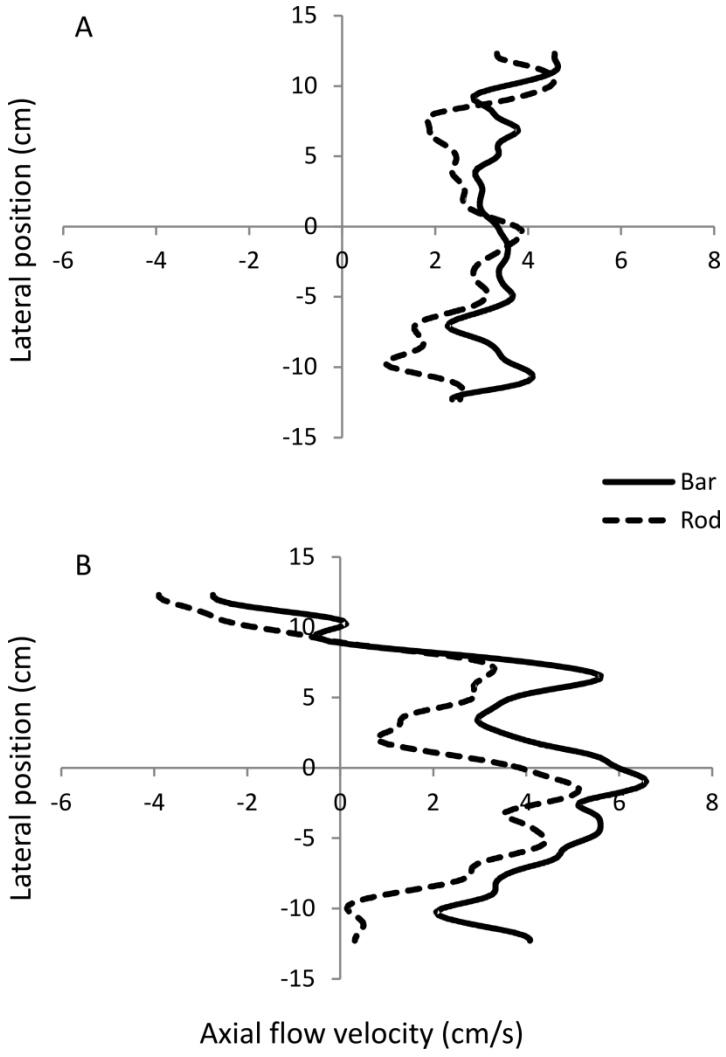

Figure 4.11. Axial flow velocity profiles from the wake of the rod (dotted line) or bar (solid line) models being actuated at (A) 0.5 Hz and (B) 2.5 Hz. Axial (upstream-downstream direction) velocity data were taken from a line extending across the wake approximately 8.5 cm behind the trailing edge of each model. In general, the bar generates slightly faster downstream flows than the rod at both driving frequencies.

between the bar and rod models (Figures 4.12 and 4.13). While being actuated at 1.0 Hz, the wake for each model again resembles a 2P wake, where laterally-directed fluid jets (open arrows, Figures 4.12 and 4.13) are produced between counter-rotating pairs of vortices on either side of the wake. The vorticity shed into the wake by the square bar tends to be lower and less visually apparent than the vorticity generated at the bar's sharp trailing edges, however (Figure 4.13). As patterns of bending within each model changed more with differences in driving frequency than differences in shape, patterns of flow around the models similarly varied the most over changes in kinematics. At a driving frequency of 0.5 Hz, high amplitude motions of the models's posterior regions drew broad regions of fluid toward each model, and lateral flows induced by the sharp-edged bar were slightly stronger than in the rod (Figure 4.14A, B). At 2.5 Hz, however, the wake no longer retained a 2P structure with distinct lateral jets but became less organized in both models (Figure 4.14C, D). The force associated with presumptive vortex rings shed into the wake at 0.5 Hz and 1.0 Hz appeared to differ between frequencies (Figure 4.15), but an ANOVA was unable to find statistically significant differences among the models or frequencies tested ($F = 0.94$, $p = 0.49$).

Discussion

The present study uses two categories of hagfish-like physical models and a systematic experimental approach to examine mechanisms of undulatory propulsion, particularly in relation to elongate anguilliform swimmers such as hagfishes. Both categories of physical models are externally actuated only at their leading edge, such that undulatory waves generated along the model passively propagate toward the trailing edge. The motion of the model is a result of interactions between the input kinematics, the model's inherent mechanical properties, and

Figure 4.12. Representative time-series of ventral-view flows generated by the polyurethane rod model being actuated at a driving frequency of 1.0 Hz in a flow tank with a constant flow speed of 8.9 cm/s. Heave amplitude = 2 cm, pitch angle = 25 degrees. Fluid velocity vectors are represented by black arrows, and the vorticity field is color-coded. Only every second vector is shown for clarity. Water flow is from left to right and the freestream velocity has been subtracted from the flow. Large open arrows represent overall fluid jet direction. At this frequency, the actuated rod has a 2P wake. A pair of vortices with a central fluid jet is visible at t = 0 s and t = 0.5 s.

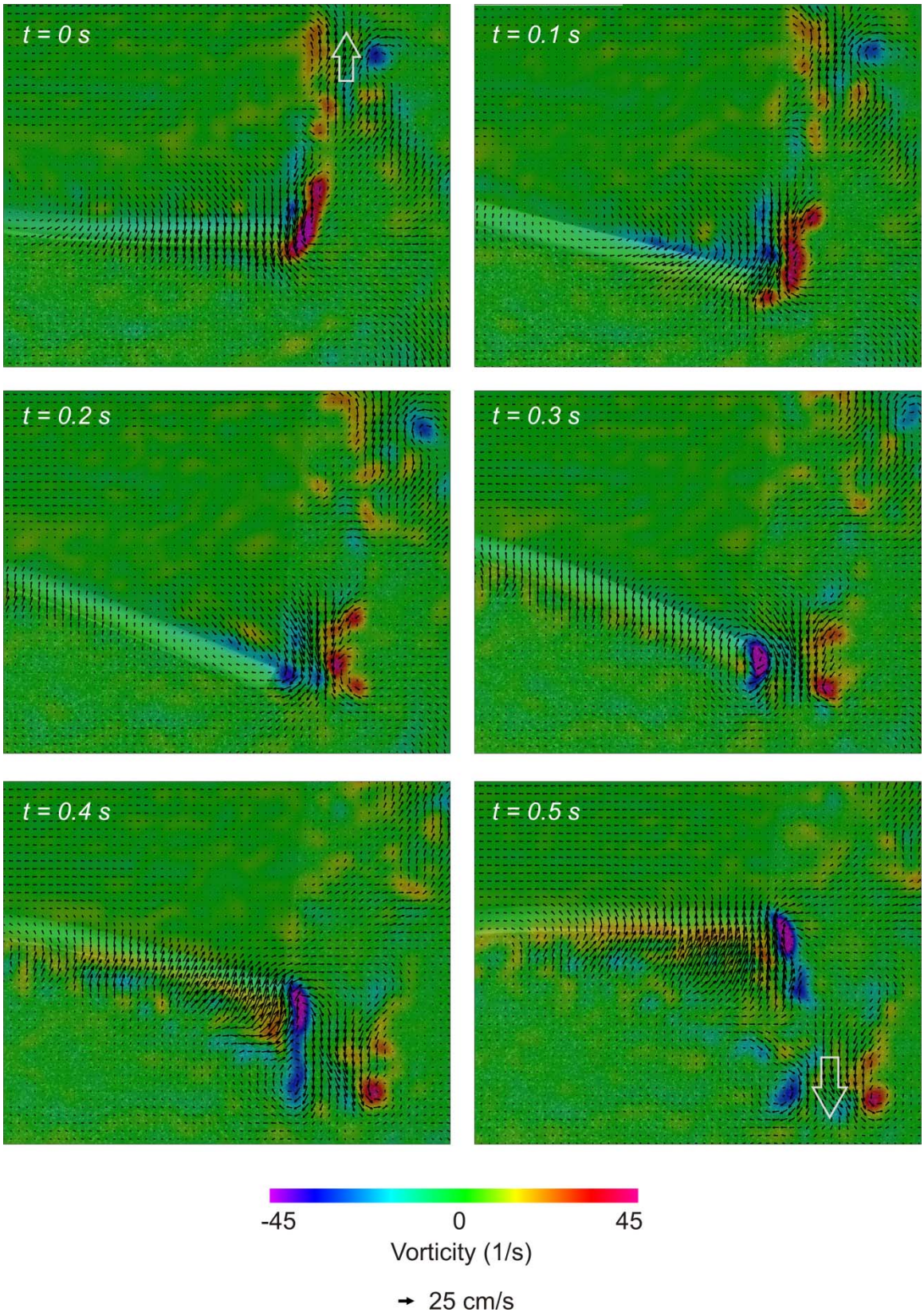

Figure 4.12 (Continued)

Figure 4.13. Representative time-series of ventral-view flows generated by the polyurethane bar model being actuated at a driving frequency of 1.0 Hz in a flow tank with a constant flow speed of 8.9 cm/s. Heave amplitude = 2 cm, pitch angle = 25 degrees. Fluid velocity vectors are represented by black arrows, and the vorticity field is color-coded. Only every second vector is shown for clarity. Water flow is from left to right and the freestream velocity has been subtracted from the flow. Large open arrows represent overall fluid jet direction. At this frequency, the actuated bar has a 2P wake. Centers of opposite-sign vorticity on either side of a fluid jet is visible at $t = 0$ s and $t = 0.5$ s.

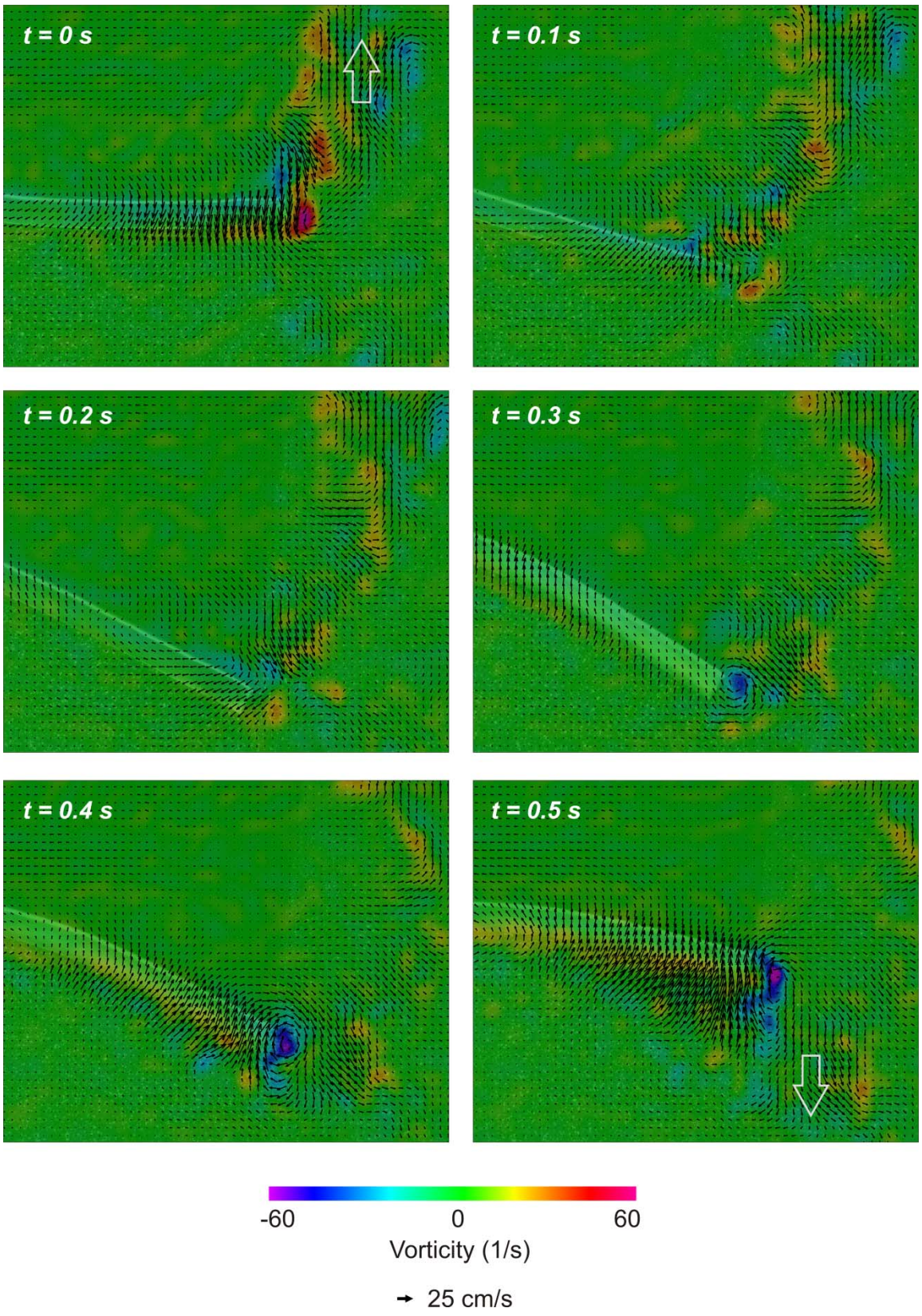

Figure 4.13 (Continued)

Figure 4.14. Ventral views of representative flow fields around the polyurethane (A,C) bar and (B,D) rod models being actuated at (A,B) 0.5 Hz and (C,D) 2.5 Hz in a flow tank with a constant flow speed of 8.9 cm/s. Fluid velocity vectors are represented by black arrows, and the vorticity field is color-coded. Only every second vector is shown for clarity. Water flow is from left to right and the freestream velocity has been subtracted from the flow. Note the different scales for velocity vectors and vorticity beneath each image. Wake structure is influenced more by driving frequency than by differences in model shape.

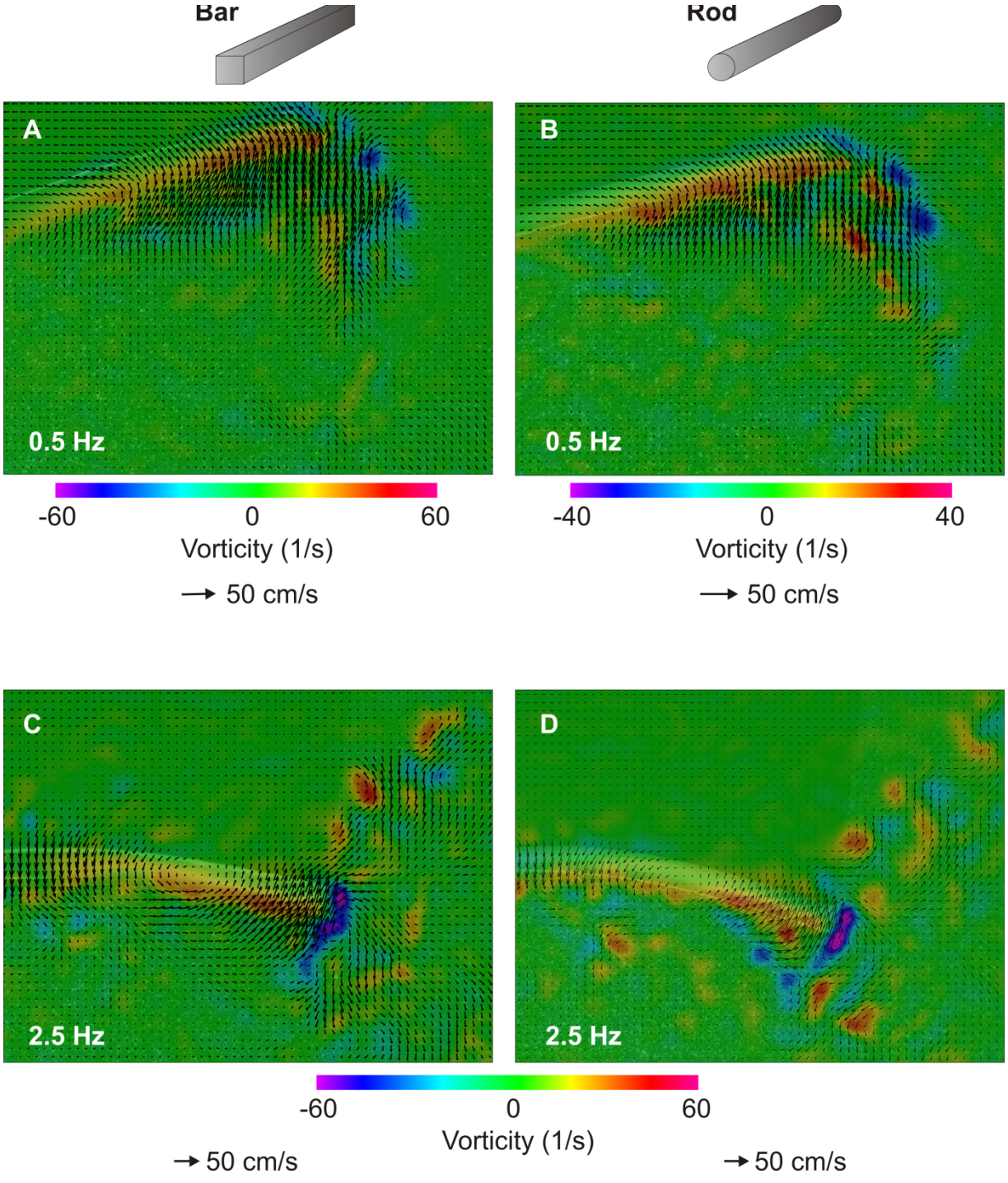

Figure 4.14 (Continued)

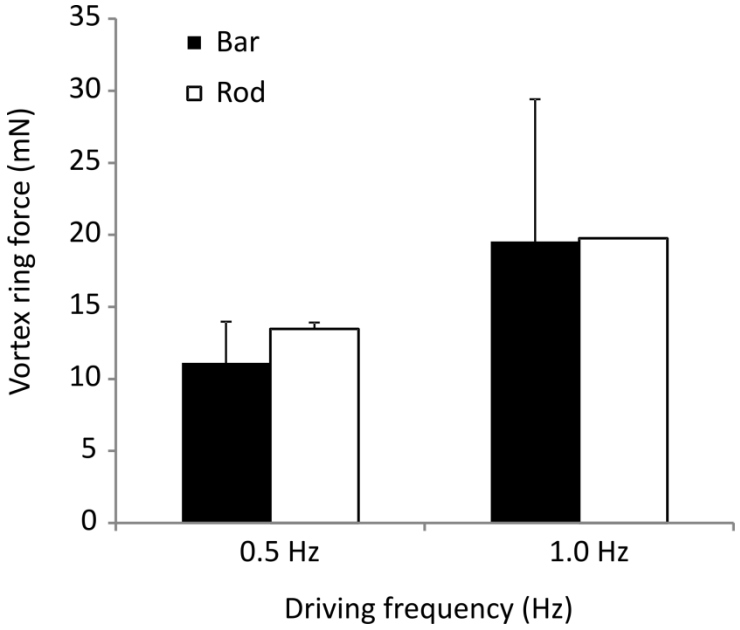

Figure 4.15. Mean force used to produce putative vortex rings (counter-rotating vortices with a central jet) in the wakes of the polyurethane bar (solid bars) and rod (open bars) models being actuated at 0.5 Hz and 1.0 Hz in a flow tank with a constant flow speed of 8.9 cm/s. Error bars are standard error of the mean. Force is generally higher at the higher frequency, but an ANOVA did not detect statistically significant differences among the models or frequencies tested (F = 0.94, p = 0.49).

external forces from the surrounding fluid (Alben, 2008). In live anguilliform swimmers, an additional determinant of body motion arises from the pattern of active muscular contraction along the length of the body (Tytell et al., 2010). In the first part of the study, a flexible plastic rectangular foil serves as a two-dimensional representation of an elongate swimmer, where foil stiffness, driving frequency, and driving amplitude are varied independently to quantify their effects on steady swimming speed and wake structure. In the second part of the study, a flexible rod and bar are used as model swimmers to more closely approximate the three-dimensional morphology of an elongate anguilliform swimmer. Driving frequency is varied to explore its effects on thrust production and wake structure in these two differently shaped 3D models. The input kinematics used to actuate the models encompass kinematic values measured from live swimming hagfishes, allowing for general comparisons between actively swimming hagfish and passively flexing models. Here, I discuss the performance of the physical models in relation to known characteristics of hagfish swimming, and consider lessons we can learn from passively undulating models to better understand locomotion by live anguilliform swimmers.

Approximating hagfish swimming with physical models

Despite lacking additional active musculature along their length to power swimming motions, the physical models studied here reproduced certain aspects of undulatory swimming also found in live, elongate anguilliform swimmers. The rectangular foil with a flexural stiffness closest to that for a whole hagfish (1.19×10^{-4} Nm^2 model *vs.* 3×10^{-4} Nm^2, *Myxine glutinosa* (Long et al., 2002)) swam at steady speeds that were similar to those for live hagfishes at comparable leading edge amplitudes and frequencies. For example, a Pacific hagfish (*Eptatretus stoutii*) with a rostral amplitude of 1.25 cm and frequency of 2 Hz swam at 26 cm/s, close to the ~23 cm/s self-

propelled swim speed by the rectangular foil of intermediate stiffness (Figure 4.3B). Similarly, an Atlantic hagfish (*M. glutinosa*) with a rostral amplitude of 2.5 cm and frequency of 1.25 Hz swam at 19 cm/s, close to the ~22 cm/s foil swim speed. For the same rectangular foil swimming at a driving amplitude of 1.5 cm and frequency of 1.5 Hz, values which would be typical for a live swimming hagfish, the structure of the wake produced by the physical model and hagfish also closely resembled each other (Figure 4.5; Chapter 3). Both produced a clear 2P wake where two pairs of vortices are shed per complete undulatory cycle (Hultmark et al., 2007; Schnipper et al., 2009). While the polyurethane bar and rod models more closely approximated the body of a hagfish or eel, the flexural stiffnesses of these models were an order of magnitude larger than that for either of these fishes (Long, 1998; Long et al., 2002). Nevertheless, actuating the bar and rod models at a heave amplitude of 2 cm and frequency of 1.0 Hz, again within the range of typical physiological values for a live swimming hagfish, also produced a wake structure similar to the 2P wake observed for steady swimming hagfish. For all of the model swimmers, formation of wake flow structures began along the length of the foil as they do in live undulating hagfish. Bending along the foil entrains fluid that travels posteriorly toward the trailing edge where it forms jets in the wake (Figures 4.6 – 4.8, 4.12, 4.13). In several cases, the fluid jets consist of flows with a substantial laterally-directed component, a condition also shared by eels and hagfishes that are hypothesized to balance thrust and drag production along the entire length of their bodies (Müller et al., 2001; Tytell and Lauder, 2004).

While the passively flexing foils were capable of achieving comparable levels of swim performance and wake organization as live hagfish, the shape of the undulatory wave in the rectangular foil models did not closely approximate the shape of the typical anguilliform body wave. Amplitude of undulation changed little along the length of the foil (Figure 4.2), while in

hagfishes and other elongate anguilliform swimmers the amplitude of body undulations generally increases from head to tail during steady swimming (Chapter 1; Gillis, 1996). It appears that simply adding rotation about the anterior body can produce amplitude variation along the body, however, as the polyurethane rod and bar models pitched about their leading edge axis and also had a non-uniform amplitude along their length (Figure 4.9).

For both the rectangular foils and the polyurethane rod and bar models, the shape of the undulatory wave was explained well by mechanical theory. For a body of uniform stiffness, the speed of an undulatory wave along the body remains constant (McHenry et al., 1995). Because wave speed is equal to the product of wavelength and frequency, an increase in frequency is accompanied by a decrease in wavelength. This was observed in the bar and rod models, where increases in driving frequency resulted in decreases in wavelength as well as trailing edge amplitude (Figure 4.9). McHenry and his colleagues (McHenry et al., 1995) similarly studied undulatory waves in physical models of pumpkinseed sunfish (*Lepomis gibbosus*) and found that tail beat amplitude also decreased with increasing driving frequency. Interestingly, Pacific hagfish also reduce their tail beat amplitude and wavelength while increasing tail beat frequency to swim at faster steady swim speeds (Chapter 1), suggesting that these particular kinematic characteristics of their undulatory wave may be entirely passive.

On the other hand, an increase in body stiffness results in an increase in the wavelength of undulatory waves along the body (McHenry et al., 1995). This was observed among the rectangular foils of different flexural stiffnesses at any given combination of heave amplitude and driving frequency (Figure 4.2). Increasing stiffness also increases wave speed (McHenry et al., 1995), which would contribute to the higher swim speeds measured for the stiffer foils (Figure 4.3). Similarly, in an experimental study of swimming in a robotic lamprey model with

tails of different stiffnesses, Leftwich et al. (Leftwich et al., 2012) found that greater tail flexibility was correlated with reduced thrust production. The hydrodynamics of the passively flexing foils in the present study also varied accordingly with changes in foil stiffness and undulatory wave shape. The shape of a body's undulatory wave, particularly at posterior regions, can influence wake structure (Tytell et al., 2010), and for the most flexible foil that was most susceptible to changing configuration under external forces, the structure of the wake changed with every change in input kinematics (Figure 4.8). In contrast, for the stiffer foils that were more resistant to deformation, general wake structure changed little (Figures 4.6, 4.7). The stiffest rectangular foil least resembled a swimming hagfish in both undulatory wave shape and wake structure, which consisted of persisting bands of vorticity representing shear layers caused by the foil trailing edge moving through the fluid (Figure 4.7). For all swim speeds and kinematic combinations observed in voluntarily swimming hagfish, the 2P wake was always observed (Chapter 3), suggesting some active control of the shape of the body undulatory wave (Long et al., 2010).

Lessons from model swimmers

Of most relevance to flexible-bodied swimmers, driving frequency appears to be a primary variable controlling steady swimming speed. For the two most flexible rectangular foils (flexural stiffness of 4.78×10^{-7} and 1.19×10^{-4} Nm^2, Table 4.1), self-propelled swimming speed responds more to changes in driving frequency than changes in heave amplitude, particularly at low frequencies that are comparable to those observed in live steady swimming hagfish (Figure 4.3A, B; Chapter 1). For example, for the most flexible foil oscillating at a frequency of 1 Hz, self-propelled speeds remain at approximately 5 cm/s despite increasing the heave amplitude at the

leading edge (Figure 4.3A). This lack of a gain in swim speed with increasing amplitude is also reflected in the flexible foil's hydrodynamics. As heave amplitude increases from 1.5 to 3.5 cm, the wake structure transitions from a 2S wake with distinct vortices (Figure 4.8, bottom panel) to an irregular and less coherent wake (Figure 4.8, top panel). In general, organized and coherent vortices in a thrust wake are associated with higher swim speeds (Alben et al., 2012). The irregularity of the wake at a high heave amplitude may be related to the irregular trajectory of the trailing edge (Schnipper et al., 2009) and distortion of the undulatory wave shape (Figure 4.2, top panel). Higher heave amplitudes were also associated with a stronger leading edge vortex, which may induce higher drag on the foil. At a constant heave amplitude of 2.5 cm, however, increasing driving frequency from 1.5 to 2.5 Hz results in a transition to an organized 2P wake (Figure 4.8, right panel).

As the whole-body flexural stiffness of Atlantic hagfish (*Myxine glutinosa*) is between the stiffnesses of the two most flexible rectangular foils, the importance of driving frequency over amplitude in controlling steady swim speed at low tail beat frequencies could be relevant to live hagfish as well. In a previous study of hagfish steady swimming, *M. glutinosa* consistently swam slower than their Pacific cousins, *Eptatretus stoutii* (Chapter 1), and tended to increase undulatory amplitude with increasing swim speeds. Other researchers have noted that this difference in swimming ability may be related to species differences in aerobic capacity for exercise (Forster, 1990), but the experiments with model swimmers here show that it may also be a mechanical consequence of expending more energy to generate larger body waves (Wu, 1977) without concomitant gains in swim speed.

Driving frequency was also a strong influence on the undulatory behavior of the square bar and round rod models. In general, the shape of the undulatory wave along the models and the

wake structure varied more with changes in driving frequency than with the shape of the models (Figures 4.9, 4.12 – 4.14). The different cross-sectional shapes of these models is relevant to anguilliform swimming because the lateral surfaces of an elongate swimming body push on the water and propel the body through it *via* fluid reaction forces. A surface with a rounded profile (i.e. rod model) should have smaller drag and added mass coefficients than a flat surface profile (i.e. bar model) (Vogel, 1994), potentially producing smaller fluid forces and thrust. Interestingly, differences in thrust production between the bar and rod models were dependent on the driving frequency. At low frequencies, the flat-sided bar generated more net thrust (Figure 4.10A), while at higher frequencies, the rod and bar models generated approximately equal amounts of net thrust (Figure 4.10A). In contrast, vortex ring force did not differ between the rod and bar at low frequencies (Figure 4.15), though these forces were mostly laterally-directed and would not contribute to forward thrust (Tytell and Lauder, 2004). The work exerted to actuate the models, however, was always greater in the bar than the rod (Figure 4.10B). This difference in energetic cost could be due to the higher bending rigidity of the bar and/or higher form drag in the bar compared to the rod. However, because the rod and bar still produced comparable amounts of net thrust, this suggests that flexible, cylindrically-shaped swimmers (e.g. eels, hagfish, salamanders, and sea snakes) can exploit reduced energy requirements to move their bodies through the water while still generating thrust along their bodies and achieving reasonable swim speeds. Furthermore, the work required to actuate the bar and rod models changed little over increasing driving frequencies spanning 0.5 to 1.5 Hz (Figure 4.10B), demonstrating that it is possible to exploit passive changes in emergent body motion and produce more propulsive force without incurring greater energetic costs. Lateral compression of tails in live anguilliform swimmers further confers savings in energy, as tapering tails require less force and energy to

move (McMillen and Holmes, 2006).

In accordance with other studies that used physical models to study swimming in flexible bodies (McHenry et al., 1995; Root et al., 1999), I support the hypothesis that anterior muscle activation on its own could conceivably power undulatory locomotion (Blight, 1977). The present study has shown that increasing contraction frequency of muscles only near the head could affect body motion at the tail, and consequently swim performance, if the body can transmit the forces along its length. Alternatively, live anguilliform swimmers could employ the same motor program to generate body bends but differences in body stiffness can result in differences in interaction with the surrounding water and resultant swim performance.

List of symbols and abbreviations

E	Young's modulus
I	Second moment of area
SPS	Self-propelled speed
COT	Cost of transport
BL	Body length = total length of the physical model
I_r	Vortex ring impulse
ρ	Fluid density
Γ	Vortex ring circulation
h	Vortex ring height
d	Vortex ring diameter
t	Time

Acknowledgements

I am grateful to George Lauder for his support during all stages of this study. Special thanks to Chuck Witt and Eric Tytell for providing invaluable Matlab code, Vern Baker, Chuck Witt, and Dan Quinn for assistance during data collection, and Erin Blevins and Li Wen for constructive discussions about this experiment and analysis. This project was supported by NSF grant EFRI-0938043 to George Lauder, the Harvard University OEB Department, and a Robert A. Chapman Memorial Scholarship granted to Jeanette Lim.

References

Alben, S. (2008). Optimal flexibility of a flapping appendage in an inviscid fluid. *J. Fluid Mech.* **614**, 355-380.

Alben, S., Witt, C., Baker, T. V., Anderson, E. and Lauder, G. V. (2012). Dynamics of freely swimming flexible foils. *Phys. Fluids* **24**, 051901.

Blight, A. R. (1977). The muscular control of vertebrate swimming movements. *Biol. Rev.* **52**, 181-218.

Carlson, R. L. and Lauder, G. V. (2011). Escaping the flow: boundary layer use by the darter *Etheostoma tetrazonum* (Percidae) during benthic station holding. *J. Exp. Biol.* **214**, 1181-1193.

Ferreira de Sousa, P. J. S. A. and Allen, J. J. (2011). Thrust efficiency of harmonically oscillating flexible flat plates. *J. Fluid Mech.* **674**, 43-66.

Forster, M. E. (1990). Confirmation of the low metabolic rate of hagfish. *Comp. Biochem. Physiol. A* **96**, 113-116.

Gillis, G. B. (1996). Undulatory locomotion in elongate aquatic vertebrates: Anguilliform swimming since Sir James Gray. *Amer. Zool.* **36**, 656-665.

Gillis, G. B. (1998). Environmental effects on undulatory locomotion in the American eel *Anguilla rostrata*: kinematics in water and on land. *J. Exp. Biol.* **201**, 949-961.

Hart, J. L. (1973). Pacific fishes of Canada. *Fish. Res. Board Can. Bull.* **180**, 1-740.

Hultmark, M., Leftwich, M. and Smits, A. J. (2007). Flowfield measurements in the wake of a robotic lamprey. *Exp. Fluids* **43**, 683-690.

Jayne, B. C. (1985). Swimming in constricting (*Elaphe g. guttata*) and nonconstricting (*Nerodia fasciata pictiventris*) colubrid snakes. *Copeia* **1985**, 195-208.

Lauder, G. V. (2000). Function of the caudal fin during locomotion in fishes: kinematics, flow visualization, and evolutionary patterns. *Amer. Zool.* **40**, 101-122.

Lauder, G. V., Anderson, E. J., Tangorra, J. L. and Madden, P. G. A. (2007). Fish biorobotics: kinematics and hydrodynamics of self-propulsion. *J. Exp. Biol.* **210**, 2767-2780.

Lauder, G. V., Lim, J. L., Shelton, R., Witt, C., Anderson, E. J. and Tangorra, J. L. (2011). Robotic models for studying undulatory locomotion in fishes. *Mar. Technol. Soc. J.* **45**, 45-55.

Leftwich, M. C., Tytell, E. D., Cohen, A. H. and Smits, A. J. (2012). Wake structures behind a swimming robotic lamprey with a passively flexible tail. *J. Exp. Biol.* **215**, 416-425.

Long, J. H., Jr. (1998). Muscles, elastic energy, and the dynamics of body stiffness in swimming eels. *Amer. Zool.* **38**, 771-792.

Long, J. H., Jr., Koob-Emunds, M., Sinwell, B. and Koob, T. J. (2002). The notochord of hagfish *Myxine glutinosa*: visco-elastic properties and mechanical functions during steady swimming. *J. Exp. Biol.* **205**, 3819-3831.

Long, J. H., Porter, M. E., Root, R. G. and Liew, C. W. (2010). Go reconfigure: how fish change shape as they swim and evolve. *Integr. Comp. Biol.* **50**, 1120-1139.

McHenry, M. J., Pell, C. A. and Long, J. H., Jr. (1995). Mechanical control of swimming speed: stiffness and axial wave form in undulating fish models. *J. Exp. Biol.* **198**, 2293-2305.

McMillen, T. and Holmes, P. (2006). An elastic rod model for anguilliform swimming. *J. Math. Biol.* **53**, 843-886.

Müller, U. K., Smit, J., Stamhuis, E. J. and videler, J. J. (2001). How the body contributes to the wake in undulatory fish swimming: flow fields of a swimming eel (*Anguilla anguilla*). *J. Exp. Biol.* **204**, 2715-2762.

Munk, Y. (2008). Kinematics of swimming garter snakes (*Thamnophis sirtalis*). *Comp. Biochem. Physiol. A* **150**, 131-135.

Ota, K. G., Fujimoto, S., Oisi, Y. and Kuratani, S. (2011). Identification of vertebra-like elements and their possible differentiation from sclerotomes in the hagfish. *Nat. Commun.* **2**:373 doi: 10.1038/ncomms1355.

Prempraneerach, P., Hover, F. S. and Triantafyllou, M. S. (2003). The effect of chordwise flexibility on the thrust and efficiency of a flapping foil. In *Proc. 13th Int. Symp. on Unmanned Untethered Subersible Technology: special session on bioengineering research related to autonomous underwater vehicles*. New Hampshire.

Root, R. G., Courtland, H. W., Pell, C. A., Hobson, B., Twohig, E. J., Suter, R. B., Shepherd, W. R. I., Boetticher, N. C. and Long, J. H., Jr. (1999). Swimming fish and fish-like models: the harmonic structure of undulatory waves suggest that fish actively tune their bodies. In *Proceedings of the 11th International Symposium on Unmanned Untethered Submersible Technology* vol. 11, pp. 378-388: Autonomous Undersea Systems Institute.

Schlichting, H. (1979). *Boundary-layer theory*. New York: McGraw-Hill.

Schnipper, T., Andersen, A. and Bohr, T. (2009). Vortex wakes of a flapping foil. *J. Fluid Mech.* **633**, 411-423.

Scott, W. B. and Scott, M. G. (1988). Atlantic Fishes of Canada. *Can. Bull. Fish. Aquat. Sci.* **219**, 1-731.

Stamhuis, E. J. and Nauwelaerts, S. (2005). Propulsive force calculations in swimming frogs II. Application of a vortex ring model to DPIV data. *J. Exp. Biol.* **208**, 1445-1451.

Tytell, E. D. (2004). The hydrodynamics of eel swimming II. Effect of swimming speed. *J. Exp. Biol.* **207**, 3265-3279.

Tytell, E. D., Hsu, C.-Y., Williams, T. L., Cohen, A. H. and Fauci, L. J. (2010). Interactions between internal forces, body stiffness, and fluid environment in a neuromechanical model of lamprey swimming. *Proc. Nat. Acad. Sci. USA* **107**, 19832-19837.

Tytell, E. D. and Lauder, G. V. (2004). The hydrodynamics of eel swimming I. Wake structure. *J. Exp. Biol.* **207**, 1825-1841.

Vogel, S. (1994). *Life in Moving Fluids: The Physical Biology of Flow*. Princeton: Princeton University Press.

Wu, T. Y. (1977). Introduction to the scaling of aquatic animal locomotion. In *Scale effects in animal locomotion* (ed. T. J. Pedley), pp. 203-232. New York: Academic Press.